

# Dynamic Frequency Planning for Professional Wireless Microphone Systems

Von der Fakultät für Elektrotechnik und Informatik  
der Gottfried Wilhelm Leibniz Universität Hannover  
zur Erlangung des akademischen Grades

Doktor-Ingenieur

genehmigte

**Dissertation**

von

Dipl.-Wirtsch.-Ing. Christoph Jürgen König  
geboren am 28. Mai 1979 in Bremen

2015

Referent : Prof. Dr.-Ing. Markus Fidler  
Korreferent : Prof. Dr.-Ing. Thomas Kürner  
Tag der Promotion : 29. Mai 2015

Dipl.-Wirtsch.-Ing. Christoph Jürgen König: *Dynamic Frequency Planning for Professional Wireless Microphone Systems*, Dissertation, © 2015

## ABSTRACT

---

In this thesis, we investigate dynamic frequency planning for professional wireless microphone systems. Besides guard intervals of their operation frequencies, these systems also have to consider the constraint of intermodulation. This necessity has its origin in the ongoing worldwide discussion on a new spectrum regulation regime, that tries to balance the high demand for unused resources by allowing the access of unlicensed systems on a non-interfering basis. In this thesis, we show that our approaches and methodologies are capable of coping with the considered complex frequency allocation problem in the new spectrum regulation regime.

An approval of these unlicensed systems will change the situation of professional wireless microphone systems considerably. Such systems are characterized by outstanding high quality of service requirements such as very low latency for psychoacoustic reasons and the prevention of any audible disturbances during operation. Today, the probability, that such disturbances occur is low due to the static resource allocation. However, this will change in the future, and these systems will have to cope with sudden interference caused by missed detections of unlicensed devices.

This marks the baseline for this thesis. Building upon basic principles of power amplifiers, Cognitive Radio, and Fourier analysis, we determine the complexity class of a dynamic frequency allocation problem. We design frequency allocation approaches with different objectives and evaluate them for typical configuration sizes and quality requirements of wireless microphone systems.

Another important aspect in the context of coexistence is the correct determination of the current radio spectrum environment. So a sensor network has to identify unoccupied resources correctly. During the International Radio Exhibition (IFA; Internationale Funkausstellung) 2013, we conducted measurements on the fairgrounds of the Messe Berlin. Our results provide insight into the current spectrum occupancy and allow conclusions regarding the design of similar sensor networks at other locations.

In the last part, we combine our findings. We introduce an architecture for a Cognitive Engine, that selects a feasible frequency allocation based on the currently reported audio quality and radio spectrum environment information. Furthermore, we present a scheme that rates the sensor data to identify the best alternate frequency in case of emerging interference.

*Index terms*— Cognitive Radio, Frequency Assignment, Intermodulation Products, Simulated Annealing

## ZUSAMMENFASSUNG

---

Die vorliegende Arbeit behandelt die dynamische Frequenzplanung drahtloser Kommunikationssysteme, wie beispielsweise drahtlose Mikrofone, bei denen, neben einem Schutzabstand der Sendefrequenzen, auch deren Intermodulationsprodukte zu berücksichtigen sind. Die Notwendigkeit für neue Verfahren ergibt sich aus den aktuell weltweit diskutierten Änderungen zur Frequenzregulierung, die versuchen, die ungebremst hohe Nachfrage nach ungenutzten spektralen Ressourcen auszugleichen und für unlicenzierte Systeme zu öffnen. Dies erfolgt unter der Maßgabe, dass kein lizenziertes System gestört werden darf. Im Verlauf der Arbeit wird gezeigt, dass das betrachtete Frequenzplanungsproblem mit Hilfe der entwickelten Methoden und Verfahren beherrschbar ist.

Eine Zulassung solcher Systeme verändert die Situation von professionellen drahtlosen Mikrofonsystemen erheblich. Diese zeichnen sich durch äußerst hohe Anforderungen an die Übertragungsqualität aus, z. B. sind aus psychoakustischen Gründen sehr geringe Latenzzeiten erforderlich und hörbare Störungen müssen unter allen Umständen vermieden werden. Bisher waren diese wegen der statischen Spektrumbelegung kaum zu erwarten, jedoch muss in Zukunft mit dem plötzlichen Auftreten unlizenzierter Geräte gerechnet werden, deren Detektionsmechanismus versagt hat.

Dies stellt das in dieser Arbeit zu untersuchende Ausgangsszenario dar. Aufbauend auf den theoretischen Grundlagen über Leistungsverstärker, Cognitive Radio und Fourier-Analyse wird die Komplexitätsklasse des Allokationsproblems identifiziert. Daran anschließend werden Frequenzplanungsverfahren mit unterschiedlichen Zielrichtungen entwickelt, um sie mit typischen Konfigurationsgrößen und Qualitätsanforderungen drahtloser Mikrofonsysteme zu evaluieren.

Ein weiterer, wichtiger Gesichtspunkt ist die kontinuierliche Erfassung des Spektrums zur Identifikation unbelegter Ressourcen. Dies geschieht mit Hilfe eines Sensornetzwerks und entsprechende Messungen wurden während der Internationalen Funkausstellung 2013 auf dem Gelände der Messe Berlin durchgeführt. Sie erlauben einen Einblick in die Spektrumbelegung während einer Großveranstaltung und lassen Rückschlüsse auf das erforderliche Design eines solchen Sensornetzwerks an anderen Orten zu.

Mit den zuvor gewonnenen Erkenntnissen wird anschließend eine Prozess-Architektur entwickelt, die situationsabhängig Entscheidungen über das zu verwendende Frequenzplanungsverfahren treffen kann und dafür die aktuelle Audioqualität und Informationen aus dem Sensornetzwerk berücksichtigt. Weiterhin wird eine Bewer-

tungsmethode für Ausweichfrequenzen entwickelt, um im Fall einer Störung auf eine andere Frequenz mit höherer Qualität zu wechseln.

*Schlagwörter*— Cognitive Radio, Frequenzplanung, Intermodulationsprodukte, Simulated Annealing



# CONTENTS

---

<b>I</b>	<b>DISSERTATION</b>	<b>1</b>
1	INTRODUCTION	3
1.1	Power Amplifiers . . . . .	4
1.2	Cognitive Radio . . . . .	13
1.3	Spectrum Analysis . . . . .	22
1.4	Application Scenario . . . . .	29
1.5	System Setup . . . . .	31
1.6	Organization of the Thesis . . . . .	31
2	RELATED WORK	33
3	PROBLEM FORMULATION	37
4	PROBLEM COMPLEXITY CLASSIFICATION	39
4.1	Complexity Classes . . . . .	39
4.2	Search Space Exploration . . . . .	41
4.3	Evaluation . . . . .	46
4.4	Discussion . . . . .	48
5	STATE-OF-THE-ART AND CONSTRUCTIVE APPROACHES	51
5.1	Replication Assignment . . . . .	51
5.2	Interference Scenarios . . . . .	53
5.3	Constructive Approaches . . . . .	55
5.4	Discussion . . . . .	62
6	ADAPTATION OF A METAHEURISTIC	67
6.1	Strategies to Solve Combinatorial Problems . . . . .	67
6.2	Problem Representation . . . . .	69
6.3	Selection of a Problem-Specific Strategy . . . . .	76
6.4	Optimization with Simulated Annealing . . . . .	78
6.5	Evaluation . . . . .	81
6.6	Outlook: Parallelization . . . . .	86
7	SPECTRUM OCCUPANCY MEASUREMENTS	87
7.1	Measurement Setup and Methodology . . . . .	87
7.2	Measurement Results . . . . .	91
7.3	Summary . . . . .	96
8	ARCHITECTURE FOR COGNITIVE DEVICES	97
8.1	Scope of our Cognitive Engine . . . . .	97
8.2	Proposed Software Framework . . . . .	98
8.3	Rating of Spectrum Scanner Data . . . . .	103
9	CONCLUSION AND OUTLOOK	109
<b>II</b>	<b>APPENDIX</b>	<b>113</b>
A	OBTAINED ALLOCATIONS	115
B	SHIFT EXAMPLE	119

BIBLIOGRAPHY	123
PUBLICATIONS	133
SCIENTIFIC CAREER	135



## LIST OF FIGURES

---

Figure 1.1	Digital transmitter and receiver system . . . . .	3
Figure 1.2	Energetic representation of PA operation . . . . .	5
Figure 1.3	Symbol and characteristics of an n-MOSFET . . . . .	5
Figure 1.4	Extended topology and current waveform . . . . .	7
Figure 1.5	PA efficiency for different operation classes . . . . .	8
Figure 1.6	Definition of distance $d_c$ . . . . .	11
Figure 1.7	Definition of distance $d_3$ . . . . .	12
Figure 1.8	Agility in the ISO OSI model . . . . .	14
Figure 1.9	Dynamic spectrum access scheme . . . . .	16
Figure 1.10	Mitola's Cognitive Cycle . . . . .	16
Figure 1.11	Signal in time and frequency domain . . . . .	23
Figure 1.12	Frequency domain discretization . . . . .	24
Figure 1.13	Two-point DFT . . . . .	26
Figure 1.14	Four-point DFT . . . . .	27
Figure 1.15	Link budget for a wireless device . . . . .	28
Figure 1.16	General system setup . . . . .	31
Figure 4.1	Sets of problem attributes . . . . .	39
Figure 4.2	Producer-Consumer pattern . . . . .	41
Figure 4.3	Impact of combination reduction techniques . . . . .	47
Figure 5.1	State-of-the-art frequency allocation strategy . . . . .	52
Figure 5.2	Considered interference scenarios . . . . .	53
Figure 5.3	Data collection during system setup phase . . . . .	54
Figure 5.4	Performance achieved by random fit . . . . .	58
Figure 5.5	Performance achieved by extended first fit . . . . .	61
Figure 5.6	Performance under interference scenarios . . . . .	63
Figure 6.1	Used utility functions . . . . .	72
Figure 6.2	Recombination example . . . . .	76
Figure 6.3	Achievable utilities by moving a link . . . . .	78
Figure 6.4	Simulated Annealing and Genetic Algorithms . . . . .	82
Figure 6.5	Dynamic frequency reallocation . . . . .	84
Figure 6.6	Increase of utility $U_F$ during optimization . . . . .	85
Figure 6.7	Parallelized Simulated Annealing processes . . . . .	86
Figure 7.1	System setup of the measurement installation . . . . .	90
Figure 7.2	Map of the area at Messe Berlin . . . . .	90
Figure 7.3	Floor plan with installed scanning receivers . . . . .	91
Figure 7.4	Overview of measured duty cycles . . . . .	94
Figure 7.5	Spatial correlation matrices . . . . .	95
Figure 8.1	Data collection during setup and operation . . . . .	97
Figure 8.2	Cognitive cycle . . . . .	99
Figure 8.3	Architecture of our Cognitive Engine . . . . .	100
Figure 8.4	Spectrum Quality Mapping function . . . . .	104

Figure 8.5	Estimated trajectory of a mobile transmitter . . .	106
Figure 8.6	Rated spectrum quality at two locations . . . .	107

## LIST OF TABLES

---

Table 1.1	Emissions created by intermodulation . . . . .	10
Table 1.2	Network types and wireless IEEE standards .	19
Table 1.3	Fourier analysis methods . . . . .	23
Table 1.4	Future coexisting systems in the UHF TV band	29
Table 4.1	Combination process . . . . .	44
Table 4.2	Evaluation of reduction approaches . . . . .	48
Table 5.1	Allocations for different bandwidths . . . . .	52
Table 5.2	Parameters for frequency allocation . . . . .	55
Table 5.3	Performance achieved by random fit approach	59
Table 5.4	Performance achieved by first fit approaches .	60
Table 5.5	Comparison of allocated devices . . . . .	62
Table 6.1	Matrices definition and prototype assignment	74
Table 6.2	Utilities before and after recombination . . . .	77
Table 7.1	DVB-T Radio Towers in Berlin Area . . . . .	88
Table 7.2	DVB-T Radio Towers' Transmission Power . .	89
Table 7.3	Scanning receiver configuration . . . . .	91
Table 7.4	Duty cycles of September, 7th 2013 . . . . .	93
Table 8.1	Lookup table for evaluation of scanner data . .	107
Table A.1	Best EFF allocations (interference-free case) . .	116
Table A.2	Best EFF allocations (interference-case) . . . .	117
Table A.3	Best Simulated Annealing allocation . . . . .	118

## LIST OF ALGORITHMS

---

Algorithm 4.1	Validate combination for $d_3$ on a CPU . . . . .	42
Algorithm 5.1	Constructive allocation approaches . . . . .	56
Algorithm 6.1	Simulated Annealing process . . . . .	79
Algorithm 6.2	Neighbor function of the annealing process . .	80
Algorithm 8.1	Create scanner data interpretation scheme . .	105

## GLOSSARY OF ACRONYMS

---

3G	Third-generation cellular systems.
ADC	Analog-to-Digital Converter.
CEN	Cognitive Engine.
CPU	Central Processing Unit.
CUDA	Compute Unified Device Architecture.
DAC	Digital-to-Analog Converter.
DC	Direct Current.
DFT	Discrete Fourier Transform.
DSP	Digital Signal Processor.
DTFT	Discrete Time Fourier Transform.
DVB-T	Digital Video Broadcasting – Terrestrial.
ECC	Electronic Communications Committee.
EFF	Extended First Fit.
ETSI	European Telecommunications Standards Institute.
FAP	Frequency Assignment Problem.
FCC	Federal Communications Commission.
FFT	Fast Fourier Transform.
FS	Fourier Series.
FT	Fourier Transform.
GA	Genetic Algorithm.
GLDB	Geolocation Database.
GPS	Global Positioning System.
GPU	Graphics Processing Unit.
GSM	Global System for Mobile Communications.
GUI	Graphical User Interface.
IEEE	Institute of Electrical and Electronics Engineers.

IFFT	Inverse Fast Fourier Transform.
IM	Intermodulation.
IMP	Intermodulation Product.
ISM	Industrial, Scientific, and Medical.
ISO	International Organization for Standardization.
ITU	International Telecommunication Union.
LAN	Local Area Network.
LNA	Low Noise Amplifier.
LQI	Link Quality Indicator.
LTE	Long-term Evolution.
MAN	Metropolitan Area Network.
Mbps	Megabit per second.
MIMO	Multiple Input Multiple Output.
MOSFET	Metal-Oxide Semiconductor Field Effect Transistor.
Ofcom	Office of Communications.
OSI	Open Systems Interconnection.
PA	Power Amplifier.
PAN	Personal Area Network.
PFF	Plain First Fit.
PMSE	Programme Making and Special Event.
PSD	Power Spectral Density.
RAN	Regional Area Network.
REM	Radio Environment Map.
RLM	Radio Link Manager.
RSQ	Rated Spectrum Quality.
SA	Simulated Annealing.
SNR	Signal-to-Noise Ratio.
TS	Taboo Search.
TV	Television.
TVWS	Television White Space.

UHF Ultra High Frequency.

VCO Voltage Controlled Oscillator.

WAN Wide Area Network.

WiFi Wireless Fidelity.

WSD White Space Device.





Part I

DISSERTATION



## INTRODUCTION

Today's wireless communications systems are characterized by the requirement to deliver a growing amount of data to the users. It follows that researchers and engineers seek for solutions that increase the spectrum efficiency of systems to make the most out of the scarce radio resource spectrum.

Based on Hertz's discovery of radio waves in 1888, initial wireless transmission experiments were performed by Marconi in 1894. Starting with low Morse code rates, the development of vacuum tubes and modulation techniques enable that this communication technology faced an extensive evolution in the last century. Currently, transmission rates of hundreds of Megabit per second (Mbps) are state-of-the-art in Wireless Fidelity (WiFi) networks and there is much research and development to increase them even further.

A revolutionary improvement of wireless systems is triggered by Moore's law of computational evolution. As the performance of integrated circuits becomes more and more powerful, they can be used today for a highly-flexible system architecture that implements the time-critical signal processing as a software function. Such architecture enables very smart devices that are highly configurable and creates a new class of devices, the so-called Cognitive Radios. These Cognitive Radios can be used to perform a dynamic spectrum access by using unoccupied resources and achieve a better utilization, i.e., a higher spectrum efficiency. In the following, we will discuss general benefits and particular challenges for other wireless systems that arise with the introduction of Cognitive Radios.

We start with a brief introduction of basic principles for wireless communication. An example of a digital transmitter and receiver system we will refer several times in this work to is depicted in Figure 1.1. The lower path describes a transmitter while the upper one represents a receiver system. Both paths perform amplification and

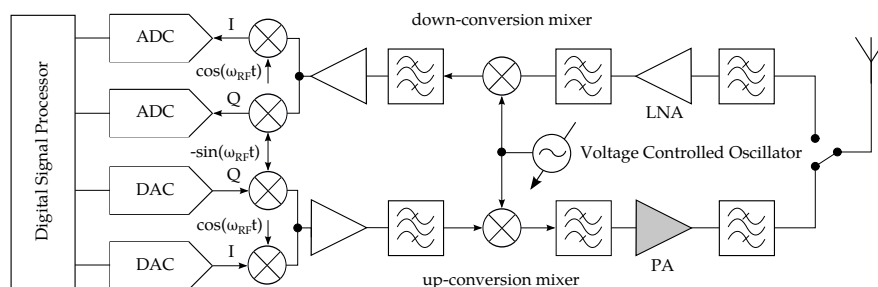


Figure 1.1: Digital transmitter and receiver system [36].

mixing operations on the signal and block unwanted parts of them with band-pass filters. Regarding the transmitter path, this thesis mainly concentrates on the characteristics of the Power Amplifier (PA) and its negative influences on the simultaneous operation of multiple wireless devices. On the receiver side, we consider the complete path. With this, we are able to analyze the radio spectrum environment to detect possible threats to our system. These threats are caused by the presence of other users and triggered by a changing radio spectrum regulation in the future.

In this chapter, we detail the underlying problems and organize the remainder as follows. For the transmitter, we show the trade-off between efficiency and distortion of PAs to identify constraints for resource allocation of wireless devices in Section 1.1. Next, in Section 1.2 we present the Cognitive Radio approach that describes a changing radio spectrum regulation from a static to a dynamic regime. These changes require methods to dynamically determine the interference level between coexisting systems and take actions to deal with them. Consequently, an additional quality constraint has to be introduced which must be considered during setup and operation in future systems and we describe the principles of spectrum analysis and determination of this quality constraint in Section 1.3. Finally, we present our application scenario that forms the basis of this thesis in Section 1.4. Though the findings in this thesis are given in the context of the system setup presented in Section 1.5, they are not limited to them. The obtained findings naturally fit to other application scenarios that face the same constraints regarding resource allocation during system setup and operation.

### 1.1 POWER AMPLIFIERS

In this section, we derive the distortion effects that occur when the power of a signal is amplified. The conclusions obtained here are significant for the problem formulation of this thesis.

In the ideal case, a power amplifier operates as efficient as possible and does not distort the output signal. Its efficiency is very important for mobile devices to achieve a long runtime while the second aspect influences the quality of the transmitted signal. However, in reality we face a trade-off between efficiency and linearity.

A linear amplification is required if a signal is generated by amplitude or a combination of amplitude and phase modulation. Signals with a constant amplitude do not require a linear amplification because their shape contains no information. Hence, its distortion does not reduce its information content. In the following, we derive analytically why a nonlinear amplification is essential for an efficient system operation.

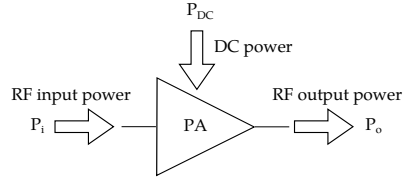


Figure 1.2: Energetic representation of power amplifier operation [16].

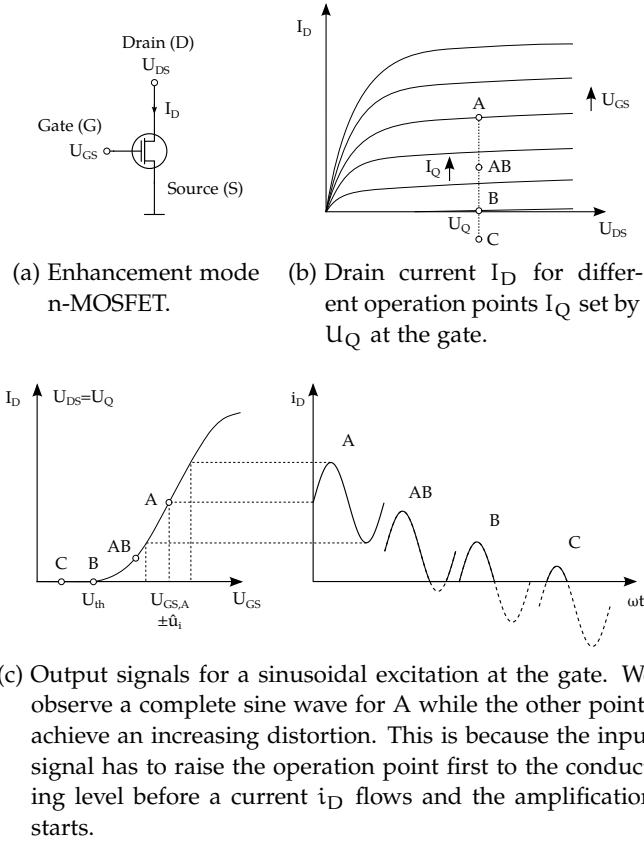


Figure 1.3: Symbol and characteristics of an n-MOSFET semiconductor for different operation points [16].

### 1.1.1 Efficiency Considerations

To analyze the efficiency of a power amplifier, we consider the energetic representation as depicted in Figure 1.2. The input power  $P_i$  is amplified with the help of the imparted power  $P_{DC}$  and results in the output power  $P_o$ . Since  $P_{DC} \gg P_i$  holds, we find the efficiency  $\eta$  as [4]:

$$\eta = \frac{P_o}{P_{DC}}. \quad (1.1)$$

It follows that a general goal in the complex power amplifier design is to minimize the required imparted power  $P_{DC}$  to increase the efficiency. To gain a closer insight into how to reduce this value, con-

sider Figure 1.3. The figure depicts the characteristics of an n-channel Metal-Oxide Semiconductor Field Effect Transistor (MOSFET) that is selected here as the representative part of a power amplifier. Other components, such as bipolar junction transistors and vacuum tubes, generally show similar characteristics [61]. Figure 1.3a shows the circuit symbol of an n-MOSFET with three connection points: Gate (G), drain (D), and source (S). In the following, we use these letters as indexes in our description and calculations to indicate current flows or voltage drops.

Essential parameters for n-MOSFET operation are voltages  $U_{DS}$  and  $U_{GS}$  that, as depicted in Figure 1.3b, set the drain current  $I_D$ . An increase of  $U_{GS}$  for a constant  $U_{DS}$  increases the drain current and sets the quiescent point (Q-point) for a particular output load. Depending on the drain current in the Q-point  $I_Q$ , the power consumption of the amplifier operation can be divided into the 4 classes: A, AB, B, and C. For instance, by setting the Q-point to A or AB, a permanent power is consumed while B or C do not trigger a flow of  $I_D$  because the transistor is disabled.

In case a superposition of voltage  $U_{GS}$  with a time-dependent signal  $\hat{u}_i \sin(\omega t)$  holds, the Q-point in Figure 1.3c moves along the characteristic curve. This movement influences a change of the drain current such that  $I_D$  also becomes a time-dependent variable  $i_d(t)$ . For example, with a sinusoidal excitation at A a steady drain current flows while at C the threshold voltage  $U_{th}$  needs to be exceeded first. Note that  $U_{th}$  refers to the cutoff voltage of the transistor. Only if  $U_{GS} + u_i(t) > U_{th}$  holds, a current  $I_D$  flows and output power at the load is implemented.

As we observe on the right side of Figure 1.3c, the achieved signal from a sinusoidal excitation for class A equals the input signal which results in a linear amplification. Contrary, a power amplifier operated at class C only amplifies some parts of the input signal which leads to a strong signal distortion. The remaining classes AB and B are in between these two extremes.

For efficiency analysis, we extend the n-MOSFET in Figure 1.3a with a Direct Current (DC) and a signal input source. Furthermore, we record the currents and voltages of an ideal network topology as depicted in Figure 1.4a [4]. The load is represented by  $R_L$  at the output. The parallel LC resonator is used to pass the fundamental frequency signal only to  $R_L$ . The components  $L_{CK}$  and  $C_B$  are used to block and pass the radio frequency signal, respectively.

As discussed before, the selection of the Q-point is an important design decision for linearity of power amplifier operation. Furthermore, this setting has a direct implication on the conduction angle  $2\phi$  that determines the length of an amplification phase. It follows that this parameter is significant for the efficiency of a power amplifier because it determines the period for the imparting power  $P_{DC}$ .

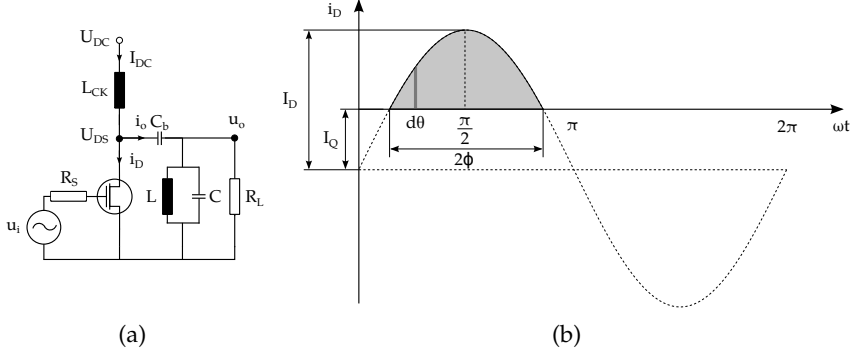


Figure 1.4: Extended n-MOSFET topology and drain current waveform for a conduction angle of  $2\phi$  (class C amplifier) [4, 61].

For further analysis, we define an angle  $\theta$  to partition the area into infinitely small pieces as depicted in Figure 1.4b. In our example, a class C amplifier operates with a cycle length of  $2\phi$  for  $2\phi \leq \pi$ , centered at  $\frac{\pi}{2}$ .

To quantify the alternating values  $i_o$  and  $u_o$  of the output network, we define their dependency of angle  $\theta$  as follows:

$$i_o = I_o \sin(\theta) \quad (1.2a)$$

$$u_o = U_o \sin(\theta) \quad (1.2b)$$

with  $I_o$  and  $U_o$  the peak values of the current and voltage, respectively. We start our analysis using (1.2a) to define the drain current  $i_D$  in dependency on  $\theta$ . Note that  $I_Q$  is negative for a class C amplifier that results in [61]:

$$i_D(\theta) = \begin{cases} I_Q + I_o \sin(\theta), & \frac{\pi}{2} - \phi \leq \theta \leq \frac{\pi}{2} + \phi, I_Q < 0 \\ 0, & \text{otherwise.} \end{cases} \quad (1.3)$$

At  $\theta = \frac{\pi}{2} - \phi$ ,  $i_D(\theta) = 0$  holds. It follows that  $I_Q = -I_o \cos(\phi)$  and (1.3) becomes:

$$i_D(\theta) = I_o [\sin(\theta) - \cos(\phi)].$$

The average drain current  $I_D$  is given by:

$$\begin{aligned} I_D &= \frac{1}{2\pi} \int_{\frac{\pi}{2}-\phi}^{\frac{\pi}{2}+\phi} I_o [\sin(\theta) - \cos(\phi)] d\theta \\ &= \frac{I_o}{\pi} [\sin(\phi) - \phi \cos(\phi)]. \end{aligned} \quad (1.4)$$

This results in an output power of:

$$\begin{aligned} P_o &= \frac{1}{2\pi} \int_{\frac{\pi}{2}-\phi}^{\frac{\pi}{2}+\phi} U_o \sin(\theta) I_o [\sin(\theta) - \cos(\phi)] d\theta \\ &= \frac{U_o I_o}{2\pi} [2\phi - \sin(2\phi)]. \end{aligned} \quad (1.5)$$

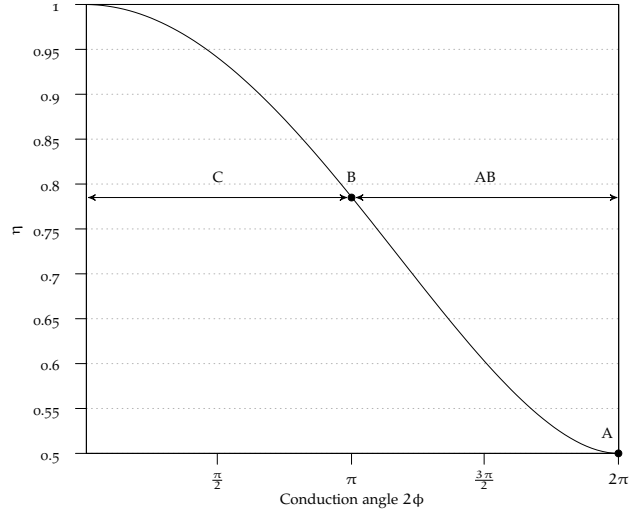


Figure 1.5: Overview of achievable efficiency  $\eta$  for different power amplifier operation classes. The highest efficiency is achieved by class C with a conduction angle between 0 and  $\pi$ . However, this mode has the highest level of signal distortion. Contrary, class A faces the lowest efficiency but a signal amplification without distortion.

In case of performance adaptation with  $U_o = U_{DS}$ , the maximum output power is given by:

$$P_{o,\max} = \frac{U_{DS}I_o}{4\pi} [2\phi - \sin 2\phi]. \quad (1.6)$$

Using (1.4), (1.6), and an input power of  $P_{DC} = I_D U_{DS}$  we find a conduction angle dependent efficiency of:

$$\eta_D = \frac{P_{o,\max}}{P_{DC}} = \frac{2\phi - \sin(2\phi)}{4[\sin(\phi) - \phi \cos(\phi)]}. \quad (1.7)$$

Figure 1.5 depicts the achievable efficiency calculated by (1.7) over the conduction angle  $2\phi$ . We observe that the highest efficiency is achieved in class C for which we have determined the highest signal distortion before. In contrast, a power amplifier operated at class A achieves the lowest efficiency but a linear amplification without distortion.

In the following, we elaborate on the consequences influenced by a nonlinear operation mode that result from an efficient amplification mode.

### 1.1.2 Distortion Analysis

As discussed before, the nonlinearity allows an efficient power amplifier operation but results in a distortion of output voltages and current waveforms that degrade the output signal quality. Therefore,



this behavior has to be correctly classified to not only fulfill requirements in terms of efficiency.

In order to identify the nonlinearity, an approximation of a power amplifier transfer characteristic is adopted. We consider an amplifier that is excited by a sinusoidal signal  $u_i(t)$ . Then, the output voltage can be expressed as a power series of the input as follows [4]:

$$u_o(t) = k_1 u_i(t) + k_2 u_i^2(t) + \dots + k_n u_i^n(t). \quad (1.8)$$

This approximation describes a memoryless system where previous states have no impact on the current state. For linear amplification, all coefficients except  $k_1$  are zero while  $k_1 > k_2 > \dots > k_n$  hold for the nonlinear case [4].

We assume that a power amplifier is operated with a conduction angle  $2\phi$  below  $\pi$  and analytically derive the generation of Intermodulation Products (IMPs) which are a consequence of this operation mode. Further, the modulation scheme and Q-point are selected such that the output signal is above an acceptable level.

To reduce the computational complexity, we perform our analysis on a power series of  $n = 3$ . This limitation can be done because higher orders only have a minor influence on the resulting signal [4, 94]. We consider an input signal  $u_i(t)$  as a combination of two signals with an equal amplitude  $A$  but different frequencies (*two-tone analysis*) [4] and find the mutual interaction between these frequencies in a nonlinear amplification as follows:

$$u_i(t) = A[\cos(\omega_1 t) + \cos(\omega_2 t)] \quad (1.9)$$

with  $\omega_1 = 2\pi f_1$  and  $\omega_2 = 2\pi f_2$ . By using (1.9) as input signal, (1.8) can be rewritten as:

$$\begin{aligned} u_o(t) = & k_1 A [\cos(\omega_1 t) + \cos(\omega_2 t)] \\ & + k_2 A^2 [\cos(\omega_1 t) + \cos(\omega_2 t)]^2 \\ & + k_3 A^3 [\cos(\omega_1 t) + \cos(\omega_2 t)]^3. \end{aligned} \quad (1.10)$$

Substituting (1.10) and ordering the terms by frequency components results in:

$$\begin{aligned} u_o(t) = & a_0 + a_1 \cos(\omega_1 t) + a_1 \cos(\omega_2 t) \\ & + a_0 \cos(\omega_1 t + \omega_2 t) + a_0 \cos(\omega_1 t - \omega_2 t) \\ & + \frac{a_0}{2} \cos(2\omega_1 t) + \frac{a_0}{2} \cos(2\omega_2 t) \\ & + 3a_2 \cos(2\omega_1 t - \omega_2 t) + 3a_2 \cos(2\omega_2 t - \omega_1 t) \\ & + 3a_2 \cos(2\omega_1 t + \omega_2 t) + 3a_2 \cos(2\omega_2 t + \omega_1 t) \\ & + a_2 \cos(3\omega_1 t) + a_2 \cos(3\omega_2 t) \end{aligned} \quad (1.11)$$

with coefficients

$$a_0 = k_2 A^2, a_1 = k_1 A + \frac{9}{4} k_3 A^3, a_2 = \frac{1}{4} k_3 A^3.$$

Table 1.1: Emissions created by  $f_1=800$  MHz and  $f_2=801$  MHz. The assumed system operation range is between 790 and 810 MHz.

Combination	Frequency [MHz]	Filterable?
$f_1 + f_2, f_2 - f_1$	1601, 1	yes
$2f_1, 2f_2$	1600, 1602	yes
$2f_1 - f_2, 2f_2 - f_1$	799, 802	no
$2f_1 + f_2, 2f_2 + f_1$	2401, 2402	yes
$3f_1, 3f_2$	2400, 2403	yes

The arguments of the cosine functions in (1.11)

$$\omega = j\omega_1 \pm k\omega_2 = j2\pi f_1 \pm k2\pi f_2$$

describe possible frequency combinations where  $j, k$  are integers in the interval  $[0, 3]$  and  $j + k$  represents the combination order. Orders with one frequency component only are named harmonics while orders with two (or more) components result in IMPs of them.

To identify harmful frequency combinations generated by the low power consuming amplification mode, we consider a wireless device transmitting between the frequencies  $f_1=800$  MHz and  $f_2=801$  MHz. Moreover, we assume a system operation range between 790 MHz and 810 MHz, i.e., signals with frequencies beyond the border of this range are filtered by the power amplifier downstream band-pass filter as depicted in Figure 1.1. The locations of the generated signals in the radio spectrum are summarized in Table 1.1. From this example, we find that all emissions are filtered except odd IMPs in the form  $2\omega_1 - \omega_2$  and  $2\omega_2 - \omega_1$ , respectively. Since our analysis is performed for  $n = 3$ , we observe the results for IMPs of third order only. However, combinations for higher orders can be calculated following the same scheme [4, 16].

From our previous finding, we derive a wireless signal which is expanded around its center frequency by odd IMPs. Now we extend our analysis and consider a setup where at least two devices operate simultaneously in the same transmission range. During transmission, each device amplifies its modulated input signal. Figure 1.6 depicts the generated IMPs up to 7th order. From this figure, it directly follows that device center frequencies need to have a specific distance  $d_c$  to avoid mutually adjacent-channel interference among the transmitted signals. The definition of this distance is the first constraint for the problem formulation of this thesis.

As we have seen, the nonlinear amplification of a modulated input signal enlarges the occupied bandwidth and initiates a distance constraint that has to be considered during resource allocation.

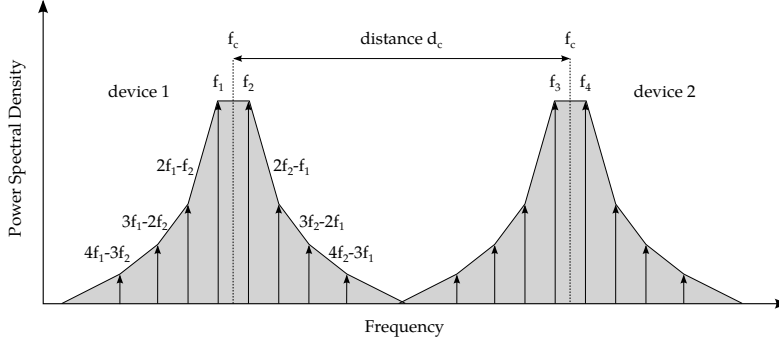


Figure 1.6: The output signal of each device is extended by intermodulation products of the input. Therefore, adjacent center frequencies  $f_c$  require a specific distance  $d_c$  to enable an interference-free operation.

Nonetheless, there is an additional effect called transmitter or reverse intermodulation between devices. In the case, that two devices operate in a spatially close range, i.e., less than 0.5 m, their output signals are mutually injected into the transmitter path of them. Since both devices use a frequency within the operation bandwidth, the band-pass filters, as depicted in Figure 1.1, are not capable of blocking the incoming signals. It follows that these incoming signals now act as an additional signal source at the power amplifier and our previous performed two-tone analysis holds again. As a consequence, further IMPs appear in the radio spectrum and have to be addressed during the overall resource allocation process.

For a simplification of the resource allocation process, we relax our view from absolute frequency values and introduce relative channels or slots to describe a system configuration without loss of generality.

To exploit all possible allocations, the typically selected slot size corresponds to the tunable frequency granularity of the underlying wireless system. It follows that each frequency dependent parameter  $p_f$  can be converted to a slot number  $s_n$  by dividing it by the slot size  $s$ :

$$s_n = \frac{p_f}{s}.$$

An example of this slot based approach for a setup with three devices is depicted in Figure 1.7. The allocation  $A$  contains three slot numbers  $a_1, a_2, a_3$  that act as center frequencies of the devices. Each center frequency has to maintain at least a distance  $d_c$  to all other center frequencies as previously described. Each pair of  $a_i \in A$  for  $i = 1, 2, 3$  induces IMPs. We store the locations of these IMPs in the set  $IMP$ . Considering these, we need to calculate their locations and check whether all devices maintain a further distance,  $d_3$ , to them. This distance is required to avoid Intermodulation (IM) adjacent-channel interference and guarantee a reliable transmission

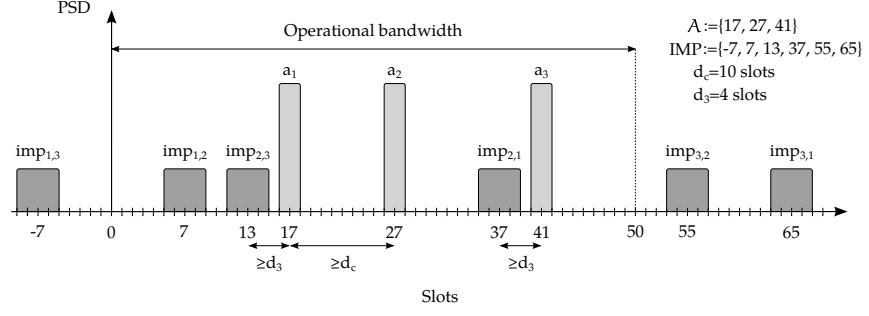


Figure 1.7: Generated intermodulation products (IMPs) by devices at slots  $a_1$ ,  $a_2$ , and  $a_3$  acting as center frequencies. In order to guarantee an interference-free operation all of the time, each device frequency has to maintain a distance of at least  $d_3$  to adjacent IMPs.

at all times. This marks the second constraint of our resource allocation. The number of IMPs grows quadratically with the number of devices. Note, however that some of the IMPs might be beyond the operation range of the system. Furthermore, IMPs face a lower signal power level and, therefore, distance  $d_3$  can be smaller than  $d_c$  [94].

Throughout this thesis, we focus on pairwise IM, i.e., at most two transmitters are spatially close to each other. Moreover, we assume that only third order IMPs cause remarkable interference to our devices because the power levels of higher orders decrease considerably. In general, an increase of values  $d_c$  and  $d_3$  results in a higher quality of the transmission. However, large distances lead to an inefficient allocation by wasting radio spectrum because the transmission quality turns into saturation at some point. It follows that our objective is a trade-off between achieved transmission quality and is directly related to the distance constraints  $d_c$  and  $d_3$ , as well as the number of simultaneously allocated devices. In the following, we term a resource allocation that fulfills both constraints as IM-free.

Our overall goal is to allocate as many devices as possible in the available operation range. Hence, we summarize our combinatorial optimization problem as follows:

$$\begin{aligned}
 & \max \quad \#A \\
 & \text{s.t.} \\
 & |a_i - a_j| \geq d_c \text{ for all } a_i, a_j \in A \text{ and } i \neq j \\
 & \underbrace{|2a_i - a_j - a_k|}_{\text{imp}_{i,j}} \geq d_3 \text{ for all } a_i, a_j, a_k \in A \text{ and } i \neq j.
 \end{aligned} \tag{1.12}$$

Note that  $\#A$  denotes the cardinality of  $A$ . Thus, our objective is to maximize the number of elements  $A$  holds. We do not use vertical bars to avoid confusion with the notation of absolute values.

## 1.2 COGNITIVE RADIO

Cognitive Radio is a topic of great interest and will play a strong role in future wireless communication systems [21]. In this section, we motivate why it is required and explain the main elements of its technology, regulation, and standardization.

### 1.2.1 *Motivation for Cognitive Radio*

In wireless communications, radio spectrum is the most important resource. Throughout the world, this scarce resource is regulated by governmental authorities. This guarantees that essential services, like Television (TV) broadcasting in the Ultra High Frequency (UHF) band, can be provided and are protected from harmful interference.

In general, these assignments base on radio technologies available at the time of the decision-making and are issued on a long-term basis. In particular, the Federal Communications Commission (FCC) in the US or national authorities in Europe have allocated radio spectrum blocks for specific purposes and assigned licenses to specific users or companies. This strategy tended to a static exclusive use of spectrum in large geographic areas. It is, however, required for several applications like TV broadcasting or mobile communication networks. Today, the major part of the radio spectrum has already been assigned to various purposes and only little spectrum is available for new emerging wireless applications and services [7].

Several studies and reports, e.g., [28, 39, 101], show a considerable underutilization of the radio spectrum, especially in the UHF TV band. This underutilization originated from the switchover from analog to Digital Video Broadcasting – Terrestrial (DVB-T) TV transmissions, which are much more efficient in spectrum and reduce the occupied resources significantly. This frequency band is very attractive for wireless services since it has good signal propagation characteristics which reduce installation costs for operators.

These findings motivate the idea for a new type of devices called Cognitive Radio that should be able to identify free radio spectrum opportunities automatically and occupy them for communication. Indeed, this is only a fraction of the necessary requirements for such devices. For example, a network of Cognitive Radio devices needs to be self-organizing such that the licensee of a desired resource is protected from harmful interference.

The increasing demand for mobile services for radio spectrum [14], to provide higher quality and data rates, accelerates the research and development activities for Cognitive Radio technology. If successful, this could revolutionize the way spectrum is allocated to achieve a much higher spectrum efficiency. Further, this could shorten the

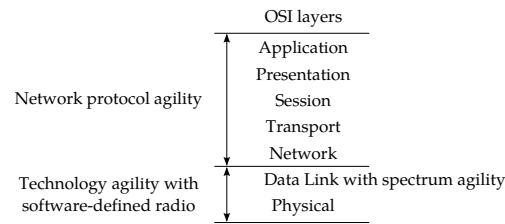


Figure 1.8: Agility in the ISO OSI model.

time to market for emerging wireless services and technologies due to lower regulation barriers.

### 1.2.2 What is a Cognitive Radio?

Cognitive Radio is a generic term for a radio that is aware of its environment and adapts its behavior according to the current situation. In order to achieve this, Cognitive Radios need to recognize their neighboring systems and must be able to adjust their transmission frequency, waveforms, and protocols to interact or coexist with them in an appropriate way. It follows that Cognitive Radios cover multiple domains of knowledge, model-based reasoning, and negotiation to maintain a radio spectrum etiquette during operation [41, 69].

An important difference of Cognitive Radios compared to traditional radios is their agility along the following items [7]:

- *Technology agility* covers the seamless operation of a device between multiple transmission technologies, e.g., WiFi or Long-term Evolution (LTE).
- *Protocol agility* refers to a dynamic reconfigurability of the communication protocol stack for interaction with discovered devices in the current environment.
- *Spectrum agility* covers strategies to exploit and occupy spectrum in an opportunistic way. This feature requires the design of efficient algorithms for coordination and cooperation, e.g., by negotiation of transmission parameters for coexisting Cognitive Radios.

In order to classify the agility schemes of Cognitive Radios in the International Organization for Standardization (ISO) Open Systems Interconnection (OSI) protocol model for communication systems, we depict an overview in Figure 1.8.

In recent years, re-programmable hardware became more and more powerful. This concept of software-defined radio aims to replace fixed implemented hardware functionalities, e.g., time-critical signal processing, by a flexible software approach. This technique enables the physical layer to become agile and offers a various number of new system parameters for configuration by the data link layer.

The network protocol stack implementations are less time-critical and mostly software-implemented in today's operating systems. Consequently, the first two agility schemes enable Cognitive Radio devices to quickly adapt to new transmission technologies and protocols. For an implementation, consider software libraries in which the matching objects are loaded for system operation according to the current requirements. Devices that are able to consider every possible operation parameter are termed full Cognitive Radios [47].

The last agility scheme mentioned is different to the others. It does not enable a specific technology or protocol but observes the parameters of the physical layer in order to configure the system efficiently to gain maximum performance in the context discovered. To determine the current radio spectrum occupation, the physical layer needs to provide a functionality that enables the data link layer to identify incumbents and spectrum opportunities for operation. This determination can be done either by spectrum sensing or querying a Geolocation Database (GLDB) with the current system position. The first approach analyzes the radio spectrum with a scanning device to identify spectrum opportunities and detect upcoming primary users, i.e., the incumbent of the spectrum resource or interference generated by other secondary user networks. The GLDB approach introduces a high administrative burden and requires a separate connection to request the spectrum occupancy data. In addition to the capability of analyzing the spectrum, the physical layer must be able to set specific operation parameters, e.g., transmission power, operation frequency, or modulation and coding schemes.

The data link layer has to evaluate the environment data provided by the physical layer, make a decision and set the parameters for system operation. This decision-making process contains the main logic and can become very complex in case of cooperation with other systems or challenging constraints during frequency allocation. Devices that consider the radio spectrum environment are named spectrum sensing Cognitive Radios [47].

Stepping back to the scenario of wireless communications, we need to find a coexistence etiquette for the users. This leads to the suggestion of a dynamic spectrum access scheme where two user roles are defined: primary and secondary users. A primary user is an incumbent and has higher priority granted by regulation while a secondary user is allowed to use unoccupied resources unless the primary user is not harmfully disturbed [3, 106].

Initially, secondary users search the radio spectrum for primary users. Frequency ranges between two primary users are called white spaces. After identifying those white spaces, secondary users or, more commonly White Space Devices (WSDs), allocate those ranges for communication as depicted in Figure 1.9. A requirement for WSD operation is to observe the occupied resources permanently for the

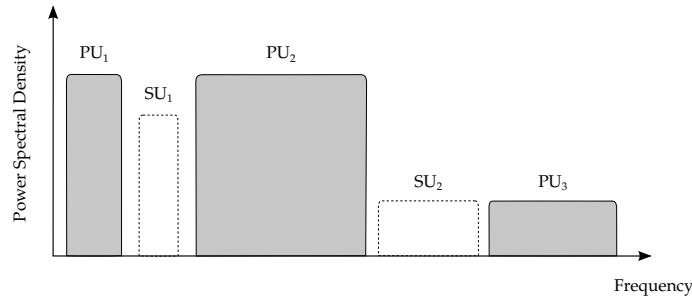


Figure 1.9: Secondary users (SUs) occupy white spaces between primary users (PUs) following the dynamic spectrum access scheme [21].

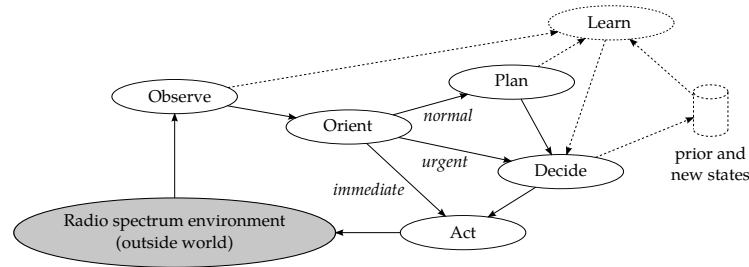


Figure 1.10: By observing the outside world, Mitola's Cognitive Cycle [69] evaluates the current situation to determine a reaction. For example, a normal threat allows to run complex schemes and select the best solution before an action is taken. Contrary, an immediate threat requires a fast determination of a reaction. All decision-makings can be used for learning purposes to guide the cycle in future situations.

occurrence of primary users. If primary users appear and occupy a frequency band that has been used by a WSD so far, the latter has to evacuate the resources immediately to avoid interference with the primary users operation. Thus, WSDs need capabilities to adapt very fast to new situations.

We summarize the process of WSD operation as originally envisioned by Mitola [69] in Figure 1.10. Following this cognitive cycle the devices process the observed environmental data, e.g., radio spectrum information, and analyzes the current situation to find a priority for further proceeding. In the case of normal operation, a possible complex algorithm with long runtime can be performed to find a new configuration. In the case of urgent or immediate situations, however, a fast determination of a reaction is required. Additionally, past situations, states, and decisions are stored in a database for learning purposes. Thereby, they can be considered during the regular operation phase. Throughout this thesis, we only consider the solid paths of the cycle and exclude learning. Our application scenario creates a very large parameter space and the probability to see a situation again is assumed to be sufficiently small. Thus, learning is unlikely to improve the decision process.



### 1.2.3 *New Spectrum Regulation Policies*

The success of Cognitive Radio is strongly related with a new spectrum management regime from regulation authorities. The process of spectrum management describes the organization of how and by whom the scarce resource radio spectrum is used. The objective is to maximize the benefit for the society by allocating resources as efficient as possible and minimizing interference among different users [13].

A worldwide high-level frequency allocation is performed by the International Telecommunication Union (ITU), which is a specialized agency of the United Nations. National authorities implement these resolutions in detail, e.g., by the definition of guard intervals or maximum allowed transmission power.

As we have seen, regulation authorities around the world manage radio spectrum in a very prescriptive way. They divide the spectrum into different frequency ranges and specify both, the delivered services and used technologies, on a long-term basis. Such a command-and-control approach is very charming for regulators, but not necessarily related to market demands or user requirements. It also has several disadvantages for incumbents and their service users, respectively.

On the one hand, the fixed approach defers the establishment of new communication services or technologies, thus, existing licenses cannot divert to new services or technologies. Although there have been license harmonizations in the past, e.g., in Europe [99, 100], the decision-making process for these harmonizations can take a long time and might not be capable of keeping up with new innovations. On the other hand, large portions of the radio spectrum are underutilized today although there is a high demand for them. This situation led to several proposals for new spectrum management regimes, i.e., the best dynamic spectrum access technique, to improve the overall efficiency [5, 21].

One possible technology and service-neutral regime is market driven. It uses exclusive resource assignments from a regulatory authority with fewer specifications. This can be seen as a just-in-time license that prevents primary and secondary users from interfering with each other. For example, by performing spectrum auctions for exclusive short-term assignments, market demands at specific locations can be better considered. Once a license is obtained, an incumbent operates, in contrast to the current regulation, any technology or service [21].

Another proposal is based on an unlicensed approach where users coexist, and everyone accepts a certain level of interference. The most successful example for such a regime used today is the 2.4 GHz Industrial, Scientific, and Medical (ISM) band. It is used for, e.g., WiFi communications by a large number of mobile devices. However, such

an approach has several consequences that were initially investigated in the field of economics. In *The Tragedy of the Commons* [38] proposed in 1968, Hardin concludes that the unregulated access of a finite, common resource by selfish individuals leads to inefficiencies due to an over-subscription of the resources. A solution, to overcome this dilemma, is to provide usage rates or other regulatory rules, e.g., primary users have to be protected against interference in any case. In the 2.4 GHz ISM band, this is achieved by regulation of the maximum allowed equivalent isotropically radiated power for each device.

Throughout this thesis, we selected a common spectrum regime with opportunistic resource sharing among users. In future radio spectrum regulation, this approach is very likely to happen as it provides large degrees of freedom for system operation.

#### 1.2.4 Applications

As suggested in Section 1.2.1, the targeted implementation of Cognitive Radio today is the use of white spaces by an opportunistic spectrum sharing approach in the UHF TV band. We find several applications that benefit from such a spectrum sharing approach and present the most interesting ones in the following.

Cognitive Radio networks can be used to provide wireless broadband access to rural areas in which the current communication infrastructure is not well developed. Typically, this is caused by high installation costs of laying wires in combination with low attainable revenues for service providers. Cognitive Radio networks are capable of bringing down those installation costs by using a wireless device at each home [7]. To achieve sufficient revenue, a large number of users has to be covered. Thus, such wireless networks need to operate with large cells, i.e., high transmission powers.

The Cognitive Radio technology can also be used in cellular networks to improve the spectrum efficiency and to cope with the rapid growth of the number of users and their demand for high data rates. To increase the capacity in a specific area, pico- and femtocells have been introduced, e.g., in LTE. These cells can be seen as minimized base stations transmitting at low power that form coverage islands inside an existing macrocell of the operator. By using the same spectrum resources, such a cell splitting provides more gain as the entire macrocell [19]. The configuration of each femtocell can be done dynamically by Cognitive Radio techniques depending on the current traffic and spectrum usage.

Another possibility to extend the capacity of a cellular network in case of overload situations is to allocate radio spectrum and offload traffic dynamically. This "data-boost" is a very interesting aspect for operators since it enables to transfer non-real-time data to white spaces to meet its quality-of-service requirement in the cellu-

Table 1.2: Network types and wireless IEEE standards [50, 98].

Distance	Coverage	Type	Wireless Std.	Frequency
1 m	Square meter	PAN	IEEE 802.15	2.4 GHz 54-862 MHz
10 m	Room	LAN	IEEE 802.11	2.4/5 GHz 54-862 MHz
100 m	Building			
1 km	Campus			
10 km	City	MAN	IEEE 802.16	>2 GHz
100 km	Country	RAN	IEEE 802.22	54-862 MHz
1000 km	Continent	WAN	-	-
10 000 km	Planet	Internet	-	-

lar network. It is assumed that this approach increases the existing capacity up to two to five times [7]. Furthermore, in the case of a common spectrum regulation regime, the radio spectrum to achieve this capacity increase comes at no additional cost for operators [7].

As we have seen, there is a lively interest in Cognitive Radio techniques to provide broadband access for rural areas and to increase the number of users and data rates in existing cellular networks. In the following, we review current Cognitive Radio standardization activities regarding Television White Space (TVWS) communication and identify coexistence threats in such networks.

#### 1.2.5 Standardization and Coexistence

The standardization activities for Cognitive Radios are an ongoing process that partially reached mature specifications. We briefly discuss the currently most relevant standards and identify aspects relevant for the application scenario of this thesis. A detailed survey on the current state of standardization can be found in [97].

Today, most of the Cognitive Radio standardization activity is performed by the Institute of Electrical and Electronics Engineers (IEEE). For instance, the IEEE 802 standard family describes different usage scenarios for a license-exempt spectrum access. In general, communication networks can be divided into several types that differ in their coverage range. We classify the most recent state-of-the-art wireless standards in Table 1.2. Moreover, we describe these different types, identify the major aims, and explain how coexistence among different systems is realized.

IEEE 802.15 covers Personal Area Networks (PANs) such as Bluetooth and ZigBee with a limited transmission range. IEEE 802.11 is a popular standard for Local Area Networks (LANs) to cover areas like buildings and campuses. IEEE 802.16 is also known as WiMAX for Metropolitan Area Networks (MANs) and intends to enable wireless broadband access within a city. IEEE 802.22 acts as a Regional Area Network (RAN) and aims to supply ranges of up to 100 km.

If we consider the desired operation frequencies in Table 1.2, we will find that most standard amendments strive to operate in the UHF TV band: IEEE 802.15.4m [51], 802.11af [49], and 802.22 [48]. This indicates that there is substantial interest in Cognitive Radio techniques not only in the research community but also from manufacturers to develop WSDs.

Besides standardization, every technical parameter or rule for radio spectrum access is subject to regulation by a governmental authority. Around the world, the FCC in the US is pioneering in defining these. Thus, in their first report [28], they introduce spectrum sensing and GLDB access as mandatory features for WSDs operation. In later reports [29, 30], this was relaxed to a mandatory spectrum sensing *or* GLDB access. The requirement for WSD networks that rely on spectrum sensing only is a reduced transmission power in comparison to networks that have GLDB access. The current regulation approach in Europe [22] is defined by the European Conference of Postal and Telecommunications Administration and bases on a GLDB approach.

The GLDB is a central entity operated by a regulation authority that administers the radio spectrum occupation for a specific area. Therefore, a Cognitive Radio device could omit sensing the spectrum and consult the GLDB to determine unoccupied radio spectrum at its position. For example, such a database could contain the locations of all TV transmitter stations and additional details like operated frequencies or transmission power.

Contrary to spectrum sensing, this GLDB approach enables detailed information about all transmitters in a specific area and prevents the risk of missed detections. A key element for successful operation is to model the signal propagation correctly to find the transmission ranges of registered users. This can be done with a proper path-loss model that accounts for the environment, e.g., gathered from a landscape map.

If compared with spectrum sensing, this approach has some drawbacks [21]. The database may be very static and does not offer the full potential of Cognitive Radios to exploit variations in spectrum occupancy over short time periods. Furthermore, an accurate propagation model is very challenging for urban or indoor environments and, depending on the desired resolution, computational intensive. It follows that highly dynamic and nomadic applications also have

to rely on spectrum sensing to detect sudden interference by other users.

In order to perform a radio spectrum analysis, spectrum sensing in the area of interest can either be done by the WSDs themselves or a scanner network in the background [41]. The usage of spectrum sensing enables the determination of currently available TVWSs and an ongoing observation of interference levels.

During spectrum sensing, the WSD network has to interrupt its transmission and identify the occupied resources. In the case, that an incumbent has appeared in the last transmission interval, all WSDs are required to move immediately to an alternate TVWS frequency. This sensing period decreases the time provided for data transmission. Thus, the scheduling of this period is a trade-off between desired sensing accuracy and achievable WSD throughput.

A further effect, which influences the overall sensing accuracy, is the signal attenuation of a wireless transmission. This mainly covers a distance dependent path loss and multipath fading from scattering, reflection, and diffraction effects related to objects and structures present in the environment. Attenuation results in strong variations of the received signal's power level, which especially appear in urban or indoor scenarios [7].

In order to determine the presence of a primary user, a scanner observes the signal for a defined time period and performs a hypothesis test. Due to the previously mentioned fading effects, a scanner might notice a deep fade and conclude the absence of a primary user or other WSDs. Hence, there is a probability of missed detections and false alarms as wrong outcomes of the decision-making process. A false alarm is equivalent to neglecting spectrum opportunities while missed detections lead to collisions with other users. It follows that WSDs aim at a low false-alarm probability to achieve a high throughput while primary users demand high protection with a low missed detection probability of WSDs. Although the regulation authorities are able to set the detection probabilities, there is a remaining risk for interference and both the incumbents and other WSDs may be affected by those missed detections.

Throughout this thesis, we apply energy detection as the spectrum sensing technique, which we further discuss in the application scenario. This method measures the energy in a certain frequency range to decide whether or not there is a primary user present by a given threshold. A problem of this method is to distinguish between noise, and a wanted signal when the Signal-to-Noise Ratio (SNR) is low which results in a high uncertainty about the presence of primary users and other WSDs. However, a feature detector, which analyzes the signals' cyclostationary behavior, improves the decision outcomes also for low-powered signals. The disadvantage of this method is that

it requires more complex algorithms and a significantly longer observation time compared to an energy detector [21].

Summarizing the above, we find that the introduction of Cognitive Radio is applicable to satisfy the increasing demand for spectrum resources by mobile communication services. This satisfaction is achieved by the identification of spectrum opportunities in an underutilized radio spectrum without interfering with an incumbent user. However, an entirely interference-free mode of operation cannot be guaranteed by WSDs for the following reasons. In a mostly deregulated spectrum, more users will be present and occupy unused spectrum resources for their communication activities. As mentioned before, the resource allocation among the users can either be done with the help of a GLDB or spectrum sensing. Both approaches have drawbacks that influence the reliability of the decisions that are made. These drawbacks are, e.g., the resolution of an underlying path-loss model to determine the allowed transmission power in a GLDB or the remaining risk of missed detections during spectrum sensing.

We can think of two possible interference scenarios. The first considers a RAN that covers a large geographical area and therefore requires a high transmission power. In such a case, it is possible that other systems operating in the same area with lower power are hidden and therefore experience interference.

A second scenario considers a data traffic offload from existing third-generation cellular systems (3G) or LTE networks. In general, this occurs in the case of high user density in urban or indoor environments (with strong multipath fading effects) during major events. Consequently, there exists an interference probability for incumbents but also among different WSDs in Cognitive Radio networks.

Besides the technical challenges for the coexistence of Cognitive Radio, there is also a political challenge. The regulators will only permit a dynamic spectrum access if Cognitive Radios prove that they occupy spectrum opportunities only and that they minimize interference with spectrum incumbents. This proof, however, depends on a successful implementation of Cognitive Radios and the establishment of a new radio spectrum regulation regime. Therefore, we face a chicken-egg problem [21] and the success of Cognitive Radio depends on the definition of spectrum access rules by regulation authorities.

We conclude that permanent spectrum sensing is required to continuously protect coexisting Cognitive Radios against sudden interference. Therefore, in the following we introduce spectrum sensing basics to achieve this.

### 1.3 SPECTRUM ANALYSIS

In this section, we describe the fundamentals of an important capability of Cognitive Radios: radio spectrum sensing to observe the

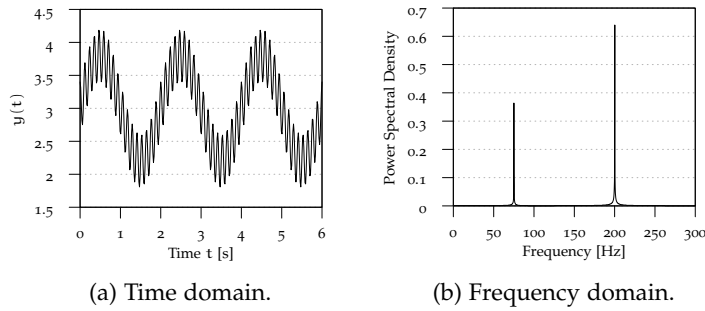


Figure 1.11: Transformation from time to frequency domain to identify a signal's spectrum components and their amplitudes.

Table 1.3: Comparison of Fourier analysis methods.

Time Domain		Frequency Domain	Method
continuous, periodic	○—●	discrete, aperiodic	FS
continuous, aperiodic	○—●	continuous, aperiodic	FT
discrete, periodic	○—●	discrete, periodic	DFT
discrete, aperiodic	○—●	continuous, periodic	DTFT

environment. This is an alternative to the GLDB to find spectrum opportunities and the only way to detect sudden interference threats caused by other systems.

Throughout this thesis, we focus on the energy detection method to determine the radio spectrum power level. This method bases on the theory published by Fourier in 1822 [31] and has fundamental importance in science and technology. We briefly describe the theory behind spectrum analysis and present an efficient approach to implementing it in a scanning device.

### 1.3.1 Overview

The Fourier analysis can be imagined as a signal transformation between time and frequency domain, e.g., to analyze a time signal's spectrum components as depicted in Figure 1.11. To achieve this, different transformation methods exist which differ depending on the input signal, which can be either continuous or discrete and periodic or aperiodic. In total, there are four time-frequency relations, and we depict them with the specific transformation method in Table 1.3.

For digital processing, as depicted in the receiver path of Figure 1.1, a discrete signal is required. It is generated by sampling the continuous signal with a specific rate by the Analog-to-Digital Converter

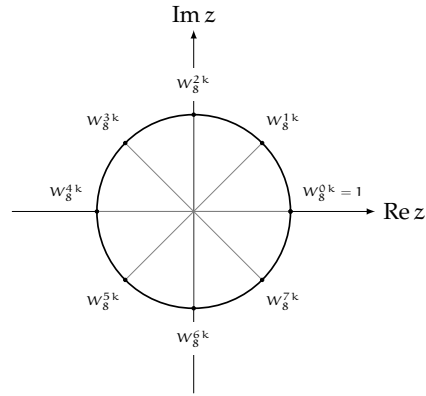


Figure 1.12: Frequency domain discretization with  $N = 8$  points.

(ADC). Following the Nyquist-Shannon sampling theorem [89], the sampling rate of the ADC must be at least two times higher than the maximum frequency of the original signal to determine them completely.

As we observe from Table 1.3, the Fourier Series (FS), Fourier Transform (FT) and Discrete Time Fourier Transform (DTFT) have continuous in- or outputs and are, therefore, not suitable for our purposes. However, the Discrete Fourier Transform (DFT) fits our needs as it contains both discrete input and output signals. It is based on the FS. In the following, we present both the FS and DFT as well as an efficient method to calculate the DFT, named Fast Fourier Transform (FFT).

### 1.3.2 Fourier Series

The common representation of a continuous input signal is the FS defined as a superposition of individual sine and cosine functions that precisely describe the signal. The complex form of such an individual function for angle  $\theta$  is given by Euler's formula:

$$e^{\pm j\theta} = \cos(\theta) \pm j\sin(\theta).$$

Note that  $j \in \mathbb{C}$  holds. For a continuous-time signal, the exponential FS is defined as [77]:

$$x(t) = \sum_{k=-\infty}^{+\infty} c_k e^{jk\omega_0 t}, \quad \text{with } c_k = \frac{1}{T_0} \int_{T_0} x(t) e^{-jk\omega_0 t} dt, \quad (1.13)$$

with  $T_0$  the fundamental period of the periodic signal  $x(t)$  and the angular frequency  $\omega_0 = \frac{2\pi}{T_0}$ .



For implementation reasons, only a limited set of functions is used for representation. This results for (1.13) in a truncated exponential FS given by:

$$x(t) = \sum_{k=-N}^N c_k e^{jk\omega_0 t},$$

where  $N$  is chosen such that the approximation error is below a defined threshold.

### 1.3.3 Discrete Fourier and Fast Fourier Transform

In the previous section, we introduced the fundamental FS concept to analyze the time and frequency domain of continuous signals. Now we consider the DFT (or discrete FS) that processes discrete signals for implementation on a computer. In order to achieve this, the signal is sampled and, therefore, we only can find an approximate solution in the time and the frequency domain, respectively.

In the time domain, the periodic signal  $x(t)$  is sampled every  $\Delta t$  to generate  $N$  values for further processing. In contrast to the FS, the DFT only uses a limited set of individual functions for the representation in the frequency domain, i.e., the overall granularity of the method is limited by this. With the shorthand symbol  $W_N = e^{-j2\pi/N}$  we divide the unitcircle of the frequency domain into  $N$  parts as depicted in Figure 1.12. These parts define the pool of available spectrum components and it directly follows that a higher value of  $N$  results in a higher resolution.

For each sample  $k \in N$ , the DFT generates a linear combination of available spectrum components:

$$X[k] = \sum_{n=0}^{N-1} x[n] W_N^{nk}, \text{ with } k = n \in [0, N-1].$$

Note that  $nk$  is an exponent of  $W_N$ . For a sample length  $N$  the runtime complexity to determine  $X[0], \dots, X[N]$  is in  $\mathcal{O}(n^2)$ , because we have to sum up  $N$  samples for each of the  $N$  spectrum components.

For a more efficient DFT computation, Cooley and Tukey [18] published 1965 the FFT algorithm. An important property of this method is that it requires  $N$  samples,  $N = 2^i, i \in \mathbb{N}$ . We determine the DFT for two and four points before we generalize the process to the radix-2 FFT.

Starting with a two-point DFT, i.e.,  $N = 2, k \in [0, N-1]$ , we obtain:

$$X[k] = \sum_{n=0}^1 x[n] W_2^{nk} = x[0] W_2^{0k} + x[1] W_2^{1k}. \quad (1.14)$$

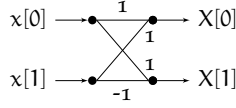


Figure 1.13: Signal-flow graph of a two-point DFT.

Because  $W_2^{0k} = e^{-j0} = 1$  and  $W_2^{1k} = e^{-j\pi k} = (-1)^k$ , we simplify (1.14) to:

$$\begin{aligned} X[0] &= x[0] + x[1] \\ X[1] &= x[0] - x[1]. \end{aligned}$$

More general, this becomes:

$$X[k] = x[0] + (-1)^k x[1] \text{ with } k \in [0, 1].$$

The signal-flow or butterfly diagram of a two-point DFT is depicted in Figure 1.13 and illustrates the computation process of the output coefficients. Next, we calculate the four-point DFT as:

$$X[k] = \sum_{n=0}^3 x[n]W_4^{nk} = x[0]W_4^{0k} + x[1]W_4^{1k} + x[2]W_4^{2k} + x[3]W_4^{3k}.$$

Using the periodicity of the weighting factors, we simplify this to:

$$\begin{aligned} W_N^{nk} &= e^{-j(2\pi/N)nk} \\ W_4^{0k} &= 1 \\ W_4^{1k} &= e^{-j(\pi/2)k} = (-j)^k \\ W_4^{2k} &= e^{-j\pi k} = (-1)^k \\ W_4^{3k} &= W_4^{2k}W_4^{1k} = (-1)^k W_4^{1k} \end{aligned}$$

and find that:

$$X[k] = (x[0] + x[2](-1)^k) + (x[1] + x[3](-1)^k)W_4^{1k}. \quad (1.15)$$

If we define the two variables for even and odd weighting factors,  $x_e[n] = x[2n]$  and  $x_o[n] = x[2n + 1]$  with  $n \in [0, 1]$ , respectively, (1.15) can be written as:

$$X[k] = (x_e[0] + x_e[1](-1)^k) + (x_o[0] + x_o[1](-1)^k)W_4^{1k}.$$

Note that the terms inside the round brackets are two-point DFTs:

$$\begin{aligned} X_e[m] &= x_e[0] + x_e[1](-1)^m \\ X_o[m] &= x_o[0] + x_o[1](-1)^m \text{ with } m \in [0, 1]. \end{aligned}$$

Again, we use the periodicity of  $X_e$  and  $X_o$  to simplify this expression:

$$\begin{aligned} X_e[2] &= x_e[0] + x_e[1](-1)^2 = X_e[0] \\ X_e[3] &= x_e[0] + x_e[1](-1)^3 = X_e[1]. \end{aligned}$$

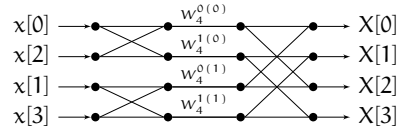


Figure 1.14: Signal-flow graph of a four-point DFT.

It follows that the four-point DFT can be summarized as:

$$\begin{aligned} X[0] &= X_e[0] + X_o[0]W_4^{1(0)} = X_e[0] + X_o[0] \\ X[1] &= X_e[1] + X_o[1]W_4^{1(1)} = X_e[1] + X_o[1]W_4^1 \\ X[2] &= X_e[0] + X_o[0]W_4^{1(2)} = X_e[0] - X_o[0] \\ X[3] &= X_e[1] + X_o[1]W_4^{1(3)} = X_e[1] - X_o[1]W_4^1 \end{aligned}$$

and the term  $W_4^{1(k)}$  changes to  $W_4^1$  for the chosen value of  $k$ .

We observe that a four-point DFT is computed by the generation of 2 two-point DFTs and the recomposition of them. The signal-flow that illustrates this is depicted in Figure 1.14. More general, we write:

$$\text{4-point DFT of } x[n] = [\text{2-point DFT of } x_e[n]] + [\text{2-point DFT of } x_o[n]].$$

The definition of higher order DFTs follow the same scheme [77]. As we observe from the butterfly diagrams, an initial division of even and odd sample indexes enables a recursive implementation because there are no interconnections between the preceding coefficients. The algorithm to determine this is called FFT. While the DFT calculation requires  $\mathcal{O}(n^2)$  operations, an implementation of the presented FFT scheme only requires  $\mathcal{O}(n \cdot \log(n))$  operations [77].

#### 1.3.4 Link Budget Considerations

The FFT previously described enables to determine the power level efficiently at a particular frequency. In the following, we use this to define the final constraint for the resource allocation. To find the relationship between signal, noise, and interference power levels, we depict the link budget calculation for a wireless device in Figure 1.15.

In general, the thermal noise  $P_N$  for electrons' movement in an electric circuit is defined by:

$$P_N = k_B BT,$$

where  $k_B$  denotes the Boltzmann constant,  $B$  the bandwidth in Hertz and  $T$  the environment temperature in Kelvin. This value is the minimum noise power level a receiver can achieve. In reality, there is a further noise figure added by the components of the receiver path. In the following, we term this level as interference-free.

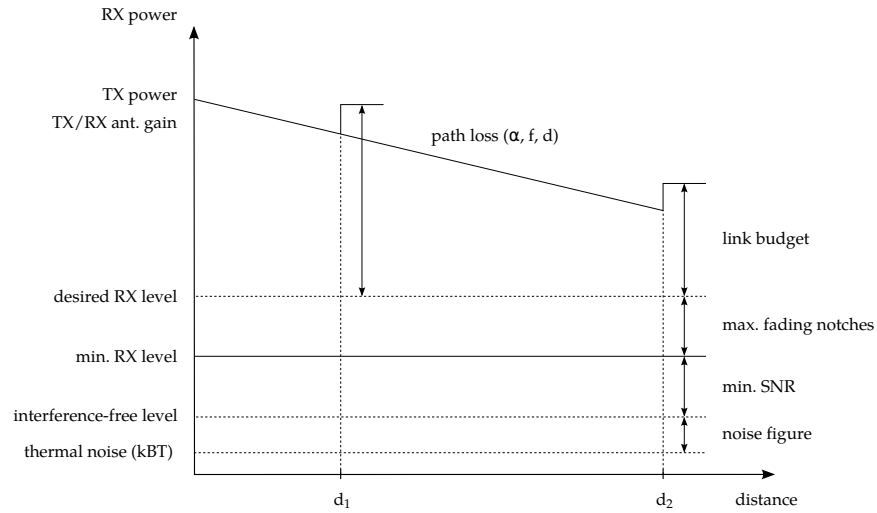


Figure 1.15: Link budget for a wireless device.

On the transmitter side, a signal is radiated by the antenna with a constant output power and then suffers path loss due to attenuation. The level of attenuation depends on the loss coefficient  $\alpha$ , the operation frequency  $f$ , and the distance  $d$  between the transmitter and receiver unit. We assume that the first two parameters are time-invariant. The received signal strength, however, highly depends on the distance to the transmitter since we assume the transmitter to be mobile. Furthermore, we consider the effect of antenna gains that increase the signal power level due to a particular radiation pattern.

In order to determine the received signal's quality, the SNR is used as a metric to describe the ratio between a desired signal and unwanted noise. Following the Hartley-Shannon theorem [40, 90], we find a lower SNR bound required for a given bandwidth and bit rate to transmit without errors in a noisy channel.

Another effect, we consider here, is the occurrence of fading notches. These are variations in the signal strength and caused by multipath propagation, e.g., by obstacles in the transmission path in the context of device mobility. An estimation of these sudden appearances of fading notches is not possible. Therefore, we use an additional margin to make the occurrence of this effect very unlikely. Taking this into account, we obtain the minimum and desired received signal strength levels that mark the lowest operation point.

To finally determine the available link budget, we sum up the interference-free noise level, the SNR, and the fading notch margin and subtract this from the desired signal power level at the receiver.

As we have discussed in Section 1.2, the available link budget might vary in the future due to the presence of interference from other WSDs that follow an opportunistic spectrum sharing approach. This additional interference can be considered as an unwanted increase of noise, also referred to as co-channel interference. In the worst case,

Table 1.4: Future coexisting systems in the UHF TV band.

Standard	Type
DVB-T/T2, DVB-H	TV broadcast
PMSE	professional audio
IEEE 802.15.4m	
IEEE 802.11af	mobile data access
IEEE 802.22	
3GPP LTE Femtocell	

the link budget melts down and the SNR, i.e., the quality of our received signal, decreases to a non-acceptable level.

We draw the following conclusions. To rate frequencies for future usage by our system, we have to consider their current noise and interference level as important quality indicator. This new coexistence situation is caused by changes in regulatory regimes and creates a new topic for spectrum management. It follows that this noise and interference level at a specific frequency is the final constraint we have to consider for resource allocation throughout this thesis.

#### 1.4 APPLICATION SCENARIO

The UHF TV band is very attractive for future Cognitive Radio applications due to its underutilization and favorable signal propagation characteristics. Today, this band is used by TV broadcasting services in coexistence with Programme Making and Special Event (PMSE) systems, i.e., professional wireless microphones or in-ear monitors, on a non-interfering basis. The current situation is very charming for such PMSE devices, because the static DVB-T transmissions do not change over time and therefore generate a very low probability of interference.

Due to the ongoing discussion and presence of several regulation authorities, we cannot anticipate the Cognitive Radio specifications in detail and how they will apply to specific areas. Some authorities might decide for a very restrictive regulation, and others might decide for a less restrictive way in the radio spectrum regulation. Further, we cannot estimate the type of Cognitive Radios available. In the worst case, all systems depicted in Table 1.4 are requested to coexist. It follows that an increase of users in the radio spectrum will also increase the probability for interference among them if protection mechanism fails.

Such a situation has several implications for future operation of PMSE systems. In general, these systems face outstanding requirements regarding the SNR to achieve a very high audio quality at all times [27]. In comparison to other voice services based on data communications networks, they do not tolerate any audible loss and demand for a very low delay for psychoacoustic reasons. Further, PMSE systems in the UHF TV band are characterized by a narrow operation bandwidth and a low transmission power that may increase the probability for missed detections during spectrum sensing performed by other systems.

To achieve a long operation time of mobile PMSE devices, their energy consumption must be kept at a low level, which implies that the PA is driven in a nonlinear mode. Due to the used frequency modulation scheme, the distortion level of transmitted signals is manageable, and system operation becomes very efficient [94]. As a consequence of this PA operation mode, they have to face the constraints  $d_c$  and  $d_3$  during the frequency resource allocation as described in Section 1.1.

To further guarantee a high audio quality with superior user experience, an efficient way, to protect PMSE systems from interference, is required. Either, these systems rely on the underlying GLDB path-loss models and spectrum sensing performance of WSDs or become spectrum agile and initiate actions to protect themselves from interference.

In this work, we focus on the second aspect by using a network of scanning devices performing energy detection as sensing method. We rely on this method because it enables a fast evaluation of present energy in the radio spectrum. In contrast, having detailed knowledge from a feature detector does not prevent the occurrence of missed detections and adds more complexity to the devices. A further method, to achieve cooperation between Cognitive Radio devices, is the introduction of a common control channel. However, this puts the responsibility back to regulation authorities and requires again static spectrum assignments. Having a mostly deregulated radio spectrum and the drawbacks of a GLDB and spectrum sensing in mind, we conclude for our application scenario the following: the most practicable way to protect future PMSE systems is the usage of a spatially large spectrum scanning network.

Throughout this thesis, we take future challenges of PMSE systems as an example to derive general methods to allocate frequencies efficiently in any radio spectrum situation considering the complex constraints of adjacent-channel and IM interference. Furthermore, we present a framework to detect and react to changes in the radio spectrum caused by coexisting users following the Cognitive Radio paradigm.

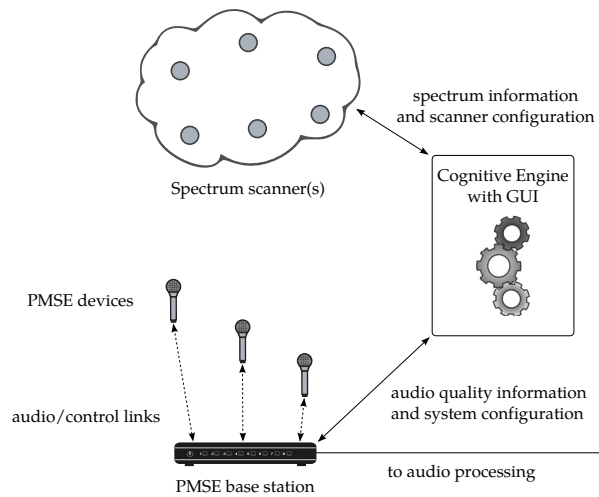


Figure 1.16: General system setup.

## 1.5 SYSTEM SETUP

The general system setup, we use throughout this thesis, is depicted in Figure 1.16. We make use of a scanning network, which permanently observes the radio spectrum in the operational area and reports detected power levels over a wired connection to a Cognitive Engine (CEN). Note that the scanning network may also consist of a single scanning node, e.g., for the mobile operation case.

The PMSE base station acts as a Radio Link Manager (RLM) and is capable of remotely control the devices and to determine the audio quality of each link. The CEN transmits the system configuration to the base station and requests the audio Link Quality Indicator (LQI) of each device for evaluation. The communication between them is also done over a wired connection, too.

Finally, a Graphical User Interface (GUI) is available for user interaction with the CEN. However, we do not cover implementation details of an RLM with LQI determination [11], primary user detection schemes, or GUI and consider these as given by external vendors. Further, we assume that the wireless channel to remotely control the mobile devices achieves a sufficient small bit error rate and all commands are timely processed by the mobile devices. In this work, we focus on decision-making in the CEN. We consider the challenges for frequency allocation of PMSE systems and develop strategies to achieve efficient solutions.

## 1.6 ORGANIZATION OF THE THESIS

In this work, we focus on efficient methodologies for decision-making in a CEN. From our presented application scenario and system setup, we derive the following research topics:

- What are efficient methods to solve the described frequency allocation problem considering the unexpected appearance of other users in the radio spectrum?
- What are the limitations in a static and especially dynamic radio spectrum case?
- What is the minimum number of scanning devices to fully sense the spectrum? What is the UHF TV band occupation during a large fair event nowadays?
- How can we interpret the reported spectrum data to identify the best alternate frequencies during operation?
- How can we setup a CEN to achieve the desired behavior?

The remainder of this thesis is organized as follows. Chapter 2 discusses related work in the context of frequency assignment in general and PMSE in particular. Further, we consider measurement studies on available spectrum occupancy and identify open issues. Based on this, we analyze available CEN architectures and rules for the fusion of spectrum data.

In Chapter 3, we formulate the problem statement of this thesis.

The complexity class of our problem is determined in Chapter 4. Based on this, we identify suitable methods to solve it efficiently.

In Chapter 5 we present the state-of-the-art approach for PMSE frequency allocation. Further, we introduce two constructive allocation approaches and evaluate them with the state-of-the-art in different interference scenarios.

An alternative methodology is presented in Chapter 6, that initially introduces a data representation of the underlying allocation problem. Using this representation, we develop a local-search methodology and evaluate it in a radio spectrum scenario with sudden interference. The main difference between the approaches presented in the chapter before is that we maintain a given number of links but minimize the experienced interference.

In Chapter 7, we leave the field of frequency planning and investigate spectrum occupancy in the UHF TV band by indoor measurements with a large spectrum scanning network. Further, we derive suggestions for a correct dimensioning of such a grid to detect interferer at an early stage.

Chapter 8 combines the previous findings. We introduce an architecture of a CEN and present a location-based rating scheme to determine the quality of alternative frequencies with the help of a scanning network.

Finally, Chapter 9 sums up this thesis and presents open issues for future work.



RELATED WORK

---

In this chapter, we briefly discuss related work. We divide it into three individual parts, namely frequency allocation, spectrum measurements, and spectrum data fusion in a CEN.

The central part of our work is related to the field of Frequency Assignment Problems (FAPs), and several surveys of them exist, e.g., [2, 24, 37, 60, 71]. One of the challenges therein is known as *fixed spectrum problem*. Here, the operational bandwidth is fixed, and a number of links have to be distributed such that the overall interference level of the frequency allocation is minimized or eliminated [71, 91, 93].

In general, FAPs have to consider co-channel, adjacent-channel, and IM adjacent-channel interference during the assignment process. In the literature, the IM constraint is mostly ignored due to its computational complexity or its negligibility in the application scenario, e.g., [35, 46, 70, 92].

Nevertheless, there are also works that account for IMPs, e.g., the authors in [23, 66] focus on determining exact solutions for small operational bandwidths. As we see in the following, this is infeasible for typical PMSE system bandwidths, because our selected granularity divides the frequency range of 72 MHz into 2880 possible slots. An initial estimation about the number of possible combinations can be done by the binomial coefficient with  $n$  the candidate space and  $k$  the number of allocated devices. Hence, this results in a non-handleable number of allocations due to the combinatorial explosion.

A closely related work to ours is [93]. It considers the constraints mentioned and aims to minimize a cost function for a cellular frequency assignment. The concluding recommendation of the authors, to achieve solutions in feasible times, is to neglect IMPs. Our application scenario, however, requires to consider them to achieve a high audio quality.

To solve FAPs in general, several strategies were proposed. These include, e.g., Artificial Neural Networks, Genetic Algorithms (GAs), Hill Climbing, Simulated Annealing (SA), or Taboo Search (TS) [44, 45, 91, 93]. However, due to different underlying problems and optimization objectives, there is no general statement about the method to use possible. Thus, a careful analysis of the underlying problem is required to identify a suitable solution strategy.

Another very closely related work in the field of frequency planning, especially for PMSE systems, uses a stochastic approach to sequentially generate an IM-free allocation [20]. During runtime, it randomly determines a candidate frequency and accepts it for operation

if all interference constraints were met. Given a certain bandwidth, it follows that the maximum number of links that can be allocated is also random and depends on the sequence of accepted slots. However, as we present in the remainder of this thesis, our developed approaches are capable of outperforming this stochastic approach.

As described before, a permanent radio spectrum observation is the only way for PMSE systems to determine the current interference situation. Therefore, the second part of our work covers the real-world performance of a spectrum scanning grid to protect the PMSE systems. It follows that a better understanding of the current spectrum usage can help them to evaluate and develop efficient coexistence scenarios.

The characterization of spectrum usage through measurements has become an intensively studied subject in recent years. However, measurement campaigns carried out mainly focused on characterizing country-specific and long-term spectrum usage. Those measurements were done using a single spectrum analyzer mostly located in an outdoor environment. Comparatively, there is only little knowledge about how spectrum usage varies within large indoor areas, for example within a large fairground or theater which is of great interest for PMSE systems.

A common finding in the related literature is that spectrum resources are currently underutilized. In general, several studies have shown that spectrum utilization significantly varies in different frequency bands for a given geographic location and at a given time. However, the different studies cannot be easily compared, since investigations were done in different countries. For example, findings from the US [67, 87], Europe [43, 65, 75, 103], Asia [52], or Latin America [78], vary by the different spectrum regulation in these countries.

Measurement studies performed so far mainly focused on either characterizing long-term spectrum usage over a large frequency range [75] or to a smaller extent, for specific wireless systems. For example, the authors in [43] investigate the particular occupation of Global System for Mobile Communications (GSM), 3G, and 2.4 GHz WiFi. Most of the measurement campaigns were carried out in an outdoor environment relying on a single spectrum analyzer. The authors in [104] perform a large-scale measurement study of the UHF TV band in a densely populated environment for both indoor and outdoor scenarios. They conclude that WSDs find more spectrum resources indoors which is caused by the blocking effects of building walls and utilize these resources. However, only little work has been presented that regard spectrum measurements carried out with a spectrum analyzer network capable of scheduling and combining scanning jobs [53].

To fill this gap with respect to the requirements of PMSE systems, we conduct an extensive spectrum measurement study in the UHF TV band at the fairground of the Messe Berlin during the International

Radio Exhibition (IFA; Internationale Funkausstellung). The IFA is the world's leading fair for consumer electronics expecting more than 200 000 visitors. Therefore, we consider the IFA a very interesting environment to investigate the indoor spectrum occupancy.

In the final part of our work, we aim to bring together all topics investigated before to run a CEN. Derived from the basic concepts envisioned in [41, 69], CEN architectures were described in, e.g., [63, 84, 86]. They are characterized by metering the radio environment parameters and setting the radio system parameters according to some predefined goal. In our approach, we rely on this general principle and adapt it to the specific requirements of PMSE systems. That is, we aim to achieve the highest possible audio link quality under strict delay constraints while considering the presence of IMPs.

To provide Cognitive Radios with a view of the radio spectrum environment beyond their sensing range, the concepts of an Available Resource Map [62] and, build upon, Radio Environment Map (REM) [107] have been introduced. These maps are knowledge databases collecting spectrum occupancy and related environment information and make a considerable contribution to a successful operation of Cognitive Radios.

REMs contribute to cognition by building knowledge via processing and combining multi-domain information from sensors, GLDBs, and regulatory authorities. Regarding the processing of spectrum measurements collected from sensors, they require an efficient spectrum data fusion rule in order to characterize the interference situation as exact as possible [32, 68, 79, 105]. In the literature, there exist three basic approaches for spectrum data fusion: a channel is considered busy if all (AND), at least one (OR), or the majority (N out of M) of the sensing nodes report an occupied spectrum [102]. It is well known that these strategies lead to inefficiencies caused by under- or overestimations of the current situation. On the one hand, if the AND or majority rule is performed, the probability of missed detections is large, which results in possible interference to the primary users. On the other hand, the OR rule can lead to a large number of false positives degrading secondary user performance by forcing them to needless reallocations.

In this work, we use the REM concept and combine it with a location-based approach to achieving a better spectrum data fusion. First, we present a CEN architecture that considers the specifics of PMSE systems and evaluate its performance regarding the response time that it requires to react in case a harmful interference is detected. Second, we propose a location-based data fusion approach that considers the distance between an operated PMSE system and interference signals and helps the CEN to rank spectrum resources and to determine alternate frequencies. Thus, if an interference situation requires a frequency reallocation of the system, it enables the CEN

to prioritize alternative frequency candidates for the reassignment process and to determine a solution that achieves the highest audio quality for the current situation.

We summarize the related work to this thesis as follows. FAPs are a well-investigated topic that, however, mostly ignore the presence of IM due its complexity. Next, measurement studies about radio spectrum occupation are mostly performed by a single scanning unit in an outdoor environment. This neglects several propagation effects, e.g., multipath propagation, that especially occurs in an indoor environment. Finally, the related work provides decision rules to combine spectrum data from a scanner network and to detect the presence of other users. These decision rules lead to under- or overestimations of the current situation.

## PROBLEM FORMULATION

---

In this chapter, we summarize our findings from Chapters 1 and 2 to formulate a problem statement of this thesis.

The worldwide discussion about regulatory changes to an opportunistic spectrum sharing approach with Cognitive Radio enables a more efficient spectrum usage. However, this creates new coexistence challenges for system operation in TVWSs. At the moment, it cannot be predicted which rules the regulatory amendments will finally specify. However, for a generic system that is supposed to work all over the world in every regulatory environment, it is worthwhile to assume the most deregulated radio spectrum scenario as the worst case.

The key to a successful operation in this new environment is the efficient allocation of available spectrum resources by a CEN. This process implements the cognitive cycle as depicted in Figure 1.10 and requires a software architecture to consider the specific constraints of our FAP.

Given the application scenario, our PMSE system consists of one base station and several mobile terminals with exclusive wireless links that face the problem of IM. Today, static configurations are used to set up such systems and require a specific radio spectrum pattern for operation. In the changed regulation regime, we cannot assume that these patterns still exist. Hence, as a first use case we require a universal approach to deal with any given radio spectrum environment. For this case, we can rely on a GLDB or spectrum scanning grid to determine the available TVWSs for operation. This implies that the current situation of the radio spectrum does not change over time, i.e., the audio quality is always at an acceptable level.

As a second use case we consider a dynamic reconfiguration during operation caused by a changing radio spectrum, i.e., a decreasing audio quality that requires fast reactions. This is much more challenging because the system is probably requested to operate with less resources than before but requires to determine an alternative solution within a very short period of time. For this use case, we cannot solely rely on a GLDB, but have to evaluate the data of a spectrum scanning grid to determine the best alternate frequencies without WSDs or other spurious emissions to maintain a high audio quality of our system.

Both use cases lead to the following problem statement that are focused in this thesis:

**Determination of efficient methods to dynamically allocate resources in a time-variant radio spectrum environment considering the constraint of intermodulation.**

Our aim is to configure a number of mobile devices efficiently while complying with constraints  $d_c$ ,  $d_3$ , and the co-channel interference that influences the achievable SNR, which highly impacts the audio quality. Throughout this thesis, we investigate both use cases which the second is an extension of the first one. In the first one, we allocate devices in a static spectrum environment whereas we aim to find IM-free allocations.

Then we evaluate the second use case with a time-variant spectrum environment to find not necessarily IM-free but optimized frequency allocations with minimized interference. To achieve this, we investigate the strength of a spectrum scanning grid and determine the achievable performance by indoor measurements during a large fair. We use the results from this measurement campaign to develop a location-based ranking approach which enables the system to rate the available resources and to determine the best alternative frequency in the case of necessary system reconfigurations.

## PROBLEM COMPLEXITY CLASSIFICATION

---

In this chapter, we identify the runtime complexity of our FAP by mapping it to an existing proven problem. Further, we perform an enumeration of the search space to identify characteristics of the solutions. Based on the knowledge gathered during this process, we develop promising strategies to solve our problem in feasible time.

### 4.1 COMPLEXITY CLASSES

In complexity theory, decision-making problems were analyzed to determine the runtime or memory consumption of algorithms that solve these problems. However, as introduced in Chapter 1, we face an optimization and not a decision-making problem in this work. But, we are able to transform an optimization into a decision-making problem by converting the objective from "Minimize  $f(x)$ " to "Is there a solution  $x$  such that  $f(x)$  is below a threshold?". This can be done because an algorithm that solves the optimization problem, is also capable to solve the decision-making problem by an additional comparison. It follows, that the implications for decision-making problems which we will describe in the following, can be extended to optimization problems as well [33].

Every decision-making problem for which we can obtain an algorithm with polynomial time complexity, belongs to complexity class P. It is well known that those problems can be efficiently solved on a deterministic Turing machine like today's computers. P is considered to be a subset of the class NP that contains all problems that can be solved by a non-deterministic Turing machine with polynomial time complexity [33].

According to the current state of knowledge, P is supposed to be a genuine subset of NP, i.e.,  $P \neq NP$  holds. However, the proof of

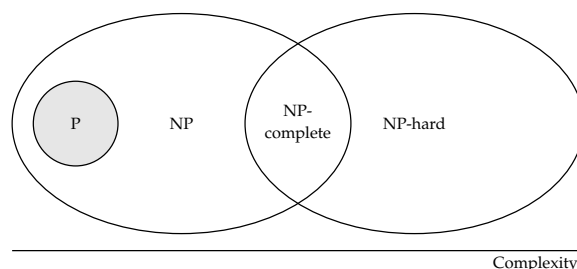


Figure 4.1: Relationship between the sets of problem attributes (assumption:  $P \neq NP$ ).

this assumption is a Millennium Problem of the Clay Mathematics Institute [15], and will have profound implications for several fields in science and technology.

Assuming that  $P \neq NP$  holds, there is a further subset in NP holding NP-complete problems [17] as depicted in Figure 4.1. Those kind of problems can be transformed into one another by a polynomial transformation, i.e., there exists an algorithm of polynomial time complexity that is capable of converting them into each other. The remaining problems that can be transformed into an NP-complete one but are not themselves in NP, are called NP-hard. Finding solutions for these kind of problems is very complex or impossible [33].

Problems, which belong to class P, can be efficiently solved on today's computers, i.e., the runtime of the algorithm can be polynomially approximated for a given input size. In contrast, the runtime of algorithms to exactly solve, e.g., NP-hard problems grows exponentially for a given input size on today's computers [33]. A general statement about the runtime complexity to solve problems that belong to NP or NP-complete is not possible as long as the proof  $P \neq NP$  is unsolved. However, most of these problems are not efficiently solvable on today's computers.

In the literature [33, 54], lists of proven NP-complete and NP-hard problems exist. These can be used as a reference to determine the complexity attributes of a studied problem, and to select a strategy to solve it. We identified the *facility dispersion problem* [25, 82] from the field of Operations Research as similar to our introduced FAP. This problem covers a location problem of  $n$  facilities in a network of  $N$  nodes. It tries to maximize the minimum (*max-min*) distance between the facilities. To analyze a solution, each pair of the selected facilities needs to be evaluated. This maps to our introduced FAP as follows. The fully meshed network is represented by the number of  $N$  available frequency slots. Each device frequency acts as a facility and has to maintain the minimum distance  $d_c$  to all others. As a constraint, each pair of device frequencies create IMPs that make other device frequencies unusable. This is different to the existing problem but will not affect the overall runtime complexity of our problem. In the work of [83], the authors show that the max-min facility dispersion problem belongs to the class of NP-hard problems.

Due to the fact that an NP-hard problem is intractable but we have no knowledge about the characteristics of the solutions at this time, we completely enumerate the search space for small bandwidths. To reduce the load, we verify different methods to reduce the search space by excluding as many invalid assignments as possible. The achieved IM-free solutions can be analyzed to identify specific characteristics and to develop an allocation strategy that adapts to these.



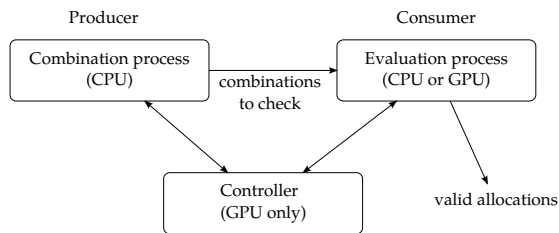


Figure 4.2: Software architecture with Producer-Consumer pattern to evaluate combinations using different processing units. A controller observes the states and interacts with both processes.

## 4.2 SEARCH SPACE EXPLORATION

In this section, we perform a search space exploration to determine the characteristics of our underlying assignment problem. We show that checking possible allocations on a Central Processing Unit (CPU) with sequential processing is not feasible and present an approach to finding solutions with massive parallelization on a Graphics Processing Unit (GPU).

### 4.2.1 Software Architecture

Our software architecture separates the generation from the evaluation of combinations. We choose the Producer-Consumer pattern as a variant of the Publisher-Subscriber design pattern as presented by the authors of [12] to provide the overall basis for our approach. As depicted in Figure 4.2, we choose a CPU as a producer to generate all combinations for a given range that meets constraint  $d_c$ . The consumer process in turn evaluates the combinations for the second constraint  $d_3$  and returns all valid allocations. In contrast to the producer process, the consumer can either be hosted on a CPU or a GPU. Note that, in case a GPU is used, an additional controller is required to take over the initial setup and the signaling between producer and consumer process. This signaling is used to, e.g., coordinate memory access between them.

Initially, we consider a consumer that operates on a CPU and sequentially processes a single combination  $C$  with  $n$  items. The pseudocode of an implementation for this is depicted in Algorithm 4.1. In general, the algorithm uses a bitarray to identify whether or not a slot is occupied by a device. To ensure an IM-free operation, we additionally mark the slots in a guard interval of  $d_3 - 1$  slots around each device frequency as occupied. Note that the size of the bitarray needs to be extended by two times the guard interval. This extension is required to ensure the correct distance evaluation in case an IMP resides in the guard interval of the first or the last element of the com-

---

**Algorithm 4.1** Pseudocode to validate a combination holding distance  $d_3$  on a CPU.

---

**Input:** Combination  $C$  and constraint  $d_3$

**Output:** Combination  $C$  is valid (boolean)

```

// Setup bitarray to find occupied and free slots: determine
// boundaries with guard interval gi
gi ← d3-1
min_slot ← min(C)-gi
max_slot ← max(C)+gi
bitarray.set_size(max_slot-min_slot) // Set up bitarray size
bitarray ← 0 // Mark all bits as free
// Mark each device slot and surrounding guard interval
// slots in bitarray as occupied
n ← size(C)-1
for i ← 0 to n do
    for d ← -gi to gi do
        | bitarray[gi + C[i]+d] ← 1 // Mark bit as occupied
        end
    end
end
// Validate locations of all IMPs and device slots
for i ← 0 to n do
    for j ← 0 to n, j ≠ i do
        | imp ← 2C[i]-C[j] // Calculate IMP
        | if imp > min_slot and imp < max_slot and bitarray[gi + imp]=1
        | then
        | | return false; // A device is interfered by imp
        | end
        end
    end
end
return true; // No device is interfered by any imp

```

---

combination, respectively. Further, this extension requires that we have use a single guard interval as offset value while accessing the bitarray.

After initialization, we calculate the location of each IMPs and evaluate the validity of the given combination with the help of the bitarray. In case one IMP collides with a device frequency, the algorithm immediately terminates and returns the combination is not a valid allocation to the producer. Contrary, in case no IMP collides with a device frequency, the combination becomes valid. We observe that the required two nested for-loops result in a runtime complexity of  $O(n^2)$ , and it follows that this approach quickly becomes very time-consuming and therefore is unfeasible for our purposes.

In an alternative approach, we use a GPU as a consumer and implement the evaluation procedure within the Compute Unified Device Architecture (CUDA) framework. This can be imagined as a matrix

calculation, whereas each field is simultaneously computed by a general calculation rule. The main difference to the previous approach is that the consumer now does not evaluate the single but a large number of combinations at a time. To achieve this, we distribute the combinations to be checked among  $n^2$  available GPU cores, launch related IMP calculations, and evaluate constraint  $d_3$ .

The final analysis performed by each CUDA thread depends linearly on the combination's length. That is, after the IMP calculation we have to check constraint  $d_3$  for each item of the corresponding combination to decide if it passes and becomes a valid allocation.

In comparison to our previously described sequential approach running on a CPU, the GPU as a consumer leads to an improvement considering the overall processing time. Here, the expensive runtime operation, to evaluate constraint  $d_3$ , can be performed in parallel that reduces the runtime complexity to  $\mathcal{O}(n)$ . Thus, the required enumeration time decreases significantly.

In the following, we make use of the GPU approach to exploring the search space of our considered FAP and verify different methods to reduce the number of combinations in the producer process. Furthermore, we determine a statistic of achievable IM-free allocations for a small bandwidth.

#### 4.2.2 Reduction Methods

We have no a priori knowledge about the specifics of the search space. Therefore, we concentrate on the producer process to generate all possible combinations for an unoccupied radio spectrum. To reduce the load of the consumer process, the combination algorithm for a complete enumeration should exclude as many invalid combinations as possible. In the following, we describe our identified reduction approaches and rate their performance.

##### *Brute force approach: considering all combinations*

A brute force approach without any knowledge about the properties and characteristics of the underlying problem generates all possible combinations and then evaluates the constraints  $d_c$  and  $d_3$ , respectively. However, this results in an unfeasible number of combinations, i.e.,  $\binom{n}{k}$  combinations for  $n$  the number of available slots and  $k$  the number of assigned links.

We adapt the constraint  $d_c$  that every element for a valid allocation needs to hold a specific distance  $d_c$  to adjacent links. That is; we can improve our producer process to select only those candidates that meet the required distances and remove all others. The outcome of this process is depicted in Table 4.1. We refer this approach as brute force that simultaneously acts as ground truth to evaluate the alternative methods.

Table 4.1: Possible combinations for 50 slots with  $d_c = 16$ 

Algorithm output		# of devices
(0,16,32,48)	first combination	4
(0,16,32,49)	second combination	4
...		
(0,16,34)		3
...		
(1,17,33,49)		4
...		
(49)	last combination	1

*Finding a combination's unique key to remove duplicates*

A reduction of the number of combinations can be done by removing combinations that have the same fingerprint. We name the sequence of distances between adjacent elements as the fingerprint of a (sorted) combination, e.g., combination (0, 25, 82, 157) has  $(25 - 0, 82 - 25, 157 - 82) = (25, 57, 75)$  as unique fingerprint.

We use this fingerprint as follows. A combination and a corresponding one with an inverted fingerprint have the same characteristics regarding the IM constraint and either both of them fulfill it or not. This property can be used because in case we invert the fingerprint and consider the resulting combination, the IMPs of them will be reallocated in such a way that the constraints  $d_c$  and  $d_3$  are met again.

This characteristic results from the linear operation during the calculation of IMPs and we come across with the same situation as in the non-inverted case. Therefore, if an allocation is valid, the corresponding allocation with an inverted fingerprint is also valid. It follows that we do not need to check the inverted combination explicitly, since we cannot gather any new information about the search space from it. Hence, this nearly halves the number of combinations.

During the generation of combinations, we observe that two combinations with the identical fingerprint, i.e., one combination with an inverted fingerprint of the other, do not occur directly in sequence. Therefore, we have to store each fingerprint and check for their presence before we put a combination to the consumer. Since the number of combinations is very large, this method requires a high memory capacity on the host system.

*Ignore already disturbed candidates by IMP pre-checking*

Another approach to reducing the number of combinations is to identify those distances of a selected candidate to IMPs that have already been created by previous items of the current result set.

Recall that during combination, we do not consider the positions of IMPs because a complete check, as presented for the CPU producer process before, is very time-consuming. However, we can exclude a large number of invalid allocations by considering the current result set and doing a simple pre-check regarding IMPs as follows. If we assume that all combinations include 0 as the first element,<sup>1</sup> we can double all elements of the current result set (except 0) to find the locations of  $(n - 1)$  IMPs quickly. Hence, with 0 present in the result set, we are able to check whether or not the current candidate meets the required distance  $d_3$ . For example, with  $d_c = 16$  and a current result set of  $(0, 16)$ , one IMP resides at  $2 \cdot 16 = 32$ . Therefore, the directly following candidate 32 will be rejected. Due to the constraint  $d_3 = 5$ , the next valid candidate is 37, i.e., all combinations between 32 and 37 can be ignored.

*Ignore combinations with the number of elements below a threshold*

Our aim is to allocate a specific number of devices in the available radio spectrum. Therefore, we can define a threshold for a minimum combination length to ignore those who are predictable below them. We denote the number of elements in a combination as the combination's length. For a combination to be feasible, its length has to be larger than the threshold from the number of devices. Thus, if this does not hold, further generation of combinations can be terminated.

This reduction approach can be realized by considering the combination process as follows. We assume that our algorithm moves from left to right in the available candidate space. Then, we examine the number of links in the current result set and the remaining candidate space to decide whether we can reach the requested number of devices. If the residual space is not sufficient to achieve the threshold, i.e., we cannot support the requested number of devices; we stop further processing. All following candidates beyond the current position will also stay below this threshold, and therefore, these combinations can be ignored. In such a case, we step back to a branch that achieves the threshold again and continue to generate combinations.

The key factor of this reduction technique is to know the threshold of achievable allocations for a specific operation range, i.e., trade-off between a high and low number. On the one hand, setting the threshold to a high value probably results in receiving no valid allocations because none of them passes the IMP check. On the other hand,

<sup>1</sup> We see in the following reduction approach that we can make this assumption without losing any valid allocations.

setting the threshold to a low value, results in a large number of combinations to be checked by the consumer process, which thwarts our desired feature.

#### *Ignore constantly shifted combinations*

The final reduction approach takes advantage of the following characteristic. The IMP for links  $a_1$  and  $a_2$  can be calculated as derived in (1.11). By adding a constant offset  $o$  to both of them, we obtain:

$$2(a_1 + o) - (a_2 + o) = \text{imp}_{1,2} + o. \quad (4.1)$$

From (4.1) we observe that an IMP is shifted the same way in the radio spectrum as the links generating them. It follows that we can neglect all combinations after the first number has changed, e.g., combination  $(0, 16, 32, 48)$  becomes the same as  $(1, 17, 33, 49)$  or  $(2, 18, 34, 50)$ , where each element is shifted by one slot to the right.

Since our objective is to maximize the number of links in an allocation, we do not lose any feasible combination by this approach. That is because the omitted results have the same or a smaller number of allocated links.

### 4.3 EVALUATION

Before we start our evaluation, we need to verify that the reduction techniques presented in Section 4.2.2 generate the same results as the brute force approach, i.e., there are no valid allocations removed by mistake. For each technique, we compare the gathered result sets with the one achieved by the brute force approach.

After verification of the different reduction methods, we start to evaluate them for a slot size of up to 160 slots. We depict our gathered results in Figure 4.3.

We observe that the number of combinations growth exponentially with the number of available slots. The reason for a linear grow at small slot numbers is due to parameter  $d_c$  that limits the outcome of the combination process to a certain level. Since PMSE systems usually do not face such small operation bandwidths, we neglect this effect here.

As expected, the brute force approach without any reduction technique generates the highest amount of combinations. The method, which removes duplicates by identifying the unique fingerprint, obtains the second highest number. The approach that does the IMP pre-check crosses the unique fingerprint reduction technique at a size of around 90 available slots. This indicates that the IM pre-check approach can reduce the slope. The lower slope has its origin in the number of allocated links. Hence, for a larger amount of allocated links a larger number of IMPs is generated. These IMPs make more

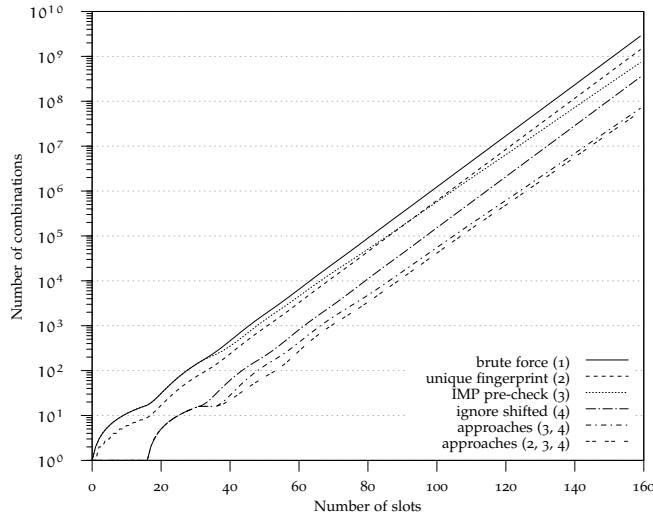


Figure 4.3: Outcome of different combination reduction techniques for a given slot size and  $d_c = 16$ . In general, the number of combinations grow for larger bandwidths exponentially.

candidates unusable and it follows that the number of combinations is reduced in such cases. The method to ignore shifted combinations results in the next highest reduction of them.

Next, we investigate two combinations of the reduction methods. The first is the IMP pre-check (3) joined with the ignore shifted approach (4) while the second additionally uses the unique fingerprint reduction method (2). Note that we have to exclude the minimum number of elements approach here because the number of links that can be allocated depends on the number of available slots.

As we observe in Figure 4.3, both graphs of the combined approaches are close to each other with (2,3,4) performing slightly better. However, due the unique fingerprint evaluation this approach consumes a large amount of memory whereas approach (3,4) achieves a comparable result with less memory consumption.

From these findings, we make the following conclusions. Each approach is capable of reducing the number of combinations to be checked. Applying all of them performs only slightly better than the IMP pre-check and ignore shifted technique but faces the drawback of a high memory consumption. Note that the IMP pre-check is the only approach capable of reducing the slope while all others are in parallel with the brute force graph.

Finally, we analyze the obtained results for a domain space of  $n=160$  slots. Note that in this case, we use the minimum length approach with a threshold of 8 links to terminate the process if the combination length is predictable below this number. We depict our gathered results in Table 4.2. As we observe for the brute force approach, there is a very large number of combinations available. By applying each of the reduction methods, this number can be reduced

Table 4.2: Evaluation of our reduction approaches for 160 slots (4 MHz) with  $d_c = 16$  and  $d_3 = 5$ .

Approach	# combinations	%
brute force (1)	2 818 276 950	100
unique fingerprint (2)	1 409 511 989	50
IMP pre-check (3)	727 534 616	25.8
min. length, $t_4 \geq 8$ (4)	1 431 442 738	50.8
ignore shifted (5)	346 206 190	12.3
approaches (2-5), $t_4 \geq 8$	26 517 820	0.95
approaches (3-5), $t_4 \geq 8$	29 067 361	1
unique allocations (8 links)	81 376	0.003

to  $\approx 1\%$  of the numbers generated by the brute force approach. Thus, with our approaches, we are able to exclude almost 99% invalid combinations from the consumer process.

If we consider the number of unique allocations with the maximum number of allocated links we will find that these combinations occur very rarely. For example, combinations with an element size of 8 that meet the constraints  $d_c$  as well as  $d_3$  represent only 0.003%, i.e., 30 ppm of all combinations. It follows that we face a very large search space with a very small number of valid solutions. Furthermore, there are not a unique but several global optima holding the same number of elements present.

We analyzed the obtained solutions by determining the distances between the allocated links and considering their occurrence frequency. Unfortunately, we observed an almost chaotic behavior of these distances and could not identify a specific pattern.

#### 4.4 DISCUSSION

From the obtained results, we can make the following observations. To explore the search space of our problem, a GPU is capable of calculating the IMPs more efficient than a CPU. Hence, the usage of a GPU enables us to perform a search space exploration for a comparatively small bandwidth and determine specifics of the solutions.

As depicted in Figure 4.3, the number of combinations grows exponentially although the reduction techniques presented are capable of reducing their number to  $\approx 1\%$  of the original value. This leads to the conclusion that our introduced reduction methods are not able to solve the problem deterministically in polynomial time. This, however, does not show that there exist no such a reduction method.



Hence, for typical operational bandwidths of PMSE systems a complete enumeration is not a viable way. For example, a bandwidth of 72 MHz results in a slot size of 2880 slots. To explore this space in a time as short as required during system operation is unfeasible. We conclude that the determination of exact solutions is not a suitable approach for larger bandwidths. Therefore, an alternative way, to find a feasible frequency allocation, is required. A possible option is to use heuristics to find near optimal solutions in a significantly reduced amount of computation time. However, in general there is no guarantee to find the (globally) optimal solution with such approaches.

In general, heuristics can be divided into *constructive* and *local search* methods [8]. The first method starts with an initially empty set and inserts links, e.g., using a greedy scheme until a solution is complete. Typically, such approaches are very fast but often return inferior results.

The second method starts from a given initial solution and tries to replace it by a better one that is located in the neighborhood of the current solution in the search space. It follows that a problem-specific algorithm, to create this new solution, is required. In comparison to the first method, such a heuristic is capable of increasing the quality of an existing solution but also requires more computation time.

In Chapter 5 we explain the state-of-the-art approach for frequency allocation of PMSE systems. Then, we develop constructive heuristics for frequency allocation and evaluate their performance for different interference scenarios in comparison to the state-of-the-art. Further, we identify their benefits and limitations.

An approach for frequency allocation that bases on a local search is investigated in Chapter 6. We initially derive a data representation for the underlying problem and determine a suitable metaheuristic to solve it then efficiently.



## STATE-OF-THE-ART AND CONSTRUCTIVE APPROACHES

---

In this chapter, we describe the currently applied frequency allocation procedure for PMSE systems. There exists an elegant way to assign a large number of devices to the radio spectrum. This assignment is done by replicating an allocation for a small number of devices and generate a new one holding a multiple number of devices. We present the details of this procedure and evaluate its strength for different interference scenarios.

Furthermore, we introduce two constructive allocation approaches that are capable to adapt to any given spectrum situation and evaluate them against the state-of-the-art. The results presented in this chapter have been partially published in [57].

### 5.1 REPLICATION ASSIGNMENT

This state-of-the-art strategy makes use of the characteristic that shifting device frequencies shifts the associated IMPs in the same way. The data sheets of PMSE manufacturers specify that at most 16 devices can be allocated to an 8 MHz TV channel such that the distances between their frequencies results in low quality. This allocation can be elegantly replicated choosing the TV channels of the replication such that the IMPs arise in common frequency ranges. Hence, this approach can be adapted to allocations with high-quality constraints. Here, we found that at most 11 devices can be allocated to an 8 MHz TV channel.

Figure 5.1 illustrates this strategy. Starting from an allocation with 16 devices in an 8 MHz TV channel, we duplicate and shift it to the next or subsequent IM-free channel in the spectrum. Doing this, we occupy 24 MHz or 32 MHz, respectively, and are able to allocate at most 32 devices. Thus, a system that spans 24 MHz holds the same number of devices as a system spanning 32 MHz. However, the 32 MHz system provides more flexibility to adapt to interference.

To further extend the number of devices, we use the compact allocation that spans 24 MHz. We duplicate it, and shift it to achieve an allocation that covers 72 MHz operational bandwidth and holds 64 devices in total. We observe that the occupied bandwidth is always three times larger than the bandwidth used by the system. This observation is explained by the IMP calculation, which indicate that the devices with the lowest and highest operation frequencies interact with each other. Note that all IMPs outside the operation range

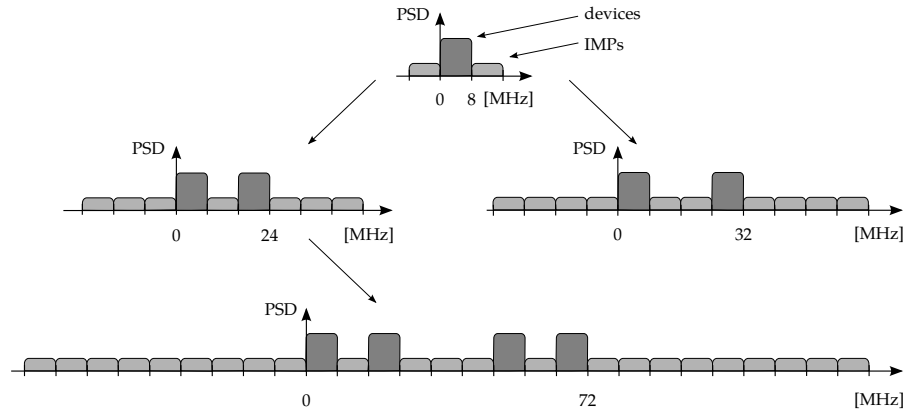


Figure 5.1: State-of-the-art frequency allocation strategy. A configuration for an 8 MHz TV channel is replicated to occupy 32 MHz or, more compact, 24 MHz. Furthermore, this can be replicated again to occupy 72 MHz.

Table 5.1: Allocations for different operational bandwidths.

B [MHz]	TV channels occupied	# of devices	
		LQ	HQ
8	{1}	16	11
24	{1, 3}	32	22
32	{1, 3} or {1, 4}	32	22
72	{1, 3, 7, 9} or {2, 4, 8}	64 or 48	44 or 33

can be filtered. However, we see in the following chapter that it is important to know their location.

We conclude that to achieve the allocation of a given number of devices, the replication-based allocation strategy requires a spectrum that is not occupied by other users in certain TV channels as given in Table 5.1.

Throughout this thesis, we use these values for the number of devices and the occupied bandwidths as reference that can be allocated to benchmark our introduced algorithms. In Chapter 1 we explained the need for new allocation strategies that can adapt to any given spectrum situation. As we see in the following section the number of PMSE devices, which can be allocated using the replication strategy, reduces considerably.

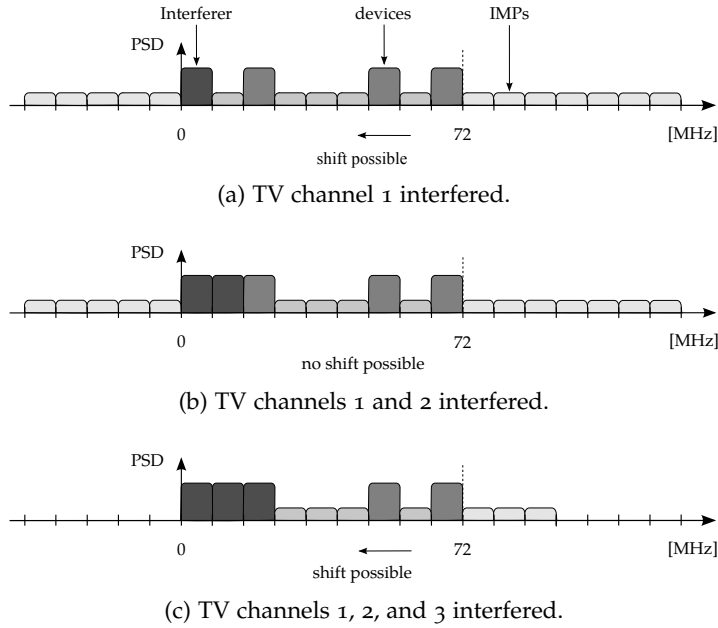


Figure 5.2: Considered interference scenarios for an operational bandwidth of 72 MHz with up to three TV channels that are unavailable for PMSE systems. Each additional interfered channel decreases the number of allocatable devices.

## 5.2 INTERFERENCE SCENARIOS

In Chapter 1, we introduced the Cognitive Radio paradigm with opportunistic spectrum sharing. As a result, PMSE systems have to cope with non-predictable interference situations caused by other users and need to overcome them in an efficient way. Hence, their aim is to maximize the number of devices in the available spectrum achieving a defined audio quality in feasible time.

We present three possible interference scenarios and discuss how the replication strategy performs on those. We concentrate on a scenario with 72 MHz operational bandwidth. From Table 5.1, we find with the replication strategy two possible configurations: i) TV channels (1,3,7,9) with 64 devices, and ii) TV channels (2,4,8) with 48 devices. Figure 5.2 depicts the three scenarios considered. Note that configuration ii) can be shifted by one TV channel to the right and a further configuration exists for TV channels (3,5,9) with 48 devices.

In scenario (a), we evaluate the case that only TV channel 1 experiences interference. Only configuration i) is affected by this such that it reduces the number of TV channels that can be used to three. Hence, the number of devices, which fits into the operation bandwidth decreases from 64 to 48 devices. Note that a blocked TV channel implies that we can alternatively shift the remaining allocation with TV channels (3,7,9) to the left, such that the new configuration with TV channels (2,6,8) arises.

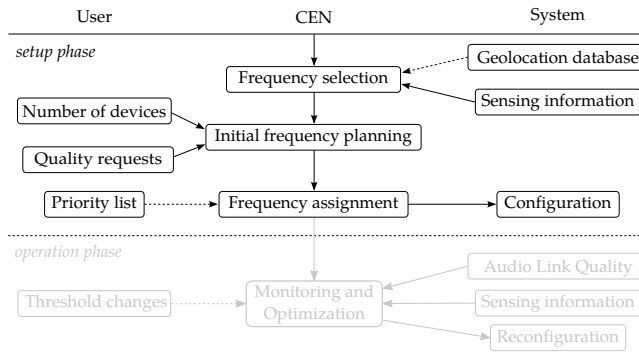


Figure 5.3: Interaction with user and other system components during the setup phase to collect relevant information for initial frequency planning.

In scenario (b), additionally TV channel 2 is interfered. Following the replication strategy, configuration i) still provides three TV channels holding up to 48 devices in total. Configuration ii), however, loses one of its channels and now can only allocate up to 32 devices. Note that those IM-free allocations cannot be shifted in the remaining available spectrum such that the arising new configuration provides more than 48 devices.

Finally, in scenario (c), the first three TV channels are interfered. As a result, both the configurations i) and ii) are affected and only contain two IM-free TV channels with up to 32 allocated devices.

The previously presented replication strategy is very elegant and quickly achieves the allocation for a system configuration. However, as we have seen for different interference scenarios, this strategy becomes inefficient since in the case of interference the numbers of devices that cannot be assigned increases.

In the following, we investigate two constructive frequency assignment approaches with respect to IM-free allocations and evaluate their performance against the replication strategy. We divide the workflow of our CEN into a setup and an operation phase as depicted in Figure 5.3. During setup, the CEN collects environment data and the requirements of the user to configure the system. During operation, the CEN monitors the audio quality of each link as well as the spectrum environment to detect threats and trigger necessary actions to reconfigure the system.

Initially, we focus on the setup phase, i.e., our system is required to adapt to any given spectrum environment with static interference. In later chapters, we further identify methods and approaches to cope with a radio spectrum scenario that dynamically changes during system operation. If the audio link quality suddenly degrades, our system is required to reconfigure immediately.

Table 5.2: Used parameters during frequency allocation.

Parameter	LQ	HQ
bandwidth B [MHz]	8, 24, 32, 72	
slot size s [kHz]	25	
device bandwidth $b_d$ [kHz]	200	
distance $d_c$ [kHz]	$\geq 400$	$\geq 600$
distance $d_3$ [kHz]	$\geq 125$	$\geq 200$
allowed power level $p_t$ [dBm]	$\leq -115$	

### 5.3 CONSTRUCTIVE APPROACHES

Before we present our constructive approaches, we introduce the environment and operation parameters used for evaluation [26]. They are summarized in Table 5.2 and enable a comparison between the different allocation methodologies. We selected the typical system operation bandwidths of today’s PMSE systems and defined the required distances  $d_c$  as well as  $d_3$  to achieve a low and high audio quality, respectively. Finally, we defined a threshold for the power level to identify interfered slots and exclude them from operating.

We start our evaluation in an interference-free situation. Our goal is to characterize the performance of both quality requirements in terms of how likely it is to find a feasible allocation containing a specific number of devices.

The pseudocode of our constructive approaches, namely random and first fit, is depicted in Algorithm 5.1. It starts with an initialization of the frequency candidate set. We only select candidates that comply with a guard interval towards our radio spectrum boundaries since we do not want to interfere with neighbors by placing a device directly onto the first or last possible slot. The set of candidates is generated from information about primary users that is, e.g., gathered from a GLDB and sensed power levels from the radio spectrum. All frequencies, that are not occupied by a primary user and whose power levels are below a certain threshold, are considered as possible candidates. After this initialization, we run either the random or first fit approach. Finally, the algorithm returns the generated allocation.

#### 5.3.1 *Random Fit*

When performing the random fit approach, a candidate slot is uniformly drawn and removed from the candidate set. If the constraints  $d_c$  and  $d_3$  are met for all already stored device frequencies, the can-

---

**Algorithm 5.1** Constructive frequency allocation approaches. The vectors contain sensor information with flag indicating the presence of a primary user and the power level at a specific frequency.

---

**Input:**  $B$ ,  $s$ ,  $b_d$ ,  $p_t$  (as defined in Table 5.2), `first_candidate`, `is_primary_user[]`, and `spectrum_power_level[]`

**Output:** frequency allocation  $A$  that meets the constraints  $d_c$  and  $d_3$

```

// find guard interval  $g_i$  to boundaries and set up
  candidates
 $g_i \leftarrow b_d / (2s)$ 
for  $i \leftarrow g_i$  to  $B/s - g_i$  do
  | if not is_primary_user[i] and spectrum_power_level[i]  $\leq p_t$  then
  | | candidates.append(i)
  | end
end
// start constructive allocation
switch approach do
  | case random fit
  | | while candidates  $\neq \emptyset$  do
  | | | // uniformly draw an index between 0 and (size-1)
  | | | | of the candidate set
  | | |  $i \leftarrow \text{uniform}(0, \text{size}(\text{candidates}) - 1)$ 
  | | | candidate  $\leftarrow \text{candidates}[i]$  // map index to a candidate
  | | | // by delete, indices right to  $i$  are shifted left
  | | | candidates.delete(i)
  | | | if accept(candidate) then
  | | | | // insert candidate to allocation
  | | | | A.append(candidate)
  | | | end
  | | end
  | case first fit
  | | candidate  $\leftarrow \text{candidates}[\text{first\_candidate}]$ 
  | | candidates.delete(first\_candidate)
  | | A.append(candidate)
  | | while candidates  $\neq \emptyset$  do
  | | | candidate  $\leftarrow \text{candidates}[0]$  // always select index 0
  | | | // by delete, indices right to  $i$  are shifted left
  | | | candidates.delete(0)
  | | | if accept(candidate) then
  | | | | // insert candidate to allocation
  | | | | A.append(candidate)
  | | | end
  | | end
  | end
endsw
return  $A$ 

```

---



didate is accepted and is added to the allocation. The algorithm terminates, if no more candidates are available.

Due to the serial and random drawing of candidate slots, this approach lets a high number of possible combinations unexplored. Therefore, it is important to perform a large number of experiments to achieve significant results for evaluation. This requirement holds especially in the case of large operation bandwidths since the search space, as described in Chapter 4, becomes very large.

We stop the algorithm after ten million experiments and plot the histograms in Figure 5.4. Note that each histogram faces a different scaling on the x-axis.

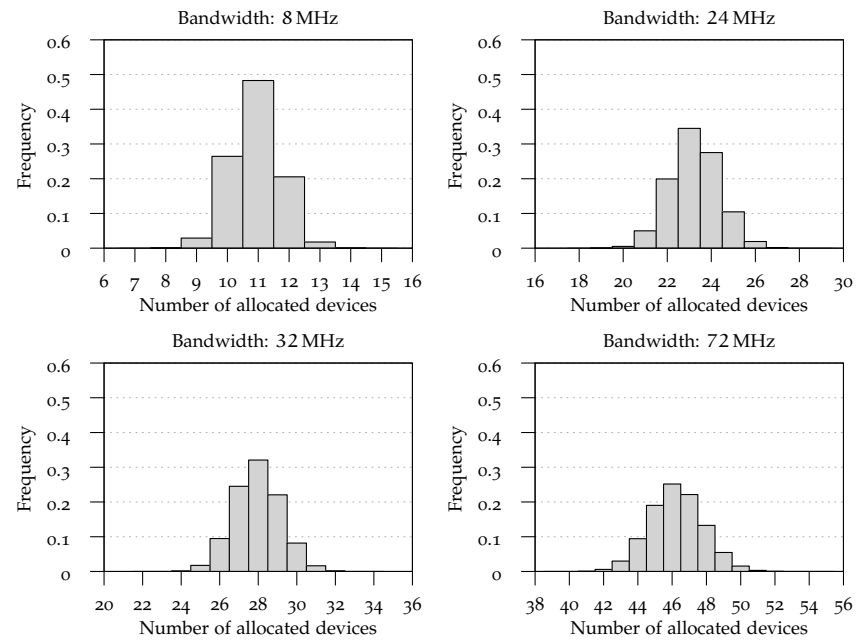
A general observation from all histograms is that the spectrum efficiency, i.e., the number of allocated devices divided by the operational bandwidth, decreases for larger bandwidths. This efficiency decrease is because the number of IMPs rapidly increases with the number of allocated devices, which implies that more frequencies cannot be used by further ones. Further, the probability distributions become flatter for larger system operation bandwidths. This indicates that it is less likely to find an allocation of a high number of devices.

For instance, for an interference-free 8MHz TV channel and low-quality requirements, we observe that in almost 50% of the trials the algorithm achieves to allocate 11 devices. The allocation of, for instance, 15 devices is also possible. However, the algorithm is less likely to find a feasible allocation. After ten million trials, the algorithm found only four possible allocations with 15 devices.

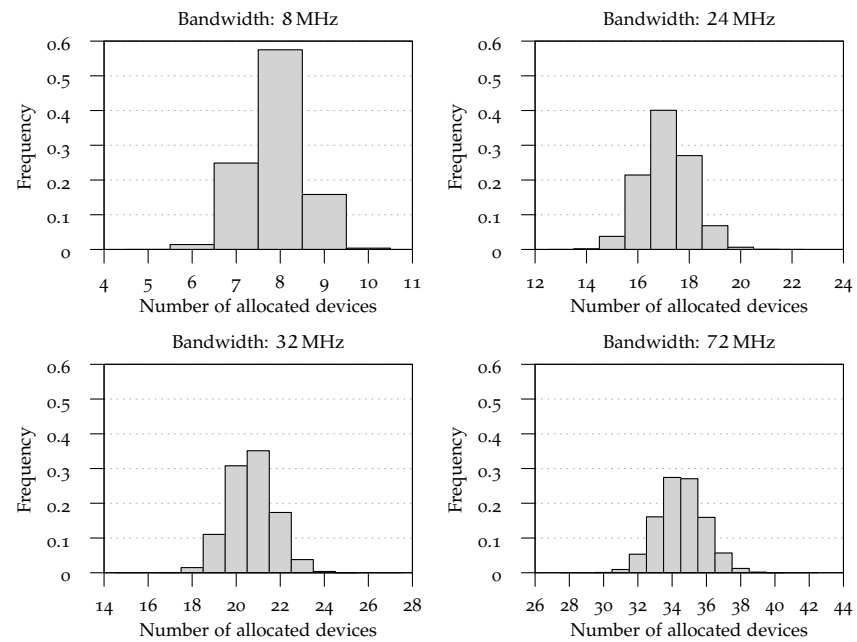
If we consider the results obtained for high-quality requirements, we find an identical relationship between the number of allocated devices and the available bandwidth. However, the overall number of allocated devices is smaller in this case because the distance constraints are more restrictive than for low-quality.

We summarize in Table 5.3 the minimum and the maximum number of devices we found for each experiment. It also presents the mean computation time<sup>1</sup> with confidence intervals required to find a single feasible allocation. As we observe, the confidence intervals are very small and indicate a stable allocation process. The achieved computation times for a specific bandwidth are for low-quality requirements at most 15% larger than those for achieving an allocation with high-quality requirements. The less required time is originated by, the more restricting distance constraints that reduce the necessary checks for a valid allocation. Further, the results show that our implementation works, e.g., for a bandwidth of 72 MHz in terms of [ms] on a common x86 single core CPU to achieve an individual allocation.

<sup>1</sup> The evaluation was done on an Intel T7500 CPU with 2.2GHz and 2GB RAM on a single core running Ubuntu 12.04.



(a) Low-quality requirements.



(b) High-quality requirements.

Figure 5.4: Histograms of the number of allocated devices (interference-free scenario) with the random fit approach for different bandwidths and quality requirements after ten million trials.

Table 5.3: Performance of the random fit approach (interference-free scenario) after 10 million trials each.

<b>B [MHz]</b>		<b>devices</b>	<b>mean time [<math>\mu</math>s]</b>	<b>(0.95 CI)</b>
8	LQ	7...15	158	( $\pm 0.02$ )
	HQ	5...10	137	( $\pm 0.04$ )
24	LQ	18...29	612	( $\pm 0.03$ )
	HQ	13...22	542	( $\pm 0.06$ )
32	LQ	22...34	872	( $\pm 0.04$ )
	HQ	15...27	784	( $\pm 0.1$ )
72	LQ	39...55	2549	( $\pm 0.2$ )
	HQ	28...42	2239	( $\pm 0.14$ )

### 5.3.2 First Fit

In this section, we introduce an alternative method to solve the allocation problem and name it Plain First Fit (PFF). This approach starts at the left boundary of the radio spectrum and moves to the right to select a candidate slot. Each candidate that satisfies the interference constraints  $d_c$  and  $d_3$  is inserted into the allocation. Thus, this behavior generates a deterministic solution for a specific candidate set, i.e.; we only need to perform a single experiment to achieve the solution.

An enhanced version of the PFF approach, we denote as Extended First Fit (EFF). With EFF, we set the first link to a predefined frequency and then apply the PFF to allocate the rest of the devices. This slight change in the allocation method highly improves the performance of the allocation process, because this first link changes the acceptance order of following candidates and the locations of their IMPs. Again, our achieved allocations are deterministic in this case.

By allocating a single link before the allocation starts, we have to perform in total a number of experiments that equals the number of available candidate slots. An increase of allocated links prior to the execution of PFF results in a large number of experiments, e.g., two pre-assigned links generate a quadratic number of experiments. Thus, the EFF approach converges to a brute-force approach that tries all possible combinations.

The pseudocode of the EFF approach is depicted in the second branch of Algorithm 5.1. Note that PFF can be derived from it by setting the first link to the lowest available slot index. As for random fit, we start with an identification of the candidate set of the radio spectrum. Following that, the predefined first link is inserted into the

Table 5.4: Performance of first fit approaches (interference-free scenario).

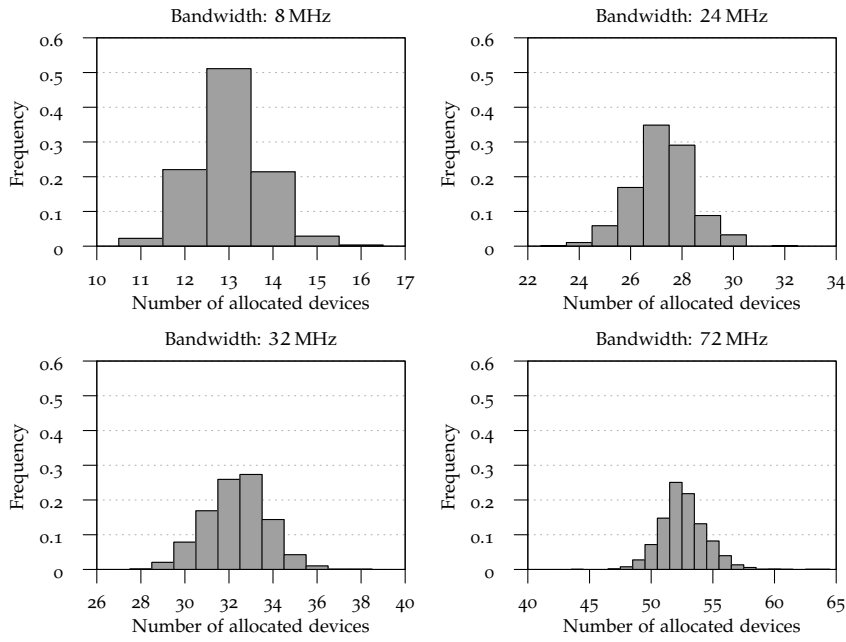
B [MHz]	Plain		Extended	
	LQ	HQ	LQ	HQ
8	13	10	11...16	8...11
24	27	23	23...32	16...24
32	33	27	28...38	21...32
72	52	45	43...64	32...50

allocation and therefore removed from the candidate set. As long as the candidate set is not empty, the candidate at the utmost left position is selected as the next candidate and inserted into the allocation if constraints  $d_c$  and  $d_3$  are met. After termination, the algorithm returns the generated allocation.

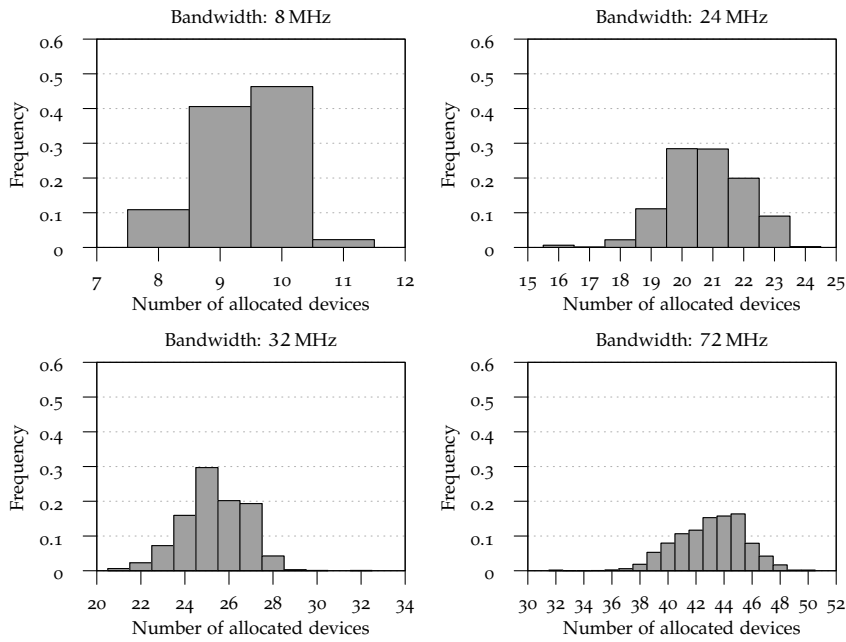
We now evaluate the performance of the presented first fit approaches in an interference-free scenario. To obtain their solutions, both approaches require a processing time comparable to that of the random fit approach. However, by their allocation strategy they ignore to investigate large parts of the search space.

As for the random fit, we evaluate the first fit approaches for different operation bandwidths and depict the results in Table 5.4. We observe that the EFF is capable of outperforming the PFF for all investigated bandwidths and quality requirements.

For further investigation, we depict the histograms for the EFF approach in Figure 5.5. Note again that each histogram faces a different scaling on the x-axis. We observe by comparing the link numbers achieving the highest probability in Figure 5.5 in most of the cases equals the link numbers of the allocation found by PFF in Table 5.4. This means in the long run that a random selection of the first link index achieves the same performance than starting from the utmost left position. The required computation time to perform all EFF experiments is low, e.g., for a bandwidth of 72 MHz with low-quality requirements the execution takes about 7 s on the used hardware. This short runtime enables us to perform all EFF experiments and thus, always obtain an allocation with the number of links at least equal to the result obtained by PFF. In the following, we concentrate on the performance of EFF and neglect an explicit evaluation of PFF, which is the degenerated case of EFF with the first link index set to the first candidate.



(a) Low-quality requirements.



(b) High-quality requirements.

Figure 5.5: Histograms of the number of allocated devices (interference-free scenario) with the EFF approach for different bandwidths and quality requirements.

Table 5.5: Comparison of allocated devices (bandwidth: 72 MHz).

Scenario	Replication		Random Fit		Ext. First Fit	
	LQ	HQ	LQ	HQ	LQ	HQ
interference-free	64	44	39...55	28...42	43...64	32...50
one channel (a)	48	33	36...51	26...39	43...64	32...46
two channels (b)	48	33	33...47	24...36	40...61	29...42
three channels (c)	32	22	29...43	21...33	32...48	27...38

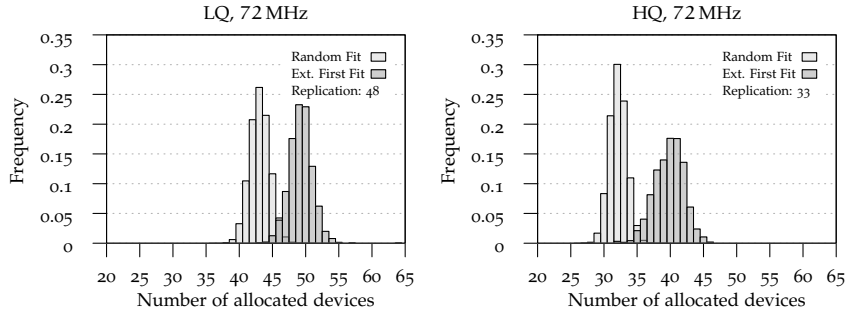
#### 5.4 DISCUSSION

Now we compare the performance of our frequency planning approaches with those obtained by the replication strategy. Again, we consider low- and high-quality requirements for different interference scenarios. The experiments with random fit are repeated 10 million times, while EFF is executed with one initially allocated link for each possible position of this link. Table 5.5 summarizes the results obtained for the interference-free scenario as well as for each of the three interference scenarios that have been depicted in Figure 5.2. The required time, to achieve an allocation, is in the same order of magnitude as in the previous runs and thus, omitted.

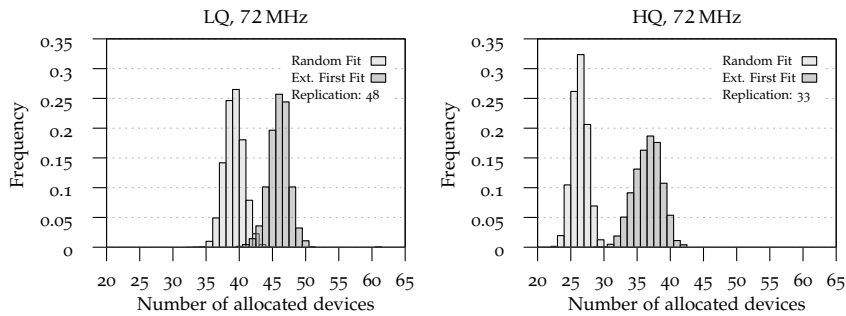
We begin with a comparison in the interference-free scenario. As we observe from Table 5.5, the results for the random fit approach are not as strong as the results obtained from the EFF or replication approach. That is, the maximum number of devices, which can be allocated, is higher with either the EFF or the replication approach. For example, for an operational bandwidth of 72 MHz with low-quality requirements both approaches can allocate 64 devices whereas the random fit approach allocates at most 55 devices with a low probability. Thus, for an interference-free scenario both the EFF and the replication provide better results than random fit, i.e., they allocate more devices in the radio spectrum.

In the following, we evaluate the performance of the three interference scenarios (a), (b), and (c), respectively, as defined in Section 5.1. The results for random fit and EFF are depicted in Figure 5.6.

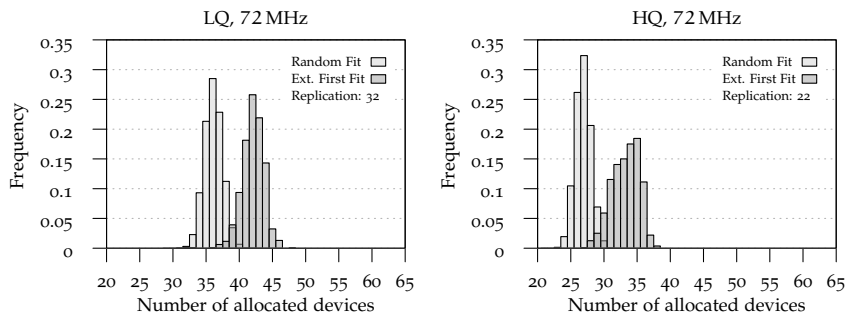
For the scenario with TV channel 1 interfered, the results are depicted in Figure 5.6a. We find that for low-quality requirements, the random fit approach most probably finds a smaller number of allocated devices than the replication offers and EFF outperforms them both. For high-quality requirements, however, there is a high probability to find a larger number of allocated devices by random fit and EFF. It follows that both our approaches outperform the replication



(a) Scenario with TV channel 1 interfered.



(b) Scenario with TV channels 1 and 2 interfered.



(c) Scenario with TV channels 1, 2, and 3 interfered.

Figure 5.6: Histograms of the number of allocated devices for different interference scenarios and an operational bandwidth of 72 MHz. In such situations, the EFF approach always outperforms the random fit and the replication approaches.

for the high-quality constraint with a high probability. Of these, EFF achieves a better performance. Note from Table 5.5 that the EFF is able to allocate to low-quality requirements the same number of devices as in the interference-free case. This results from the fact that the allocation in the interference-free case does not hold a link in the last TV channel. Thus, this allocation can be shifted by one channel to the right without reducing the number of allocated devices.

Regarding scenario (b) in Figure 5.6, we observe that this interference situation has the same impact on the replication approach as the scenario with only TV channel 1 interfered. This is caused by the replication characteristic where TV channel 2 is not used by PMSE links but only contains their IMPs. Thus, the replication approach still allocates 48 devices in the low-quality case and 33 in the high-quality case. However, for the approaches random fit and EFF the candidate set is, in fact, reduced when TV channels 1 and 2 experience interference.

We find from Figure 5.6b that in the low-quality case all allocations determined by random fit provide for 48 devices, i.e., random fit less efficiently allocates devices in the remaining spectrum than the replication strategy. In contrast, as we find in Table 5.5, the EFF is capable of finding a solution with almost 61 devices. Note that the occurrence of allocations with a large number of devices is very rare and therefore not visible in the histograms. In the high-quality case, however, it is possible for both approaches to find allocations with more than 33 devices and, thus, to outperform the replication strategy. When we compare the histograms for random fit and EFF, we observe that EFF more likely achieves better allocations.

Finally, we present the gathered results for a scenario with TV channels 1, 2, and 3 interfered. The corresponding histograms are depicted in Figure 5.6c. We observe that both the random fit and the EFF approach outperform the replication strategy for both quality requirements.

We conclude that the optimal frequency planning for PMSE devices strongly depends on the current interference situation. In some interference scenarios, the replication strategy performs the best, e.g., all TV channels except the required ones are interfered. In such cases, the EFF approach presented is not able to allocate 64 devices because the link locations generated with EFF are more distributed within the radio spectrum than the replication strategy. We find that EFF outperforms the random fit approach in all investigated interference scenarios regarding the number of allocated devices and required processing time. However, in future PMSE systems cannot rely on finding exactly one of the selected interference scenarios and must, therefore, be able to cope with changing spectrum environments. Having this in mind, our EFF approach outperforms the replication since it provides a general strategy that can adapt to any given spectrum situa-



tion. Nevertheless, we envision a hybrid frequency planning process that combines the strength of both the replication and EFF approach. With the help of classification techniques, a frequency planning entity like the CEN is able to identify interference scenarios and apply the best planning approach on those. We depict the best-obtained solutions by EFF in Appendix A.

Our approach also faces some drawbacks. We do not know in advance, how many devices will be utmost allocated in the radio spectrum. A way, to overcome this, is to decrease the quality of the achieved solutions. That is, increase the acceptance threshold  $p_t$  to find more candidates or reduce the distances  $d_c$  and  $d_3$  between the device frequencies. This quality decrease, however, will not give an optimal solution in every case. Consider, for instance, that our approach is able to assign more devices than requested, given certain values for  $d_c$ ,  $d_3$ , and  $p_t$ . Thus, the found allocation is not optimal, because we could increase the quality of the solution by the allocation of fewer devices with larger values for  $d_c$ ,  $d_3$ , or less for  $p_t$ .

Regarding a dynamic radio spectrum where links of our assignment can be disturbed and then require a new assigned frequency, our aim is to keep the number of link rearrangements as small as possible. This is, because every change of a frequency induces the degradation of a device's quality for a certain time. It follows that the random fit is a more suitable approach for reallocation because the EFF reassigns all devices that use a frequency larger than the frequency of the interferer.

During operation, our approach always needs some vacant spectrum. Otherwise, we would run out of candidates at some point of operation if we tried to keep a constant quality. A dynamic adaptation of the quality requirements  $d_c$ ,  $d_3$ , and  $p_t$ , however, becomes with the approaches presented very complex. This complexity occurs because a change of the quality parameters would only apply for a reallocated link. For the existing ones, this results in an ambiguity situation during evaluation which quality parameter holds for a considered link and the generated IMPs of the allocation.

We summarize our findings until now as follows. The introduced EFF approach is capable of adapting to any given radio spectrum situation. In most of those situations, it achieves a higher performance than the existing replication strategy. Further, we achieve frequency allocations in very fast response times for a static radio spectrum environment. However, the requirement, to assign a given number of devices and a timely dynamic radio spectrum environment, are the limitations of them. To address these, a more sophisticated mechanism that monitors the allocation process is needed. In the following chapter, we relax the strict compliance with quality constraints to achieve a higher degree of freedom during frequency planning.



In the previous chapter, we pointed out a constructive allocation method is capable of adapting to any given radio spectrum situation. However, it faces drawbacks regarding the number of allocated links and the occurrence of sudden interference. To overcome these limitations, we relax the strict quality requirements  $d_c$  and  $d_3$  in the following and present strategies to solve combinatorial problems in general.

To identify a suitable solution methodology for our FAP, we introduce a data structure that represents the characteristics of the FAP. By using this structure, we are able to adapt a general strategy to the problem specifics and evaluate its performance in a static and dynamic spectrum scenario, respectively. The results presented in this chapter have been partially published in [59].

### 6.1 STRATEGIES TO SOLVE COMBINATORIAL PROBLEMS

In the past 30 years, a new kind of algorithm has emerged that attempts to combine several basic heuristic methods into a higher level framework and to achieve solutions more efficiently. These algorithms were summarized under the term *metaheuristics* which was initially introduced in [34] in 1986. A concise definition is given in [95]: "A metaheuristic is a high-level problem-independent algorithmic framework that provides a set of guidelines or strategies to develop heuristic optimization algorithms."

Remember that all our selected strategies start with an initial solution and perform a local search by executing a specific function. When designing such a function, there are two conflicting parameters have to be accounted for: exploitation and exploration of the search space. If the focus is on exploitation, only little modifications to an existing solution are made. These little modifications lead to a slow convergence and an increased likelihood to remain in a local optimum. A stronger focus on exploration, however, might ignore the existing solution and attempts to find a new one by chance which enables to overcome local optima. Thus, the specific function is requested to balance these two parameters to achieve solutions in an efficient way.

Currently, there exist several metaheuristics in the field of combinatorial optimization. Here, we evaluate Genetic Algorithms (GAs), Simulated Annealing (SA), and Taboo Search (TS) here for their applicability to efficiently solve our introduced FAP.

GAs were introduced by the authors of [42] in 1975. These algorithms are population-based and inspired by natural evolution following the "survival of the fittest" principle.

A population consists of a number of individuals of which each holds a set of genomes that determines its fitness. During runtime, the algorithm performs genetic operations on the genomes of each individual to create a new generation of individuals with higher fitness.

The first action is to select individuals randomly as parents and recombine their genomes at a specific crossover point to create new individuals for the next generation. The idea is that parents with a high fitness will create new individuals that also achieve a high (or higher) fitness. As in nature, genes might be flipped by mutations. This unexpected behavior enables the algorithm to create individuals that are different from existing ones and, thus, can overcome local optima.

All operations named before are probabilistic, e.g., the selection operation might also pick individuals with lower fitness for the subsequent recombination and/or mutation process. The algorithm finally terminates if a given fitness threshold is reached or a predefined time has expired.

To map our FAP to the specifics of a GA, we assume that each individual represents a frequency allocation which induces in a specific fitness. The genomes are encoded by a bit stream containing zeros and ones to indicate whether or not they are occupied by a device. The total length of this stream depends on the operational bandwidth of the underlying system.

SA was introduced by the work of [55] in 1983 and bases on structure reordering in metal during a cool down process. The general principle is that a high temperature offers the atoms a large degree of freedom to reorder themselves within the structure. During annealing, this degree of freedom decreases. At a certain temperature, the metal becomes solid again with a reordered structure.

SA adapts this process by starting with an initial (unstructured) solution and a given system temperature. During annealing, the initial solution is modified by a neighbor function. The result is accepted as the new solution if its utility is higher than the one before. If the utility is smaller than the one before, it can still be accepted as the new solution with a certain system temperature dependent probability. The ability of accepting worse solutions enables a wide investigation of the search space and avoids to remain in local optima. The algorithm terminates if a given utility is reached or the system has cooled down to a predefined temperature. Hence, the cooling schedule determines the overall runtime of the algorithm.

The final metaheuristic, we describe here, is TS that was introduced in [34] in 1986. Starting from an initial solution, TS keeps track of

already performed optimization steps to guide the search into different directions, i.e., steps that have already been done are taboo in future to avoid the regeneration of solutions. During operation, the algorithm creates a number of neighbor solutions and selects their best as the new solution. However, the new best solution might be worse than the initial yet this enables the method to escape from local optima. The algorithm terminates if a given utility is reached or a predefined time has passed.

GAs come with a set of genetic operators. In contrast, for both SA and TS we need to define a specific neighbor function to generate a new solution from a given one. Within our problem, we can move a link in the radio spectrum either to the left or to the right and evaluate the outcome of this action. The challenge of this operation is to determine a suitable link, and both the direction and the offset of the shift operation.

In the following, we define data structures for a problem specific view on our FAP to identify a suitable metaheuristic to solve it efficiently.

## 6.2 PROBLEM REPRESENTATION

In this section, we introduce data structures to represent the FAP described in Chapter 1. Furthermore, we define operations to add and shift links, whereas the latter is of great interest during the optimization phase. In Appendix B, we present a detailed example of the data structures and operations to understand the shift of a link.

### 6.2.1 Problem Relaxation

As we have seen in Chapter 4, given an operation range there exists a maximum number of links that can be allocated IM-free. In case we operate this maximal number and experience sudden interference, we can either shut down the affected links or relax the problem constraints to further maintain the number of links. Note that in the latter case the allocation cannot be considered as IM-free anymore.

In the following, we concentrate on the problem relaxation of (1.12). Remind that this problem was defined as:

$$\begin{aligned}
 & \max \quad \#A \\
 & \text{s.t.} \\
 & \quad |a_i - a_j| \geq d_c \text{ for all } a_i, a_j \in A \text{ and } i \neq j \\
 & \quad \underbrace{|2a_i - a_j - a_k|}_{\text{imp}_{i,j}} \geq d_3 \text{ for all } a_i, a_j, a_k \in A \text{ and } i \neq j.
 \end{aligned}$$

That is; we want to maximize the number of links in  $A$  and meet the constraints  $d_c$  and  $d_3$  in any case. To start the relaxation, we assume a device allocation  $A$  with a given number of  $n$  links:

$$A = (a_1, \dots, a_n) \text{ for all } a_i \in \mathbb{N}_0,$$

where  $a_i$  represents the carrier frequency slot of link  $i$ .

To consider the strength of adjacent-channel interference, we determine the distance  $d_c$  for each link pair:

$$d_{c_{i,j}} = a_i - a_j \text{ for all } a_i, a_j \in A \text{ and } i \neq j.$$

As mentioned before, we additionally face the constraint of IM adjacent-channel interference. Remember that IM adjacent-channel interference is generated by IMPs and degrades the quality of the transmission. To consider its strength, we calculate  $d_{3_{i,j,k}}$  of a single IMP and link as:

$$d_{3_{i,j,k}} = \underbrace{2a_i - a_j - a_k}_{\text{imp}_{i,j}} \text{ for all } a_i, a_j, a_k \in A \text{ and } i \neq j.$$

For a given allocation  $A$ , the total number of distances, i.e.,  $d_c$  and  $d_3$  values that we have to take into account depends on the number of links in  $A$ .

Finally, we formulate an objective for our relaxed optimization problem. Each distance  $d_c$  and  $d_3$  that is generated by allocation  $A$  is evaluated by an individual utility function  $U_{d_c}$  and  $U_{d_3}$ , respectively. Our aim is to maximize the overall utility  $U$ , i.e., the sum of  $U_{d_c}$  and  $U_{d_3}$  to minimize adjacent and IM adjacent-channel interference:

$$\max_A U \text{ with } U = \left[ \sum_{d_{c_{i,j}}} U_{d_c}(d_{c_{i,j}}) + \sum_{d_{3_{i,j,k}}} U_{d_3}(d_{3_{i,j,k}}) \right].$$

The main difference of this objective to (1.12) is the relaxation of the binary constraint of IM-freeness by tolerating a certain amount of interference. In the following section, we present our data structures and used metrics for an efficient evaluation of those structures to achieve this goal.

### 6.2.2 Data Structures

Initially, we introduce two  $n \times n$  auxiliary matrices  $P$  and  $Q$ , with  $n$  the number of links. The first matrix is defined as a lower triangular matrix:

$$P_{n \times n} = \begin{pmatrix} p_{1,1} & & 0 \\ \vdots & \ddots & \\ p_{n,1} & \cdots & p_{n,n} \end{pmatrix}$$

The second one follows the regular matrix definition:

$$Q_{n \times n} = \begin{pmatrix} q_{1,1} & \cdots & q_{1,n} \\ \vdots & \ddots & \vdots \\ q_{n,1} & \cdots & q_{n,n} \end{pmatrix}$$

Since a link cannot perform intermodulation with itself, we set  $p_{i,i} = q_{i,i} = \infty$  for  $i = 1, \dots, n$ .

The first data structure is a matrix  $A$  of size  $1 \times n$  to store the frequency allocation of  $n$  links. We then compute the channel spacing between each possible pair of elements in  $A$ , i.e.,  $d_c$  and write them as matrix  $B$  of size  $n \times n$ . Note that for each link pair  $a_i$  and  $a_j$   $d_{c_{i,j}} = -d_{c_{j,i}}$  holds. Thus, we write matrix  $B$  as a matrix  $P$  to store all channel spacing values that are relevant for the computation of adjacent-channel interference. Each element  $b_{i,j}$  in  $B$  is given as:

$$b_{i,j} = d_{c_{i,j}} = a_i - a_j \text{ for } i, j = 1, \dots, n \text{ and } i > j. \quad (6.1)$$

For the computation of IM adjacent-channel interference we need to calculate the channel spacing between each element  $a_i$  in  $A$  and all occurred IMPs. The resulting matrix  $C$  of size  $n \times n$  is of type  $Q$ . The elements  $c_{i,j}$  are calculated according to (1.11), which becomes:

$$c_{i,j} = 2a_i - a_j \text{ for } i, j = 1, \dots, n \text{ and } i \neq j. \quad (6.2)$$

In the next step, we define a matrix  $D$  of size  $n \times n$  to store the distances  $d_3$  between each IMP and each link. Note that the matrix elements are not scalars but vectors of size  $n$ . This vector can be imagined as a further dimension for each element of the matrix. To find the subtraction of a IMP as scalar value with a vector, we define the auxiliary vector  $H$  that is a  $1 \times n$  matrix of ones. With this, each element of matrix  $D$ , i.e., the distances  $d_{3_{i,j}}$  for an element  $d_{i,j}$  of matrix  $D$  can be calculated for the  $n$  links as:

$$d_{i,j} = c_{i,j} \cdot H^T - A^T \text{ for } i, j = 1, \dots, n \text{ and } i \neq j. \quad (6.3)$$

Now that we have calculated the distances  $d_c$  and  $d_3$  for each link and IMP pair, we determine their utility. We define the utility function  $u_B(d_c)$  to evaluate the distance  $d_c$  of a link to its adjacent links as:

$$u_B(d_c) = \begin{cases} 3(d_c - 6), & \text{for } 0 \leq |d_c| < 4 \\ 2(d_c - 7), & \text{for } 4 \leq |d_c| < 8 \\ d_c - 6, & \text{for } 8 \leq |d_c| < 16 \\ 10, & \text{for } |d_c| \geq 16 \end{cases}$$

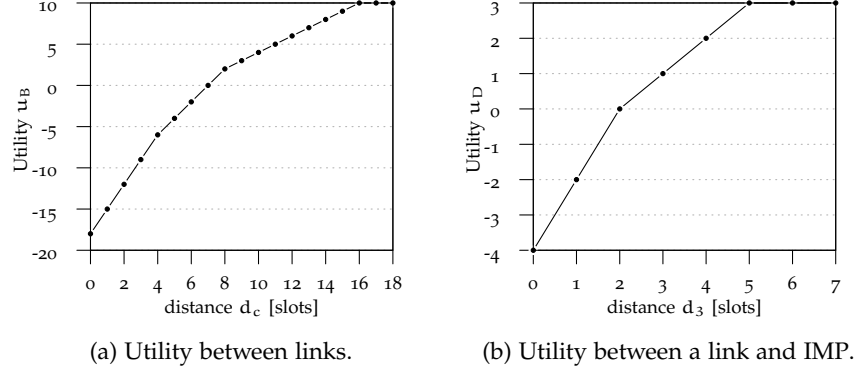


Figure 6.1: Used discrete utility functions.

For the evaluation of distance  $d_3$  between a link and an IMP, we define utility function  $u_D(d_3)$  as:

$$u_D(d_3) = \begin{cases} 2(d_3 - 2), & \text{for } 0 \leq |d_3| < 2 \\ d_3 - 2, & \text{for } 2 \leq |d_3| < 5 \\ 3, & \text{for } |d_3| \geq 5. \end{cases}$$

Figure 6.1 depicts both  $u_B$  and  $u_D$ . Note that both utility functions are discrete piecewise functions and penalize smaller distances stronger than larger ones. This corresponds to the fact that a smaller distance decreases the achievable audio quality more than a larger one. In case the distances are equal or greater than a certain threshold, the maximum utility is returned. It is worth mentioning here that these threshold values represent our targeted guard intervals to achieve an IM-free operation with low audio quality requirements. Naturally, these functions can be adapted to the operated hardware or the specific quality requirements of the user and do not limit the generality of our approach.

The utility functions are used to determine candidate links to be shifted to another frequency slot so that by improving their associated  $d_c$  and  $d_3$  values their shift increases the total utility of the allocation. This candidate link identification is the key functionality of our approach. To identify those candidate links, we have to define a metric that can assess the distance values located in the matrices B and D, respectively.

The two most interesting aspects during the evaluation of a candidate link are i) the strength of received interference by all other links and ii) the strength of added interference to all others. We show in the following that we can only apply the second aspect in acceptable computation time.

Regarding the first aspect, we need to evaluate all rows and all columns in matrices B and D except the row and column of our considered link. Then, we need to generate link pairs and evaluate their



generated interference to the considered link. It follows that this evaluation requires the assessment of a large number of link pairs that grows quadratically. For example, by appending a further link to the allocation, i.e., adding an additional column and row to each matrix, the number of elements to assess increases by the order of  $n^2$ . Thus, for a small number of links the evaluation of aspect i) is feasible but does not scale well to a large number of links as focused on in this work.

To evaluate the current configuration with respect to aspect ii), we need to iterate the row and column of the link in the matrices B and D, respectively. To quickly identify the link with the lowest utility, i.e., the one that creates the most interference, we introduce the vectors E and F that store the sum of the individual utilities of the distances stored in B and D:

$$e_i = \sum_{j=i+1}^n u_B(b_{j,i}) + \sum_{j=1}^{i-1} u_B(b_{i,j}) \quad (6.4)$$

$$f_i = \sum_{j \neq i}^n u_D \text{ with } u_{d_{3i,j}} = \sum_n (u_D(d_{j,i}) + u_D(d_{i,j})). \quad (6.5)$$

The first element in (6.4), adds the link distances of matrix B for column  $i$  from the main diagonal to the last element. The second element in (6.4) considers row  $i$  and the summation starts at the first element and stops when the main diagonal is reached. In (6.5), we determine the overall utility of the distances between a link and IMPs. To determine  $f_i$ , we consider the  $i$ -th row  $i$  and the  $i$ -th column of matrix D except the element  $(i, i)$ . Remember that the elements in D are vectors. So for each of the considered elements this results in an additional summation of  $n$  values to find the individual utility of link  $i$ .

We give a summary of our introduced data structures in Table 6.1. In the following, we describe the required link insertion and movement operations in detail.

### 6.2.3 Add a Link to the Allocation

To add a further link to our introduced data structures, we need to insert a new field to the back of each vector and append a new column and row to each matrix, respectively.

First, we append the new link to A. The corresponding additional row of matrix B contains the calculated distances of the new link to the existing ones. At the same time, we find the utility of the new distances and add their sum to vector E.

In the next step, each additional row and column of matrix C is evaluated to calculate the location of new IMPs. With an updated

Table 6.1: Matrices definition and prototype assignment.

Matrix	Type	Element	Description
A	$1 \times n$	scalar	all operated links
B	P	scalar	distances between links
C	Q	scalar	all IMPs generated by A
D	Q	vector	distances IMPs and links
E	$1 \times n$	scalar	individual utility of $\alpha_i$ from B
F	$1 \times n$	scalar	individual utility of $\alpha_i$ from D
H	$1 \times n$	scalar	helper vector containing only ones

matrix C, we also need to evaluate the additional row and column of matrix D to calculate the distances between new IMPs and existing links. Furthermore, we have to access all remaining elements of D and append the distance of an existing IMP and the new link to each element. Again, we find the utility values simultaneously and add or update them in vector F, respectively.

As we have seen, the insertion of a new link is not complex. In most of the cases, we have to iterate a row and a column of size  $n$  to calculate the relationship of the new link to existing entries. Furthermore, the utility values can be updated in parallel with the corresponding distance calculations.

#### 6.2.4 Shift a Link to a New Position

During optimization, we shift a link by an offset  $o$  and evaluate the ability of this new position. The goal is to find an allocation with higher utility, i.e., with less interference.

By shifting link  $\alpha_k$  in A by offset  $o$ , there are  $(n-2)(n-1)$  IMPs that are affected by this. It follows that these IMPs in matrix C and the distances in the matrices B and D have to be recalculated. Additionally, the utility vectors E and F have to be adapted to these changes and require an update.

Due to the selected matrix structure and the characteristics of the IMP calculation, we perform the shift operation by adding or subtracting a delta to the existing values. In the following, we describe the necessary operations to find this delta in detail.

For an update of A, the offset  $o$  can be added to element  $\alpha_k$ . Note that a positive offset indicates the shift of a link to the right in the radio spectrum. The values in the matrices, however, are updated in two different ways, depending on whether we consider their rows or columns.

For matrix  $B$  that holds the distances between links, we iterate column/row  $k$  and decrement/increment the existing values by offset  $o$ :

$$b_{j,k} = b_{j,k} - o, \text{ with } j = 1, \dots, n \text{ and } j > k \quad (6.6a)$$

$$b_{k,j} = b_{k,j} + o, \text{ with } j = 1, \dots, n \text{ and } j < k. \quad (6.6b)$$

The requirement to decrement(increment) the distance value has its origin in (6.1). Recall that  $b_{j,k} = a_j - a_k$ , so shifting a link shifts the distance. To update vector  $E$ , we increment it by the difference between the old and the new distance utility value.

Matrix  $C$  stores all IMPs, so we perform the following two operations to shift link  $k$  by offset  $o$ :

$$c_{j,k} = c_{j,k} - o, \text{ with } j = 1, \dots, n \text{ and } j \neq k \quad (6.7a)$$

$$c_{k,j} = c_{k,j} + 2o, \text{ with } j = 1, \dots, n \text{ and } j \neq k. \quad (6.7b)$$

The definition of two different operations is originated by (1.11). With (6.7a), each IMP in column  $k$  of matrix  $C$  is decremented by the offset value while (6.7b) increments each row  $k$  of matrix  $C$  by the double offset value. Naturally, these updates further introduce changes in the distance matrix  $D$  and it follows that these elements also require an update.

The necessary changes for matrix  $D$  are more complex than before since the elements of the matrix are vectors themselves. For a shift operation, we have to iterate the  $k$ -th column and  $k$ -th row and update all elements of the vectors  $d_{j,k}$  and  $d_{k,j}$ . For all other elements of matrix  $D$ , we only update the  $k$ -th element of vector  $d_{i,j}$  with  $i \neq j \neq k$ . Furthermore, the IMP calculation in (1.11) implies that the offset, to be added to the current value, depends on the element we currently process. To overcome with this, it is useful to define an additional auxiliary vector  $S$  of size  $1 \times n$ . Depending on the input parameters  $i$  and  $j$  that represent the current position of the element, we determine the specific offset coefficients to calculate the new distance values in matrix  $D$  as:

$$S_{1 \times n}(i, j) := \begin{cases} s = 2, s_k = 1 & \text{for } i = k \\ s = -1, s_k = -2 & \text{for } j = k \\ s = 0, s_k = -1 & \text{for } i \neq j \neq k. \end{cases} \quad (6.8)$$

This coefficient vector achieves for input parameters  $i$  and  $j$  a default value with an exception at the position of the shifted link. For example, in the first case every element of  $S$  holds a value of 2 except for element  $k$  where the value becomes 1. Note that the case  $i = j = k$  is not recognized due to the undefined main diagonal in matrix  $D$ .

We apply  $S$  to perform different update operations on  $D$  and explain the usage of vector  $S$  with an example in Appendix B. The first

Parent 1	0	16	37	53	79	95	116	147
Parent 2	27	43	64	80	106	122	143	159
Child 1	0	16	37	53	106	122	143	159
Child 2	27	43	64	80	79	95	116	147

Figure 6.2: Recombination example with a crossover point in the middle of the genomes.

case of (6.8) is used to update the  $k$ -th row, the second one of (6.8) is used to update the  $k$ -th column. For all other elements in matrix  $D$ , the last case of (6.8) is used. We formulate this for a complete enumeration of  $D$  as:

$$d_{i,j} = d_{i,j} + o \cdot S(i,j)^T, \text{ with } i, j = 1, \dots, n \text{ and } i \neq j.$$

Again, we are able to update vector  $F$  in parallel by finding the utility of the new distance and increment it by its difference to the previous utility.

### 6.3 SELECTION OF A PROBLEM-SPECIFIC STRATEGY

In the following, we use our previously defined data structures and operations to identify a suitable metaheuristic to solve our FAP. Recall that in Section 6.1 we introduced the metaheuristics GAs, SA, and TS.

We start with the evaluation of GAs and determine the strength of the operators recombination and mutation. Initially, we neglect the selection operation, because it is an upstream operation of the other two operations.

A recombination example with two frequency allocations achieving the highest utility, i.e., IM-freeness, is depicted in Figure 6.2. The crossover point is in the middle of the genomes. New individuals are generated by switching both second halves of the parents. We expect that this operation creates at least individuals with a utility equal to the parents' utilities. However, as we observe from Table 6.2, both child allocations receive a utility worse than those of their parents. An improved recombination approach uses the relative distances between the frequencies. This will prevent the utility degradation regarding constraint  $d_c$  for, e.g., links 4 and 5 of the second child but regarding constraint  $d_3$ , this approach also receives a utility worse than their parents. The reason for this behaviour is that the recombination of two frequency allocations results in an uncoordinated shift operation for the second half of the links, i.e., their shift offset and shift direction depends on the allocation recombined with.

Table 6.2: Utilities before and after recombination.

Allocation	Utilities $e_i$ and $f_i$	Utilities $U_E$ and $U_F$
Parent 1	70,70,70,70,70,70,70,70	560/560 (1.0)
	336,336,336,336,336,336,336,336	2688/2688 (1.0)
Parent 2	70,70,70,70,70,70,70,70	560/560 (1.0)
	336,336,336,336,336,336,336,336	2688/2688 (1.0)
Child 1	70,70,70,70,70,70,70,70	560/560 (1.0)
	<b>329,336,336,315,315,336,336,329</b>	2632/2688 (0.9792)
Child 2	70,70, <b>68,43,43,68</b> ,70,70	514/560 (0.8964)
	<b>336,319,326,300,300,312,326,329</b>	2548/2688 (0.9479)

In case of mutation, a link to flip can be identified in our representation by the lowest utility. For this link, the new position in the radio spectrum is a random selection and might improve the allocation but can also degrade. So, we conclude the following. Due to the observed massive utility degradation during recombination and a random-only (unguided) mutation operation, we find that GAs are not a suitable metaheuristic to solve our presented problem. This argumentation also holds for alternative population-based approaches.

The metaheuristics SA and TS share a common attribute: both try to improve the utility of a single allocation by modifying it. For this purpose, they require a specific function. To identify the general behavior of our FAP, we shift one link in an allocation with eight links in total and depict the individual utilities in Figure 6.3. We observe that the utility  $e_k$  of the shifted link  $k$  only depends on adjacent links that span the possible shifting range. In contrast, the utilities  $f_i$  much more limit the overall utility and do not follow a specific pattern. The achievable utility at each position of  $k$  is the shaded area, and we are able to identify four zones that create high utility values. However, there is only one zone that achieves the maximum utility, i.e., IM-freeness. This behavior recommends using a method that temporarily accepts an inferior solution to escape from local optima.

We further observe that we face a highly dynamic search space. It follows that a trajectory tracking of all shifted links as required by TS is very complex to set up and especially to evaluate during runtime. The reason for this is that each record in the taboo list is only valid for a specific link configuration which may, as demonstrated in Chapter 4, become very large. Thus, in this work we focus on a memory-less SA approach to solve our FAP.

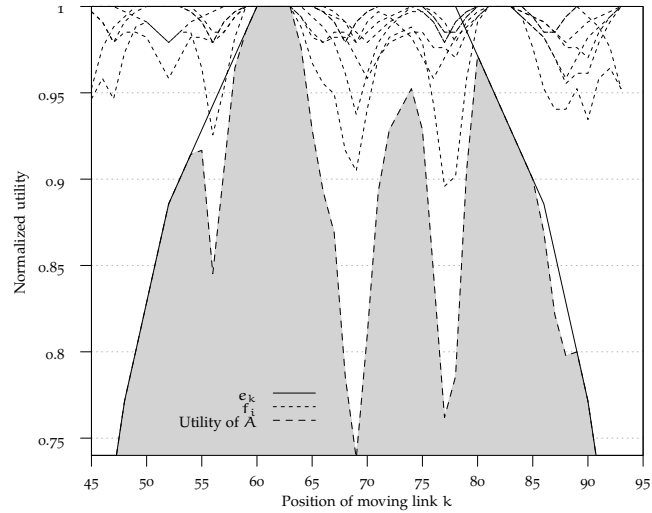


Figure 6.3: Achievable utilities for allocation  $A = \{0, 19, 44, 94, 112, 136, 154\}$  with a further link  $k$  moving from slot 45 to 93. We find four zones where the utility of  $A$  is high, i.e., a good position for  $k$ , but only one that gives IM-freeness.

#### 6.4 OPTIMIZATION WITH SIMULATED ANNEALING

In general, SA processes use a system temperature that exponentially cools down during runtime with the constant parameter  $\alpha$ . The main focus of specific SA applications is the determination of a neighbor function that modifies the current solution to be evaluated by the SA process. The probability of accepting an inferior solution then depends on the current system temperature.

In the following, we present our SA process and depict its workflow in Algorithm 6.1. The algorithm requires an initial allocation  $A$ , a number of annealing steps to perform,  $\text{step}_{\max}$ , and a maximum achievable utility value  $u_{\max}$  as input parameters.

The process starts with a shift of all interfered links in  $A$  to new positions. This is required in the case of present co-channel interference and is controlled by a CEN that permanently observes the audio link quality and radio spectrum.

Following this shift, the current allocation, as well as the utility of them, are saved as lower bound and the step counter is initialized to 0. Then, the optimization starts.

During each annealing step, the system temperature  $T$  is determined by the total number of steps, the currently performed step, and the cooling parameter  $\alpha \in [0, 1]$ . To create a new allocation for evaluation, a neighbor function shifts a link to a new position, and we describe this function subsequently in detail. Then, the outcome of this action is evaluated. If the new allocation achieves a higher utility or an inferior one is accepted, this allocation focuses the basis for the next annealing step. Note that the acceptance probability

---

**Algorithm 6.1** Pseudocode of the Simulated Annealing process. Allocations created by the neighbor function with a higher utility are always accepted while inferior ones are only accepted with a system temperature dependent probability. The algorithm returns the allocation with the highest utility.

---

**Input:**  $A, \text{step}_{\max}, u_{\max}$

**Output:** Best allocation found during optimization

```

A ← shift_interfered_links(A)
u ← utility(A)
Abest ← A, ubest ← u, step ← 0 // Initialize runtime variables
while step < stepmax and u < umax do
    T ← stepmax · αstep // Determine system temperature T
    Anew ← neighbor(A) // Modify allocation
    unew ← utility(Anew) // Evaluate new utility
    if unew > u or min(e $\frac{u_{\text{new}} - u}{T}$ , 1) > uniform(0,1) then
        | A ← Anew, u ← unew // Accept new allocation
    end
    if unew > ubest then
        | Abest ← Anew, ubest ← unew // Save best allocation
    end
    step ← step + 1 // Increment step counter
end
return Abest, ubest

```

---

for an inferior solution depends on the utility difference between the current and new allocation as well as the current system temperature  $T$ . During the overall process, we store allocation  $A_{\text{best}}$  with the highest utility. In case the number of given annealing steps have been performed or we obtained an IM-free allocation, the SA process terminates and returns allocation  $A_{\text{best}}$  to the user.

The neighbor function, to shift a link to a new position, is depicted in Algorithm 6.2. This function focuses to find a candidate link and determine the respective shift offset and direction for them to create a new allocation. To achieve that, the algorithm picks all links that achieve at most the  $m$ -th lowest utility as candidates and selects one of them following a uniform distribution. Furthermore, we grant the elimination of adjacent-channel interference a higher priority because it is a permanent appearance while IM interference only occurs in case devices operate spatially close to each other.

To improve the utility regarding distance  $d_c$  between the device frequencies, the algorithm selects all links that achieve the lowest utility value ( $m = 1$ ) as candidates. The shift direction depends on the frequency range between the candidate and the directly adjacent devices to the larger portion with a fixed offset of one slot. Hence, we are able

---

**Algorithm 6.2** Pseudocode of the neighbor function for the Simulated Annealing process. The algorithm starts with the determination of interfering links and optimizes their distances and the distances between a link and adjacent IMPs.

---

**Input:** Allocation A

**Output:** Modified allocation (neighbor) of input

```

// candidates with the worst utility (f-f)
candidates_ff[] ← A.min_utility_E(1)
// candidates with the m-th worst (or less) utility (f-im3)
candidates_fim3[] ← A.min_utility_F(m)
direction ← 1 // default direction: right
offset ← 1 // default offset: one slot
if candidates_ff.size() > 0 then
    candidate ← uniform_selection(candidates_ff)
    distance_left ← A.distance_left_adjacent(candidate)
    distance_right ← A.distance_right_adjacent(candidate)
    if distance_left > distance_right then
        | direction ← -1 // change direction to left
    end
else if candidates_fim3.size() > 0 then
    candidate ← uniform_selection(candidates_fim3)
    if bernoulli(0.5) then
        | direction ← -1 // change direction to left
    end
    offset ← 1 + geometric(p)
end
A.shift_link(candidate, direction · offset)
return A

```

---

to estimate the utility improvement by this shift operation since the  $d_c$  constraint only depends on adjacent links in the allocation.

In the case of eliminated adjacent-channel interference, we enhance the utility of the distance between a link and IMPs. This time, we cannot estimate the outcome of the shift operation because a large number of IMPs will be affected by this. Therefore, we perform a Bernoulli trial with a probability of success of 0.5 to determine the shift direction. Further, to overcome local optima, the offset we use, is now geometrically distributed with parameter  $p \in [0, 1]$ . Note that in this branch of the neighbor function all links facing at most the  $m$ -th lowest utility are possible candidates.

Finally, the selected link is shifted to the new position, and the resulting allocation is returned to the SA process for evaluation.

As we have seen, the SA process in general and the neighbor function in specific depend on random selections to determine a new al-



location. Thus, it is necessary to repeat this process several times to find a solution that the user is satisfied with.

## 6.5 EVALUATION

In this section, we evaluate our previously proposed SA algorithm in both a static and a dynamic spectrum scenario.<sup>1</sup> These can be considered as use cases for system setup and operation with suddenly emerging interference, respectively.

### 6.5.1 Static Spectrum Scenario

We perform our experiments with specific link numbers in different bandwidths as defined in Section 5.1 and compare the achieved results with the GA approach selected by the C-PMSE project [81].

To enable a comparison between both algorithms, we run them for a specific time and use the utility functions (6.4) and (6.5) to determine the utilities of the best allocation. For each iteration, we derive the mean values  $U_E$  and  $U_F$  of vectors  $E$  and  $F$ , respectively.

The SA experiments are configured with  $s_{\max} = 1000$ ,  $\alpha = 0.99$ , and an initial allocation  $A$  with equidistantly allocated links such that utility  $U_E$  is maximal. The GA experiments are configured with a population size of 50 individuals. Each of the individual holds a complete frequency allocation, a selection rate of 0.5, a crossover rate of 0.5, and a mutation rate of 0.3. These values were evaluated before and showed good results.

To further compare the results with the replication and EFF strategy that have been evaluated in Chapter 5, we use the number of link and operation bandwidths obtained as benchmark. In Figure 6.4, we depict the achieved utilities after 25 repetitions with 0.95-confidence interval for both approaches. We observe from all figures that the SA approach only needs to improve utility  $U_F$  since  $U_E$  is already at its maximum. The GA, however, attempts to improve both utilities by selection, crossover, and mutation operations but never reaches the SA level. Furthermore, the confidence intervals for the GA are much larger and indicate a high utility volatility of the achieved solutions.

During the evaluation of the SA approach, we find that a value of  $m = 1$  and a fixed offset of 1 ( $p = 1.0$ ) in our neighbor function limits its exploration capabilities. A value of  $m = 1$  selects the links obtaining the lowest utility and in the worst case, the pool of candidates contains only two links to select from. Further, an offset of 1 results in very small variations of the current solution. We find in Figure 6.3 that larger step sizes can help to overcome local optima. Therefore,

<sup>1</sup> The evaluation is done on an Intel Xeon X5650 with 2.67 GHz and 6 GB RAM running Ubuntu 12.04.4 LTS.

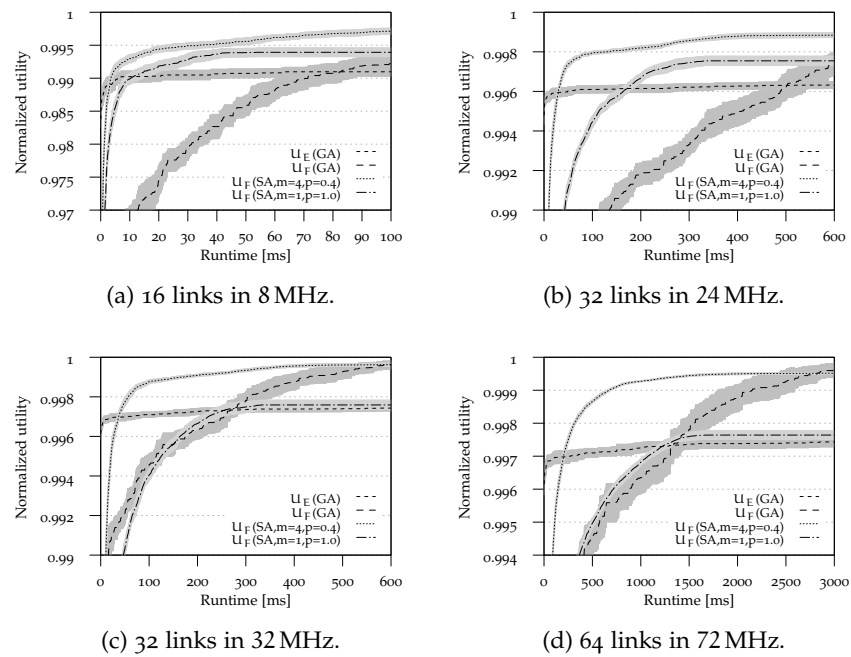


Figure 6.4: Achieved performance by Simulated Annealing (SA) and Genetic Algorithms (GAs) for different link numbers and operational bandwidths. In all cases, SA only has to improve  $U_F$  because  $U_E$  is already at its maximum. Further, the selection of links facing at most the fourth worst utility ( $m = 4$ ) as candidates for shifting and the parameter of the geometric distribution for the determination of the shift offset set to  $p = 0.4$  achieves the overall best performance.

we perform a parameter study and find during our evaluation the best solutions for a combination of the values  $m = 4$  and  $p = 0.4$ .

Important to note is that the maximum achievable utility depends on the number of links. As the number of IMPs grows quadratically, the maximum utility value grows in the same way. Most IMPs meet the required distances resulting in a high utility. It follows that the utility ratio converges to 1 as the number of links increases. Nevertheless, our aim is to get as close as possible or exactly achieve this value.

Finally, we observe that the SA is not able to find an IM-free allocation within the given optimization time. Note that the processing time naturally can be extended and we find IM-free allocations. However, e.g., for system setup, the constructive approaches that have been presented in Chapter 5 achieve better results in faster processing time.

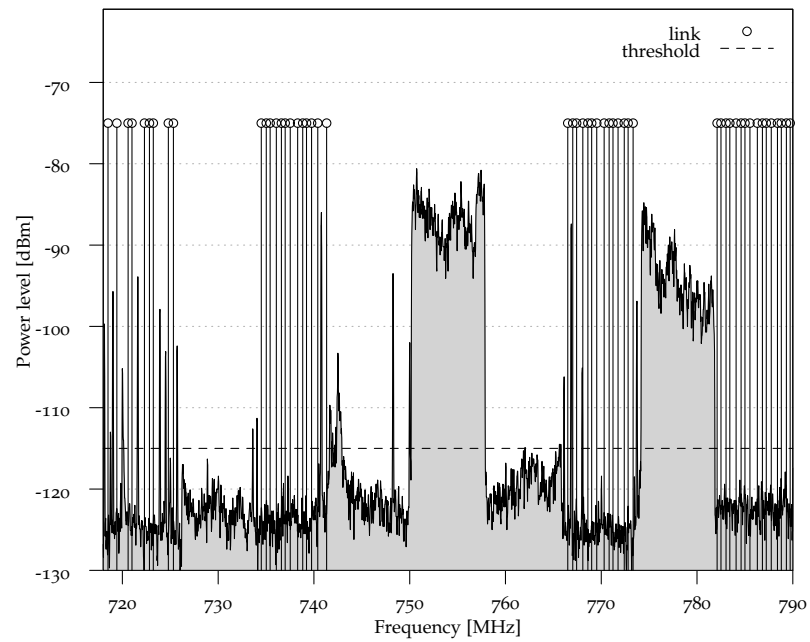
### 6.5.2 *Dynamic Spectrum Scenario*

In this section, we evaluate the reconfiguration performance of the proposed SA algorithm in case of emerging co-channel interference that affects several links. We use real-world spectrum data from an indoor measurement campaign during a large fair. From the gathered spectrum data, we selected two spectrum snapshots from September, 11th 2013 for investigation.

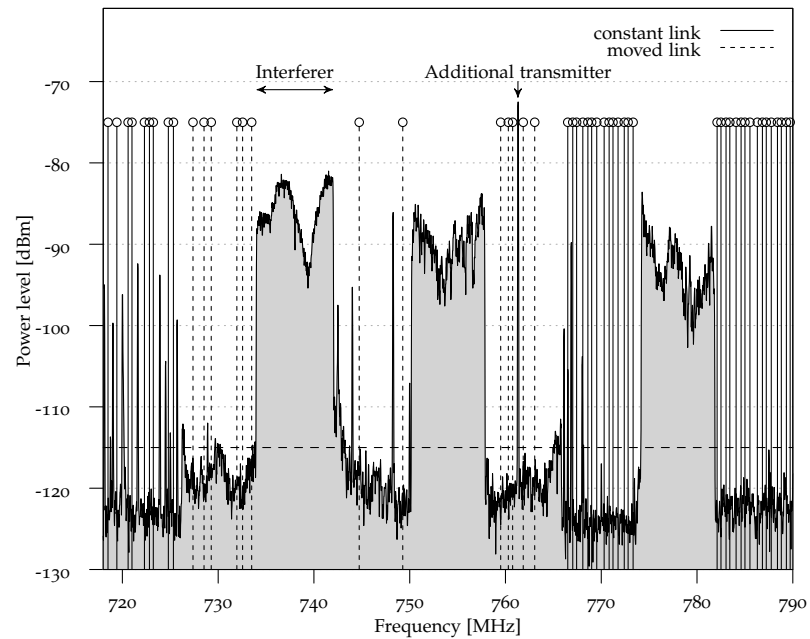
Both of them represent the spectrum occupancy in the UHF TV band between 718 MHz and 790 MHz during the day, and we attempt to utilize the resources as efficient as possible.

The first snapshot is used to initially configure the system with a maximum number of devices. To achieve high SNR values, we only select spectrum resources with a power level below  $-115$  dBm. We are able to allocate at most 52 links with low-quality, and Figure 6.5a depicts the location of those links in the radio spectrum. This IM-free allocation is generated by the replication strategy described in Section 5.1 and acts as initial allocation for the following reconfiguration.

The second snapshot in Figure 6.5b reflects a new spectrum situation. Here, an additional transmitter is present and, more interestingly, an interferer that disturbs 13 of the links. A CEN that monitors the operational environment detects this threat and triggers the reconfiguration. Thus, the SA optimization scheme attempts to reallocate the interfered links by maximizing the utilities  $U_E$  and  $U_F$ . To achieve this, the disturbed links are shifted to identified spectrum opportunities, i.e., resources below the power level threshold with sufficient distances to adjacent links. Note that the initial configuration already allocates all spectrum resources for an IM-free operation,



(a) Situation before interference occurs.



(b) Situation after interference occurred and optimization was performed.

Figure 6.5: System state before and after reconfiguration caused by the sudden occurrence of an interferer. To determine the new configuration, we performed 1000 Simulated Annealing experiments and selected the one with the lowest number of rearranged links (here: 13), followed by the one with highest  $U_E$  and  $U_F$ , respectively.

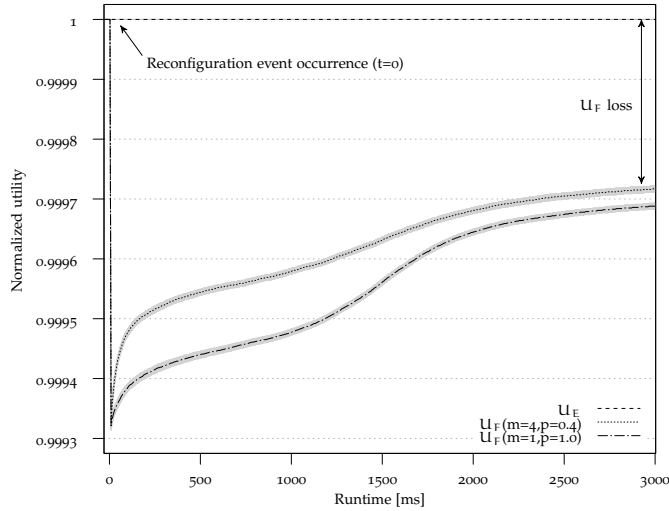


Figure 6.6: Increase of utility  $U_F$  during optimization to cope with the emerging interference event.

i.e., a constructive approach will not find any spectrum opportunity that fulfills the constraints.

We performed 1000 SA experiments in total and depicted the results in Figure 6.6. We observe that only utility  $U_F$  is affected by the emerging interferer. This means that there are sufficient spectrum resources available that satisfy the requested distance  $d_c$  between the links to avoid adjacent-channel interference. After the reconfiguration, our scheme quickly adapts to the new situation and reliably improves the solution that is indicated by the 0.95-confidence intervals with very small variations. As explained before, the selection of the parameters  $m$  and  $p$  has a great impact on the increase of the utility during the annealing process. Again, we found that  $m = 4$  and  $p = 0.4$  achieve the best results but not such outperforming as in the static spectrum scenario.

Of all generated solutions, we selected the one that requires the fewest link movements because every frequency change of a device creates an audible audio quality degradation. The next criterion is utility  $U_E$  followed by the utility  $U_F$ . This Pareto ranking [76] yields an allocation that requires the fewest frequency changes, but provides the highest audio quality.

In this dynamic case, we experience a lack of spectrum resources, i.e., we are not able to achieve an IM-free allocation again and thus, have to accept a certain quality loss. However, with the SA approach we are able to maintain the current number of operated links and offer a solution that obtains the highest possible utility. In extreme cases with large parts of the spectrum interfered, we have to modify the quality requirements, e.g., increasing the power level threshold to find further spectrum opportunities or to reduce the number of operated links.

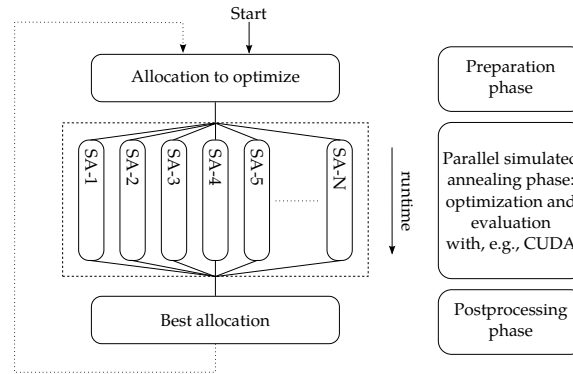


Figure 6.7: This figure depicts our proposed parallelization. We start with an initial allocation and perform  $N$  independent Simulated Annealing processes in parallel. After termination, we evaluate the utility of each to find the overall best allocation and stop or perform the optimization process again.

## 6.6 OUTLOOK: PARALLELIZATION

We have seen in this chapter that SA is a suitable metaheuristic to solve the presented FAP efficiently. Due to the random selections during the process, it is recommended to perform the SA several times. This results in a large number of solutions to select finally the best one for operation. On a single CPU, these solutions were consecutively generated which results in a limited number of solutions for a given reaction time.

For real-world systems that require such solutions in a very short time, we recommend performing a large number of optimization processes in parallel, e.g., on a GPU with CUDA framework [73]. As depicted in Figure 6.7, each process starts with the same initial solution and individually attempts to improve it. Since the proposed SA algorithm can run independently, it is applicable for a parallelized execution. Finally, the best allocation found is used for reconfiguration or acts as a starting point for further optimization.

## SPECTRUM OCCUPANCY MEASUREMENTS

---

In this chapter, we present the results of a measurement campaign conducted in Berlin (Germany) during the International Radio Exhibition (IFA; Internationale Funkausstellung) in September 2013. The measurements have been performed in order to understand the characteristics of spectrum occupation in the UHF TV band within a large indoor area. They have been done with a spectrum sensing grid which has been installed across multiple halls on the fairground at the Messe Berlin.

In the following, we present the measurement setup and report our main findings. The measurements focus on the investigation of indoor spectrum usage across several exhibition halls in the frequency range between 470 MHz and 870 MHz. We examine the statistics of the collected data, including the analysis of duty cycles and the spatial correlation to derive recommendations for dimensioning such a scanning grid at other locations. The results presented in this chapter have been published in [58].

### 7.1 MEASUREMENT SETUP AND METHODOLOGY

In this section, we motivate our measurement study and give a detailed description of the setup followed by some general comments about the spectrum environment at the measurement location.

#### 7.1.1 *Scope of the Measurements*

The measurements have been taken from the perspective of PMSE systems. Today, nomadic PMSE systems, e.g., for electronic news gathering, may already nowadays unexpectedly appear in the spectrum and create interference to fixed installations. These nomadic systems usually operate a small number of devices and, therefore, the probability of occurrence of interference is low. In contrast, it is assumed that PMSE systems also have to coexist with new upcoming cognitive wireless systems in the near future. Those WSDs will occupy large portions of the radio spectrum and will not be static as today's DVB-T systems for TV broadcasting services, but highly dynamic and opportunistic.

In both cases, uncontrolled interference may harm existing PMSE audio links by reducing their link budget that is required for a satisfying audio quality. Currently, available commercial PMSE systems react to such situations by replacing the disturbed audio links on

Table 7.1: DVB-T Radio Towers in Berlin Area.

Name	Location	d [km]
Berliner Fernsehturm (1)	52°31'14.9"N, 13°24'34"E	9.6
Berlin-Schäferberg (2)	52°25'3"N, 13°7'39.9"E	13.6
Scholzplatz (3)	52°30'27.7"N, 13°13'10.3"E	3.5

stage. This may create an extremely awkward situation as it induces an interruption of service. Thus, future PMSE systems will have to find a way to protect themselves as Cognitive Radio devices do. This means that they have to sense their environment permanently and react to changes in the spectrum usage in order to avoid audible disturbances.

To this end, the C-PMSE project [6, 81] aims to develop a research platform for the evaluation of cognitive methods for PMSE systems [9, 88] and makes use of a spectrum sensing grid with self-deployed scanning receivers [85, 96]. Remember the receiver path of Figure 1.1. Here, the scanning receivers implement the FFT in their Digital Signal Processor (DSP) unit to determine the energy present in the radio spectrum and decide whether there are other users present.

On the fairground, at the Messe Berlin, the scanning receivers have been installed across multiple halls. Furthermore, they have been connected to be controlled in a coordinated manner. Each scanning receiver is able to observe the frequency range from 470 MHz to 870 MHz. Thus, they cover the UHF TV band that is typically used for today's PMSE system operation. Furthermore, this frequency range includes the LTE down- and uplink, which is in Germany allocated between 791 MHz and 862 MHz with a duplex gap between 823 MHz and 832 MHz. Additionally, in the range of 863 MHz to 865 MHz there exists a band for ISM applications. Both the LTE duplex gap and the ISM band can be used for PMSE system operation.

### 7.1.2 Spectrum Environment at Measurement Location

According to the publicly available frequency occupancy plan for DVB-T transmissions in the Berlin area [72], there exist three radio towers that are close to the fairground. Table 7.1 summarizes their locations and the distances to the fairground.

Regarding DVB-T in Berlin, there exists a single frequency network. In such networks, spatially close radio towers transmit on the same frequencies the identical content. This results in a higher utilization of the radio spectrum with more transmitted programs and an increased coverage. We summarize the occupied frequencies for DVB-T transmissions and the power radiated by each radio tower in Table 7.2.



Table 7.2: DVB-T Radio Towers' Transmission Power [72].

Frequency [MHz]	txPower [kW]		
	1	2	3
506	20	50	-
522	120	50	20
570	50	50	-
618	20	50	-
658	120	50	-
682	100	50	20
706	50	50	-
754	10	20	-
778	10	5	-

From a regulatory perspective, the spectrum in the UHF TV band in Germany that is available for PMSE systems is currently divided into three ranges: 470 MHz–606 MHz, 614 MHz–710 MHz, and 710 MHz–790 MHz. The first two ranges are reserved for public service and private broadcasting companies. Both ranges can further be used by broadcast vehicles. The third range is intended for professional PMSE operators, e.g., for temporarily fixed installations at fairs, concerts, or theaters. Permanently fixed installations, e.g., operas or sports stadiums, can use all ranges. Note that due to the ongoing regulation activities in Germany (and worldwide, too), there might be changes in the mentioned frequency ranges and user groups in the future.

### 7.1.3 Measurement Setup

The system setup, to perform the measurements, is depicted in Figure 7.1. It applies the C-PMSE scanning grid. The scanning receivers are spatially distributed among different zones and connected by a 100 Mbps Ethernet network.

We assume that future PMSE systems will operate according to the dynamic spectrum access paradigm. Thus, each PMSE system will be controlled by a CEN. The scanning controller writes the data of each scanning receiver to a common database that can be accessed by the CENs for evaluation and to perform dynamic spectrum access actions for their attached systems. In the following, we focus on the evaluation of the scanning data in the database.

A map of the area in which the measurement campaign takes place is depicted in Figure 7.2. There are 21 scanning receivers installed in the halls such that they are distributed among 5 zones as presented in Figure 7.3. The scanning receivers in halls 18 and 20 are mounted

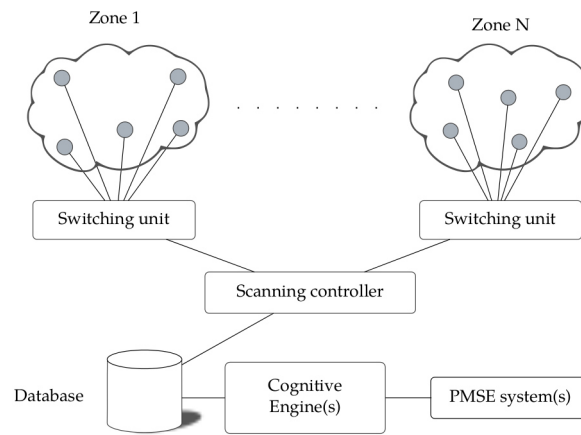


Figure 7.1: System setup of the measurement installation. The scanning receivers are distributed in several zones. The gathered data is stored in a database. The CEN(s) evaluate(s) this data and, if necessary, initiate action(s) for its(their) associated PMSE system(s).



Figure 7.2: Map of the area at Messe Berlin ( $52^{\circ}30'9.6''N$ ,  $13^{\circ}16'15.8''E$ ) [74]. The scanning receivers are installed in halls 18, 19, 20, the Palais, and the connecting corridor.

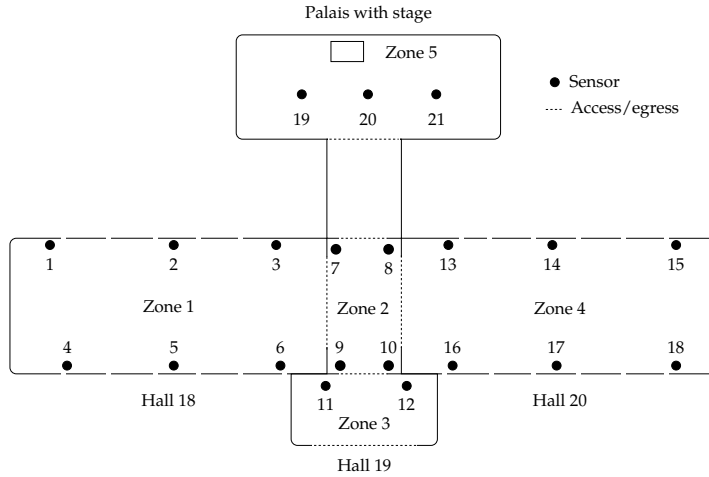


Figure 7.3: Floor plan with installed scanning receivers (schematic but true to scale).

Table 7.3: Scanning receiver configuration.

Parameter	Value
Frequency span	470 MHz–870 MHz
Resolution bandwidth	25 kHz
Number of frequency bins	16000+1
Samples per frequency bin	10
Measurement time	6 s
Measurement interval	30 s

at a height of approximately 5 m. In hall 19, the mounting height is approximately 3 m and approximately 6 m in the corridor between the halls. In the Palais, the scanning receivers reside on a projector rail at a height of approximately 3 m.

We list the detailed set of used measurement parameters in Table 7.3. The measurement time describes the time between start and end of the measurement at the scanning controller.

The scanning controller collects the data from each scanning receiver. For each frequency bin it stores the peak power level, the average power level, the noise floor, and a UTC timestamp in a common database for further processing.

In the following, we report our measurements results and evaluate the spectrum data.

## 7.2 MEASUREMENT RESULTS

In this section, we present the measurement results obtained with the previously described scanning grid. We investigate the duty cycles for

each zone and perform a spatial correlation of the scanning receiver data for a static as well as a moving transmitter device.

### 7.2.1 Duty Cycle Investigation

To determine the duty cycle of the radio spectrum, we apply generic energy detection based on the detection threshold  $\delta$ . The choice of this detection threshold  $\delta$  has a significant impact on the duty cycle computation. In general, the theoretical thermal noise floor is chosen as the threshold. This noise floor bases on the Boltzmann constant, the resolution bandwidth, and the temperature measured at the receiver plus a hardware dependent noise figure.

An experimental approach, to determine the detection threshold, is described in [64]. This work recommends terminating the input with a load resistor and determine the threshold as, e.g., the 99th percentile of the average measured power level. However, in noisy radio environments, such as expected here, this approach to determine the detection threshold is likely to overestimate the duty cycle in numerous frequencies. In fact, we compare the Power Spectral Density (PSD) measured at different locations and observe that the background noise level is about 30 dB above over the theoretical level during the day.<sup>1</sup> This noise level holds for a large part of the UHF TV band. We assume that this increase is due to the presence of LED walls for advertising or supporting presentations at the exhibition halls. Thus, we set the detection threshold to  $\delta = -90$  dBm, which is a compromise between accuracy and overestimation of the duty cycle from measured spectrum data.

In the duty cycle analysis, we focus on representative traces that describe the spectrum occupancy during the day at the different zones of the fairground (as depicted in Figure 7.3). The investigated time period lasts from 8am to 8pm (CEST). We compare the duty cycle results of all measurements days and have selected representative traces for evaluation. As an example, we discuss the duty cycle measurements obtained on Saturday, 7th September. This was the day with the largest number of visitors and the highest spectrum usage.

We have validated that zone 1 and zone 4 show very similar duty cycle results and thus, choose to present only the data of zone 1. This similar behavior can be explained by the symmetry of the exhibitions halls with similar utilization patterns and signal propagation characteristics. Figure 7.4 shows the results.

We observe that spectrum usage significantly varies with the frequency sub-bands and the measurement location. Table 7.4 summarizes the average duty cycles obtained for each zone and each frequency sub-band. Note that we follow a conservative approach and

<sup>1</sup> The thermal noise level for a bandwidth of 25 kHz at 20 °C results in  $\delta = -130$  dBm.

Table 7.4: Duty cycles of September, 7th 2013 (8am - 8pm CEST).

Duty cycle [%] ( $\delta=-90$ dBm)	Zone				
	1	2	3	4	5
PMSE band 1 (470 MHz–606 MHz)	17	17	9	17	10
PMSE band 2 (614 MHz–710 MHz)	33	33	15	32	13
PMSE band 3 (710 MHz–790 MHz)	21	16	0.6	13	0.4
LTE downlink (791 MHz–821 MHz)	59	61	6	60	60
LTE duplex gap (823 MHz–832 MHz)	0.3	0.2	0	0.4	0
LTE uplink (832 MHz–862 MHz)	2	0.6	0.3	0.2	0.8
ISM band (863 MHz–865 MHz)	2	3	0.8	5	0.6
Complete range (470 MHz–870 MHz)	22	21	7	21	11

consider for the duty cycle computation at each frequency bin only the scanner with the maximum received PSD.

We find that zones 1, 2, and 4 show similar average spectrum utilization over the complete frequency range. Zones 3 and 5, however, show in general a lower utilization. If we consider the average utilization of the complete frequency range of zone 5 is close to a half the utilization of the neighboring zones, while zone 3 utilization is one-third. Further, it is remarkable that the average utilization of the LTE downlink sub-band in zone 3 is just a tenth of the average utilization measured in the rest of the installation. This effect can be explained by the fact that the scanning receivers in zone 3 are mounted to the back of the LTE base station and therefore only observe a small amount of their transmitted energy. So we deduce that the mounting direction of the scanning receivers also has a significant impact on the achieved results. Note that we observe an average utilization in the LTE downlink of about 60%, which indicates that only two of three expected providers are active.

When considering PMSE band 3 in Table 7.4, we observe that both zones 3 and 5 show a marginal spectrum utilization compared with that of the others. As we observe in Figure 7.4, the reason is that DVB-T transmitters in this band are not detectable within zones 3 and 5. One explanation for this observation is their lower transmission power, as shown in Table 7.2, associated with a probably higher absorption level of the walls in zone 5 or, as mentioned before, an inappropriate antenna direction of the scanners in zone 3 that reduce their detection performance.

Another interesting finding regarding system operation is that for temporally narrow-band signals, like PMSE links, the average duty cycle, as given in Table 7.4, is not a reliable metric in order to make assumptions about their real spectrum utilization. As in most duty

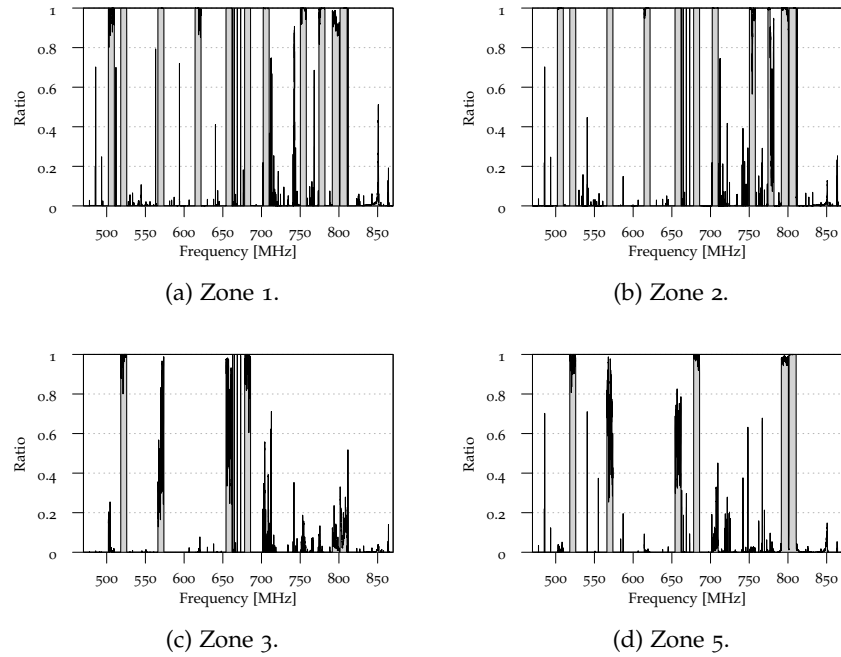


Figure 7.4: Overview of measured duty cycles with  $\delta = -90$  dBm/25 kHz collected over twelve hours (8am - 8pm CEST) on Saturday, 7th September 2013.

cycle studies in the literature, the global look at a large frequency range while considering large time periods implies that the existence of such links can only marginally affect the reported overall duty cycle. For example, if we consider a 400 MHz band for 24 h to determine the duty cycle, turning on a device with a bandwidth of 200 kHz for 1 h results in an increase of 0.002%.

Thus, in Figure 7.4 we consider the frequency dependent duty cycles to gain a much better insight into the effective spectrum utilization of such links. Due to the usage of a resolution bandwidth of 25 kHz, we are able to recognize such narrow-band signals and obtain very precise results.

### 7.2.2 Spatial Correlation

The correct dimensioning of a scanning grid is a challenging task that has a significant impact on the quality of measurement results as well as on the installation costs. Ideally, a scanning grid should deliver timely information about the existence and position of any transmitter. Thus, optimal dimensioning can only be achieved if we know in advance the kind and transmission parameters of the radio systems that attempt to coexist in the area.

From the perspective of PMSE systems, the scanning grid should be able to detect the presence of any harmful interference in their

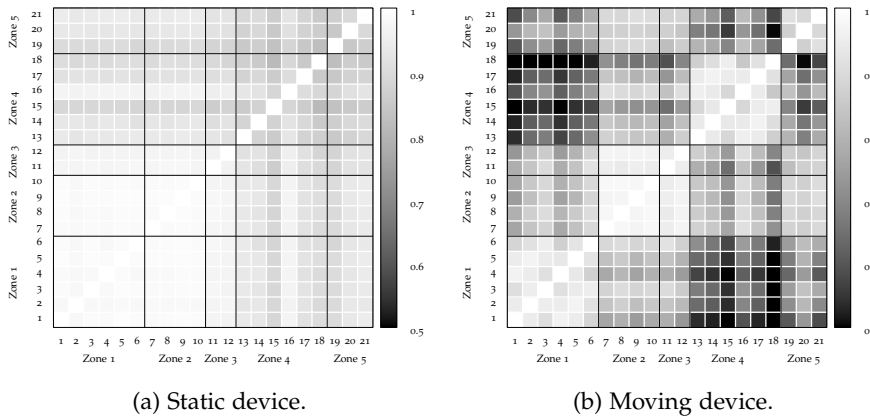


Figure 7.5: Spatial correlation matrices of the scanning receivers for two transmitting devices.

operational area. Remember that in the future, these systems have to coexist with WSDs and other nomadic PMSE systems.

In this section, we use spatial correlation as a tool to determine if the installed scanning grid is capable of detecting the presence of such coexisting systems. In the study presented, we find the correlation factors across the scanning grid for two PMSE devices that are turned on during the measurement period. The first device is static while the second device moves around the scanning grid. Figures 7.5a and 7.5b depict the correlation matrices for both cases. We use the mean of the measured power levels between each pair of scanning receivers and smooth them by an exponentially moving average with a weight of  $\alpha = 0.1$  for the previous value.

In Figure 7.5a, we observe a strong correlation between the scanning receivers of zone 1 and 2, which indicates that the active link can be found in this area. As expected, the correlation factor decreases as the distance between the measurement locations (scanning receivers) increases. For example, SCR 13 and 16 observe a stronger signal strength than SCR 15 and 18 that reside at the other end of zone 4. The overall homogeneous correlation of all scanning receivers indicates a static link, because the scanning receiver, which observes the strongest power level, does not change over time. A change would imply a decrease of the correlation factors.

In contrast, Figure 7.5b shows a different situation. We observe a strong correlation of the scanning receivers that are located in the same zone. However, the correlation is not as homogeneous as in Figure 7.5a. This difference results from a moving device that creates the strongest power level at changing scanning receivers which lowers the correlation factor across zones and increases within the zone in which the device currently resides.

If we consider all scanning receivers we note that the correlation factors are very high. So we deduce that the detection of nomadic PMSE systems can be achieved with a scanning grid with less scanning receivers. Unfortunately, we cannot give any insight into the detection performance of the grid in the case of WSD operation since we could not observe their presence in our measurement results.

### 7.3 SUMMARY

In this chapter, we presented spectrum usage results from an indoor measurement campaign in the UHF TV band. The measurements were conducted in Berlin (Germany) during a large consumer electronics fair, the IFA 2013. Our measurements focused on the investigation of indoor spectrum usage across several exhibition halls. We also considered the analysis of possible coexistence threats for PMSE systems.

We introduced our measurement setup and discussed our main findings regarding duty cycles and spatial correlation. In the next chapter, we use these measurements to evaluate and optimize the dynamic spectrum access behavior of a CEN.

We also provide our collected spectrum traces to the Cognitive Radio community.<sup>2</sup> We expect that these traces help other researchers to evaluate their architectures and algorithms with real-world data from a spatially large sensor grid.

---

<sup>2</sup> Please visit <http://www.ikt.uni-hannover.de/ifa2013.html> for further information.



In the previous chapters, we have seen that future PMSE systems require coexistence mechanisms for a successful operation in a dynamic spectrum regulation regime. The underlying interference constraints during frequency allocation pose an enormous challenge. To cope with these challenges, we combine the findings of the previously investigated topics.

In the following, we present a CEN software architecture that enables the operation of a frequency allocation algorithm that adapts to the situation. Further, we introduce a rating scheme to identify alternate frequencies in case of interference. We evaluate its performance for the mobile interferer observed during the spectrum measurements presented before. The results presented in this chapter have been published in [56].

### 8.1 SCOPE OF OUR COGNITIVE ENGINE

In Chapter 1, we argued that the static spectrum situation for PMSE systems is likely to change in the near future. This change requires the coexistence of them with emerging Cognitive Radio devices. Moreover, due to the increasing demand for spectrum resources by cellular services, the probability of sudden interference caused by detection errors is also likely to increase. Hence, future PMSE systems are required to cope with this new situation in an efficient way.

We agree with the authors in [80] that the key issue in developing a successful coexistence approach for future PMSE operation is the adoption of the cognitive paradigm by PMSE systems themselves. The key functionality to satisfy the outstanding high-quality demands

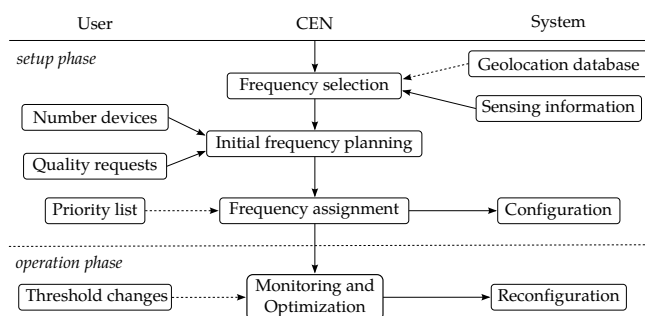


Figure 8.1: Interaction between components during system setup and operation phase.

of PMSE systems is a continuous observation of the audio link quality as well as the radio spectrum conditions.

Remember Figure 1.10 that depicted the operational context of a Cognitive Radio system. It showed that there are different levels of reactions to a threat, i.e., *normal*, *urgent*, or *immediate* actions. In general, it holds that the longer the time a system has to react, the better the quality of the response. Indeed, the decision-making process is able to do more computation cycles and thus, refine the action proposed. It follows that a software architecture of this decision-making engine, also referred to as CEN, needs to provide a dynamic selection of specific planning methods to enable such behavior.

Figure 8.1 again shows the setup and operation phase of our system. In our previous investigations, we assumed that the radio spectrum is static during setup as well as during operation. In the following, we focus dynamic changes of the systems' environment. To consider these changes, we adapt the cognitive cycle to include PMSE specifics and make decisions to cope with the current threat situation during operation. Another important aspect of decision-making in the CEN is the quality rating, i.e., to decide which action is required to meet the current interference threat or to identify the best alternative frequencies. To achieve an accurate spectrum rating, we present a location-based spectrum data fusion approach. This approach enables the CEN to rank available resources, and we evaluate it with real-world data gathered by the previously presented spectrum scanning network. Note that an adequate audio quality rating depends on the operated system and is therefore vendor specific. Thus, without loss of generality we assume that the audio quality reported by the RLM to our CEN is either very good or not acceptable.

## 8.2 PROPOSED SOFTWARE FRAMEWORK

In this section, we describe the architecture of our proposed framework and present the workflow in our CEN. Then, we evaluate the performance of our implementation that requires an immediate system reallocation in case of sudden appearing interference.

### 8.2.1 *System Model*

Traditionally, PMSE systems follow a centralized approach with a master element called base station that receives audio signals from a variable number of mobile devices over an exclusive wireless link. The radio spectrum situation is determined in advance, and mobile devices are set up manually. In case of emerging interference during operation, the disturbed mobile device is manually exchanged by a spare device. This, however, may lead to extremely awkward situations on a stage.

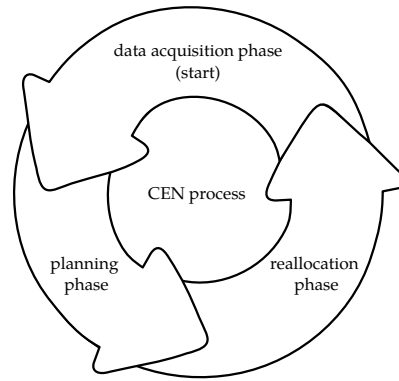


Figure 8.2: The Cognitive Engine continuously performs the depicted cycle.

In contrast, a cognitive PMSE system as depicted in Figure 1.16, executes the underlying cognitive cycle that periodically matches re-allocation steps with goals and constraints. Here, the base station acts as RLM offering an indicator about the quality of each audio link [11] to the CEN. Further, the RLM must be capable of controlling the transmission parameters of associated mobile devices remotely when requested by the CEN.

The spectrum scanner network, in turn, senses the environment using energy detection and reports the current radio spectrum occupation for evaluation to the CEN. From this data, the CEN identifies alternative operation frequencies that have a low interference level. These frequencies act as the basis for the frequency allocation algorithms during the planning phase of the cognitive cycle.

To achieve the described behavior, the CEN permanently executes a cognitive cycle as depicted in Figure 8.2. The cycle starts with a data acquisition phase of the system environment, i.e., LQI data, radio spectrum occupation, and GUI configuration settings. During the planning phase, the gathered information is evaluated, and the CEN searches for suitable frequency allocations fitting the current situation. During the reallocation phase, the best frequency allocation found is distributed to the RLM to reconfigure the system and the cycle restarts by acquiring new environment data. Note that both the planning and the reallocation phases are only performed if required. Further, to achieve more satisfying solutions, the user is allowed to modify his quality requirements or the number of operated links at any time using the GUI.

The most interesting part of this workflow is the timely determination of a new system configuration in case of changes in the radio spectrum environment. That is, the LQI of one or more devices suddenly decreases, and a new frequency allocation is required. As we have seen, this process is very challenging due to the underlying IM interference constraints. Note that the consideration of spectrum power levels is not a reliable metric for threat detection because we

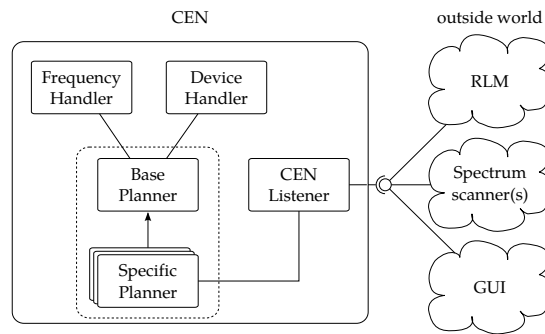


Figure 8.3: Architecture of our Cognitive Engine. It allows to use specific frequency planning algorithms depending on the current situation observed in the outside world. The connection between the system components is done via a TCP/IP interface.

are not able to distinguish between the transmissions of our system and an interfering narrow band device.

In the following, we describe the software architecture of a CEN that implements the random fit frequency planning algorithm as presented in Chapter 5 to determine the fastest system reaction possible. Remember that the SA approach causes a significantly longer processing time until it achieves a new solution and, therefore, we neglect its evaluation here. Nevertheless, our software architecture is not limited to PMSE specifics and can easily be extended by alternative frequency allocation algorithms for other Cognitive Radio systems.

### 8.2.2 Overview of Software Components

In this section, we introduce the CEN software architecture and evaluate its fastest response time to reconfigure the system in case of sudden interference. Introductions to the implementation details of other system components such as RLM with LQI determination and spectrum scanner network are given in [11] and [9], respectively. A GUI, however, is vendor-specific and therefore not considered. For the implementation, we use the C++ Boost framework [1] that offers a large library of reusable components for our purposes.

In the following, we detail the architecture of our CEN and describe its interaction with the outside world. As depicted in Figure 8.3, all system components are connected via a TCP/IP interface that dispatches the messages. Note that each of these components may run individually on its own server but also centrally on a single one. This possibility is an important design aspect of mobile operation when energy consumption is an additional constraint that limits the capabilities of the system. In contrast, a fixed installation allows the use of powerful hardware to run more complex frequency planning algorithms or achieve solutions in a shorter time.

The workflow in our CEN is controlled by a *CEN Listener*, which is modeled as a finite state machine that determines the system's reactions to incoming events. For the initial setup, the *CEN Listener* requires information from the components of the outside world, i.e., RLM, spectrum scanner network, and GUI, all necessary information for initial system setup. This information includes the number of mobile devices to serve the requested allocation quality, and the current status of the radio spectrum environment. Following this data acquisition phase, as depicted in Figure 8.2, the planning phase starts. The best frequency allocation, which has been found during this phase, is mapped to mobile devices such that the CEN knows the relationship between reported the LQI and the operation frequency. During the reallocation phase, the configuration obtained is distributed to the RLM in order to start operation.

After a successful initial setup, the system operation mode is entered. Here, the *CEN Listener* continuously acquires and monitors the LQI and radio spectrum environment to trigger necessary frequency reallocation events. Furthermore, it reacts to threshold changes received from the GUI and adapts the frequency planning algorithm accordingly to overcome unexpected situations.

In order to implement the capabilities described before, we use further software components namely *Frequency Handler*, *Device Handler*, *Base Planner*, and *Specific Planner*.

The *Frequency Handler* is a data structure that allows access to the current frequency allocation of the system. To enable the constructive allocation approaches and to generate an overall IM-freeness, it ensures that all allocated frequencies comply with the required channel spacing and do not interfere with each other. Furthermore, it also enables local-search approaches to optimize the current allocation, e.g., by implementing the neighbor function for our SA approach.

The *Device Handler* data structure maps the operation frequencies to a unique device identifier used by the RLM. In case of LQI degradation, this mapping allows the CEN to identify the affected frequency immediately to reallocate the corresponding device.

The *Planner* component hosts the frequency planning algorithm. We have selected an encapsulated architecture and divided it into base and specific functionality. The *Base Planner* holds instances of the previously described data structures and additionally keeps a snapshot of power levels from the spectrum scanning network. This snapshot is permanently refreshed by the CEN and forms the basis for the specific frequency planning algorithm.

The *Specific Planner* inherits all attributes from the *Base Planner* and implements the specific behavior for system operation, i.e., how the system is initially set up, reacts on LQI degradations, and determines alternate frequencies during operation. Further, our modular design of *Planner* components allows the use of specific frequency planning

algorithms. We set up a library of our planning algorithms investigated before, and the CEN dynamically loads one of them to cope with a threatening situation requiring *normal*, *urgent*, or *immediate* action response.

### 8.2.3 Evaluation

An overall objective of Cognitive Radio system design is to minimize its response time to a harmful situation, i.e., the time between detecting a harmful situation and providing a solution to overcome it. To evaluate our proposed architecture, we determine the individual response time of the CEN by analyzing the network traffic between the system components.

In our investigation, the response times of spectrum scanners and the RLM are not considered as they depend on vendor-specific implementations. In our setup, we emulate the spectrum scanners as the network source and the RLM as the network sink, respectively. However, this has no impact on the obtained results and does not limit the generality of our architecture.

We choose the following scenario for evaluation. In an interference-free operational bandwidth of 72 MHz with a resolution of 25 kHz, our CEN initially allocates 40 mobile devices with low-quality requirements. Note from Figures 5.4a and 5.5a that this number of devices can be allocated as long as large parts of the radio spectrum are interference-free.

During system operation, an 8 MHz wide interferer suddenly appears and affects the LQI of 6 links so that the CEN is requested to reallocate them whilst maintaining the overall quality of the devices, i.e., achieve an IMP-free allocation again. We assume that this situation requires the fastest possible response, i.e., an *immediate* action, and that the *Specific Planner* implements the random fit frequency allocation algorithm. Note that using the EFF requires comparable processing time because both find a solution after trying several candidates. To determine the response time of our CEN, we analyze the timestamps of incoming spectrum scanning data and the outgoing RLM reconfiguration request.

We perform our experiments of the described scenario and repeat them 100 times to achieve statistical significance.<sup>1</sup> The mean response time of our CEN is 138 ms with an error of 1 ms considering the 95% confidence interval.

For the C-PMSE spectrum scanning network, we used in our measurements before, the authors in [10] performed a determination of the response time. They report for a bandwidth of 72 MHz and a resolution of 25 kHz a refresh rate of 830 ms. This refresh rate implies

<sup>1</sup> The evaluation was done on an Intel T5870 CPU with 2 GHz and 4 GB RAM on a single core running Ubuntu 12.04.4.

that the PMSE system has at maximum 830 ms for reallocation between two spectrum data update events. It follows that the response time of our CEN only consumes a small portion ( $\approx 17\%$ ) of the overall processing time.

In contrast, if we perform the SA approach, we achieve a significantly longer processing time because the annealing process requires more time to determine a new configuration. The advantage of the SA approach, though, is that it is capable of maintaining the number of operated links in any case, which the constructive approaches cannot guarantee.

### 8.3 RATING OF SPECTRUM SCANNER DATA

In general, wireless communications are affected by several adverse effects on the transmission channel, e.g., fading, shadowing, and signal attenuation caused by absorption or scattering effects. Thus, a precise determination of the current radio spectrum occupation is a challenging task, especially in indoor scenarios, in which the problem of hidden terminals is likely to occur. Here, the use of a cooperative spectrum scanning network is recommended in order to achieve a high detection probability and minimize the probability of missed detections.

As discussed in the related work, there exist several rules regarding the fusion of scanner data in the literature. However, particularly in spatially large indoor spectrum scanning networks, their use cannot precisely reflect the current spectrum situation and a more sophisticated fusion rule is required to overcome the limitations of the state-of-the-art approaches.

In the following, we present our spectrum rating approach relying on a location-based spectrum data fusion rule. To determine the quality of alternative frequencies in the case of LQI degradations, it takes into account measured power levels and scanner locations. We claim that our approach enables the CEN to rate the spectrum resources in a higher resolution than existing methods from the literature.

On initial setup, we rank the scanners into different priority levels depending on their distances to the location of our systems. For example, if a scanner, which is far away from the system, reports high power levels, the CEN rates this information from scanners with a lower weight than those close to the system. Thus, the CEN is able to create a set of alternative frequencies at specific operation locations and to determine the ones with the highest quality.

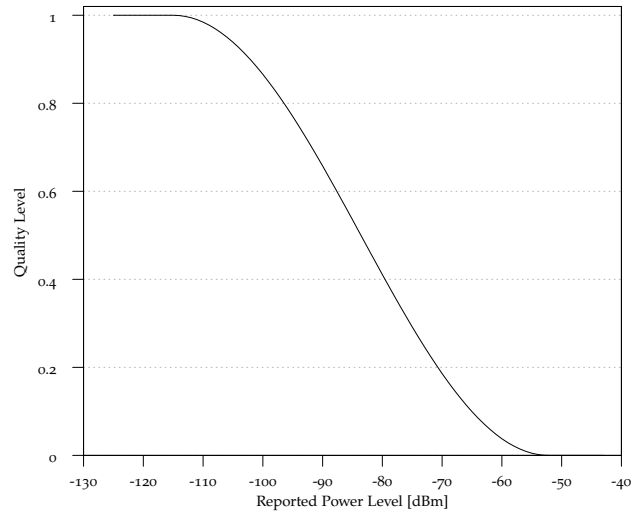


Figure 8.4: Used mapping function  $m(p)$  to determine the quality level of a spectrum power level  $p$  from a scanner. Our approach uses this level to evaluate it in relation to the position of the scanner and operated system.

### 8.3.1 Spectrum Rating

The definition of our Rated Spectrum Quality (RSQ) approach for system location  $L$  and a scanning network consisting of  $n$  scanners is given in (8.1):

$$\text{RSQ}(L, f) = \frac{1}{n} \sum_i \frac{1}{r_L(i)} m(p_i(f)). \quad (8.1)$$

Here, the power level  $p_i$  reported by scanner  $i$  at frequency  $f$  is mapped to a quality level according to function  $m(p)$  which is depicted in Figure 8.4. This mapping function reflects that a low power level corresponds to a high-quality level which decreases with the measured power level. Remember, that in the previous Chapters 1, 5, and 6 we defined a fixed noise and interference level to decide whether or not a spectrum resource is available for operation. This fixed threshold is now relaxed by the function  $m(p)$  and enables to evaluate the available link budget for each frequency. Note that this function can be adapted to specific quality requirements of both the user and the system.

The quality level of scanner  $i$  is divided by a rank  $r_L(i)$  that depends on its location. Finally, we average these values among all scanners in the network. Thus, scanner  $i$ 's rank determines the impact of its measurement on the overall RSQ.

To find the individual rank for each scanner at different system locations, we present a modified breadth-first search algorithm as depicted in Algorithm 8.1. The first input parameter is an undirected



---

**Algorithm 8.1** Pseudocode to create an evaluation view of a spectrum scanner network for the CEN.

---

**Input:** undirected graph  $G$  and initial set of scanners  $S_1$

**Output:** level scheme for interpretation of scanner data

```

result  $\leftarrow$  vector of empty sets
level  $\leftarrow$  1 // Initialize level counter
result[level]  $\leftarrow$   $S_1$  // Initialize top level scanners
forall the scanners in  $S_1$  do
| G.visit(scanner) // Mark scanner vertex in  $G$  as visited
end
// Initialization done, start to process graph  $G$ 
while number of unvisited vertices in  $G > 0$  do
| forall the vertices of current level do
| | forall the adjacents of current vertex do
| | | if adjacent is unvisited then
| | | | result[level].append(adjacent)
| | | | G.visit(adjacent) // Mark adjacent as visited
| | | end
| | end
| end
| level  $\leftarrow$  level + 1 // Increase counter for next level
end
return result

```

---

graph that represents the sensor network with scanners as nodes and connections between them as edges. The second parameter is the set of scanners that are closest to the location of our system. Those scanners are assigned the highest rank.

During run time, our algorithm visits all adjacent nodes of the current rank that have not been accessed yet and assigns them the next lower rank. Once all nodes have been accessed, our algorithm terminates and returns the obtained rank structure. With this structure, the CEN is capable of assessing all scanner power levels reported for a specific system operation location applying (8.1). Furthermore, we are able to define RSQ thresholds to classify alternative frequencies into, e.g., high, good, moderate, or low quality and use this classification during frequency planning.

### 8.3.2 Evaluation

To evaluate our proposed scheme, we use real-world traces conducted during our measurement campaign described in Chapter 7. Particularly, we choose a trace measured on September, 11th 2013 that shows a mobile device moving around the exhibition halls. A graphical representation of the scanners, two supposed locations for system operation, and an estimated trajectory of the moving device within

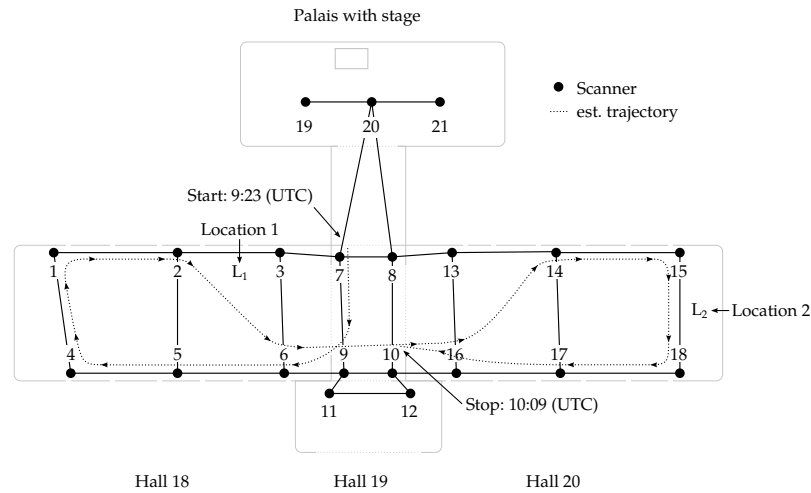


Figure 8.5: Graph representation of the C-PMSE spectrum scanner network with two assumed system operation locations  $L_1$  and  $L_2$  as well as an estimated trajectory of a moving transmitter during the IFA on September, 11th 2013.

the spectrum scanner network is depicted in Figure 8.5. For the estimation of the trajectory, we considered the scanner reporting the strongest power level at a certain time stamp.

Remember, the interpretation of spectrum data depends on the location of our system within the scanning network. If we consider the locations  $L_1$  and  $L_2$ , the ranking algorithm results in a lookup table as given in Table 8.1. For a location, this table prescribes a level for each scanner and how the reported spectrum data of them is ranked. For example, at location  $L_1$  the spectrum data from scanners 2 and 3 obtain the highest priority while the data reported from scanner 18 obtains the lowest priority.

In the following, we compute the quality of two alternative frequencies over time according to our proposed RSQ scheme for both locations and depict it in Figure 8.6. In the beginning, both frequencies achieve a high-quality rating because the reported power level from all scanners is close to the noise floor. At 9:23 (UTC) the interfering device was turned on at  $f_1=761.300$  MHz, and the quality at both locations decreases. During the walk towards location  $L_1$ , the quality at  $L_1$  decreases while at location  $L_2$  the quality increases due to the lower priority of scanners in hall 18. After entering hall 20, however, the opposite quality behavior at both locations can be observed. At 10:09 (UTC) the device was turned off and the quality returns to a high-quality rating at both locations. We observe that our quality rating follows the trajectory in a very precise way. The second alternative frequency  $f_2=762.300$  MHz is plotted as a reference. It achieves a high-quality rating at all time because it was not disturbed at any location.

Table 8.1: Lookup table for evaluation of scanner data.

Level	Location L1	Location L2
1	2,3	15,18
2	1,5,6,7	14,17
3	4,8,9,20	13,16
4	10,11,13,19,21	8,10
5	12,14,16	7,9,12,20
6	15,17	3,6,11,19,21
7	18	2,5
8	-	1,4

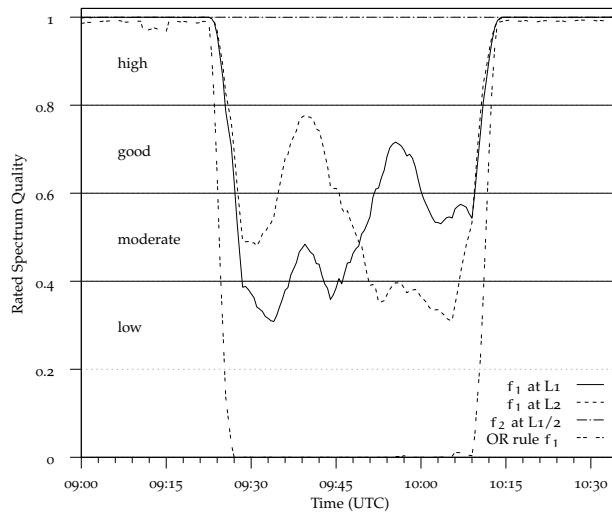


Figure 8.6: Rating of two candidate frequencies for different operation locations with our proposed RSQ scheme. The quality of the first frequency varies with the position of the interferer in the exhibition halls while the second is not affected. In contrast, during the presence of the interferer the OR rule always reports a low quality.

In contrast, if the CEN was performing the OR fusion rule, it would always determine a low-quality because at least one scanner in the network will report a high power level as long as the interferer is present. For example, the mapped quality for  $f_1$  at L2 between 9:30 and 9:45 (UTC) would be underestimated by a low-quality level although the interfering device is far away from the system and an operation could be possible. This weakness exacerbates especially for spatially large spectrum scanner networks which are, however, required to guarantee for an early detection of interfering devices to enable a proactive system operation.

We conclude that with our proposed spectrum rating scheme, a CEN is aware of the current quality level of all observed spectrum resources at any time. Further, it is capable of determining the quality of alternative frequencies in a high precision. Note that the definition of a quality threshold depends on the particular LQI decrease of the operated PMSE system and is, therefore, a vendor-specific parameter.

## CONCLUSION AND OUTLOOK

---

In this thesis, we investigated the future challenges for wireless systems caused by a mostly deregulated radio spectrum. This deregulation aims to increase the spectrum efficiency in several frequency bands by allowing the use of unoccupied resources as long as primary services are not harmfully interfered. Wireless systems, which operate in these environments and are not classified as primary services, are called Cognitive Radios.

Such Cognitive Radios implement several protection mechanisms. However, there remains the probability to misinterpret a radio spectrum situation. It follows that systems with outstanding quality requirements regarding data loss and delay, such as professional wireless microphone systems and associated audio devices, require an efficient way to determine precisely and immediately react to sudden interference that disturbs their transmissions.

In this thesis, we have identified the complexity of the underlying frequency allocation problem for these systems and have shown that this allocation problem is almost challenging nowadays. Due to the internal constraints of adjacent-channel and IM adjacent-channel interference, it cannot be solved by a complete enumeration in deterministic polynomial time. Furthermore, the introduction of Cognitive Radios adds an additional constraint of co-channel interference to the problem. This co-channel interference can suddenly occur. Hence, the corresponding constraint now becomes highly dynamic.

The state-of-the-art frequency planning approach requires a specific pattern of unoccupied radio spectrum. We cannot rely on discovering this exact pattern once the regulation regime has changed. During the problem classification, we further identified that there is a general design trade-off during the frequency allocation. So we can find either allocations with constant quality and varying link numbers or varying quality with constant link numbers. Therefore, we developed and evaluated two distinct allocation approaches based on a constructive and local-search strategy that adapts to any given spectrum situation providing solutions for both design alternatives.

Following these investigations, we moved the focus from frequency allocation to information retrieval about the currently faced situation of the system. Therefore, we installed 21 spectrum sensors on the fairground of the Messe Berlin and performed measurements during a large fair event, namely the International Radio Exhibition 2013. Based on these measurements, we identified the current spectrum

occupation and derived general design aspects for such a grid at other locations using spatial correlation.

In the next step, we combined our frequency allocation approaches and scanning grid in a decision-making engine that permanently acquires new data and takes actions to cope with interference threats. Our proposed design enables to replace the performed frequency allocation schemes to select the best one suited for the current situation.

Furthermore, we identified that the rating of alternative frequencies becomes inaccurate in spatial large spectrum scanning networks. This is, because existing rating rules also take into account interferers that reside at distant locations and thus, will not disturb the operation of our system. Therefore, we presented a location based ranking scheme that recognizes these situations and enable a much more accurate rating.

All experiments considered extreme cases for operation. Firstly, our frequency planning is done to allocate the maximum number of devices in the given radio spectrum, and we considered 64 links in a bandwidth of 72 MHz as upper evaluation benchmark. Secondly, an interfering device is turned on just in front of the system, which requires an immediate action. Finally, we assume an unlicensed radio spectrum in which only the transmission power is limited. Hence, the presented approaches are also capable of covering use cases that are not as challenging but be more likely in reality. That is, less allocated devices, a slowly upcoming interferer, or a more restricted radio spectrum regulation.

Throughout this thesis, we solved the technical problem of dynamic frequency allocation for wireless systems facing the complex constraint of IM in a possibly rapidly changing radio spectrum. We provided strategies to solve this problem efficiently and evaluated them with real-world data. Nevertheless, finding the specific rules for a new regulation regime of the radio spectrum is a political process that has to consider the interests of several user groups and reconcile them. This, however, is out of scope of this thesis.

Finally, we give an outlook on further topics for investigation we identified as future work. The most interesting aspect of research would be the tuning of the local-search approach, i.e., the neighbor function of our Simulated Annealing. For example, we could investigate the possibility of recognizing forbidden steps that have already been performed. At first sight, this is very challenging but combines the strengths of Simulated Annealing and Taboo Search, which is a further powerful metaheuristic.

Besides this research topic, there are also implementation issues to convert our presented approaches into a real-world application. As already mentioned in Chapter 3, a parallelization of our local-search algorithm will obtain more results in a given time of which a solution can be selected from. Further, the shape of our used utility functions

needs to be approved by hardware-specific measurements, i.e., the local-search utility functions  $u_B(d_c)$  and  $u_D(d_3)$ , and the quality of a certain power level  $m(p)$  to rate an individual frequency bin.





Part II

APPENDIX





## OBTAINED ALLOCATIONS

---

In the following, we depict the best allocations obtained by the EFF and SA approach. Note that the allocations for 8 MHz can also act as the basis for the replication approach described in Section 5.1. A corresponding frequency  $f_i$  in [MHz] is calculated from the tables as follows:

$$f_i = f_l + a_i \cdot s,$$

where  $f_l$  denotes the lowest operation frequency of the system in [MHz],  $a_i$  the element at slot index  $i$  from the considered allocation  $A$ , and  $s$  the slot size. In our allocations, we used a slot size of  $s = 25$  kHz.

Table A.1 Best allocations achieved by EFF as described in Section 5.3.2.

B [MHz]	Allocation
8	LQ 4, 20, 41, 57, 83, <b>104</b> , 120, 141, 172, 193, 209, 230, 256, 272, 293, 309
	HQ 4, 28, 60, 84, 124, <b>156</b> , 180, 212, 260, 292, 316
24	LQ 4, 20, <b>52</b> , 68, 89, 105, 137, 153, 179, 195, 227, 243, 264, 280, 312, 328, 497, 513, 545, 561, 582, 598, 630, 646, 672, 688, 720, 736, 757, 773, 805, 821
	HQ 4, 28, 60, 84, 124, 148, <b>196</b> , 228, 252, 284, 324, 348, 404, 436, 492, 516, 604, 652, 740, 764, 796, 820, 892, 916
32	LQ 4, 20, 41, 57, 83, <b>115</b> , 131, 152, 168, 194, 215, 231, 289, 321, 337, 358, 400, 416, 437, 453, 532, 579, 596, 732, 764, 785, 843, 860, 891, 917, 969, 1032, 1055, 1083, 1159, 1180, 1226, 1244
	HQ 4, 28, <b>76</b> , 100, 132, 156, 204, 228, 268, 292, 340, 364, 396, 420, 468, 492, 748, 772, 820, 844, 876, 900, 948, 972, 1012, 1036, 1084, 1108, 1140, 1164, 1212, 1236
72	LQ 4, 20, <b>52</b> , 68, 89, 105, 137, 153, 179, 195, 227, 243, 264, 280, 312, 328, 497, 513, 545, 561, 582, 598, 630, 646, 672, 688, 720, 736, 757, 773, 805, 821, 1483, 1499, 1531, 1547, 1568, 1584, 1616, 1632, 1658, 1674, 1706, 1722, 1743, 1759, 1791, 1807, 1976, 1992, 2024, 2040, 2061, 2077, 2109, 2125, 2151, 2167, 2199, 2215, 2236, 2252, 2284, 2300
	HQ 4, 28, 60, 84, 124, 148, 180, 204, 252, 308, 340, 388, 452, 484, 508, 540, 604, 636, 684, 796, 852, 924, 948, 1036, 1132, 1236, 1300, 1324, 1376, 1404, 1476, 1604, 1636, <b>1708</b> , 1740, 1980, 2052, 2188, 2228, 2276, 2332, 2372, 2428, 2460, 2508, 2652, 2676, 2708, 2836, 2860

Note: A bold number indicates the first allocated slot.

Table A.2 Best EFF allocations for different interference scenarios as presented in Section 5.4 (bandwidth: 72 MHz).

Scenario	Allocation
(a)	LQ 324, 340, <b>372</b> , 388, 409, 425, 457, 473, 499, 515, 547, 563, 584, 600, 632, 648, 817, 833, 865, 881, 902, 918, 950, 966, 992, 1008, 1040, 1056, 1077, 1093, 1125, 1141, 1803, 1819, 1851, 1867, 1888, 1904, 1936, 1952, 1978, 1994, 2026, 2042, 2063, 2079, 2111, 2127, 2296, 2312, 2344, 2360, 2381, 2397, 2429, 2445, 2471, 2487, 2519, 2535, 2556, 2572, 2604, 2620
	HQ 324, 348, 380, 404, 444, <b>469</b> , 516, 548, 572, 604, 644, 724, 756, 780, 852, 892, 1020, 1052, 1076, 1172, 1196, 1244, 1276, 1332, 1364, 1444, 1516, 1852, 1892, 2028, 2052, 2100, 2236, 2292, 2332, 2356, 2396, 2468, 2492, 2524, 2548, 2596, 2676, 2788, 2844, 2876
(b)	LQ 644, 660, <b>692</b> , 708, 729, 745, 777, 793, 819, 835, 867, 883, 904, 920, 952, 968, 1137, 1153, 1185, 1201, 1222, 1238, 1270, 1286, 1312, 1328, 1360, 1376, 1397, 1413, 1445, 1461, 2123, 2139, 2171, 2187, 2208, 2224, 2256, 2272, 2298, 2314, 2346, 2362, 2383, 2399, 2431, 2447, 2616, 2632, 2664, 2680, 2701, 2717, 2749, 2765, 2791, 2807, 2839, 2855, 2876
	HQ 644, 668, 700, 724, 764, 788, 820, 844, 892, 948, 980, 1028, <b>1096</b> , 1124, 1180, 1204, 1276, 1324, 1364, 1396, 1420, 1500, 1532, 1652, 1868, 1916, 1956, 1988, 2012, 2132, 2164, 2188, 2228, 2284, 2428, 2452, 2564, 2596, 2684, 2780, 2836, 2860
(c)	LQ 964, 980, <b>1012</b> , 1028, 1049, 1065, 1097, 1113, 1139, 1155, 1187, 1203, 1224, 1240, 1272, 1288, 1457, 1473, 1505, 1521, 1542, 1558, 1590, 1606, 1632, 1648, 1680, 1696, 1717, 1733, 1765, 1781, 2443, 2459, 2491, 2507, 2528, 2544, 2576, 2592, 2618, 2634, 2666, 2682, 2703, 2719, 2751, 2767
	HQ 964, 988, 1020, 1044, 1084, 1108, 1156, 1188, 1212, <b>1260</b> , 1284, 1372, 1396, 1428, 1452, 1492, 1516, 1564, 1628, 1652, 1956, 1980, 2028, 2052, 2132, 2156, 2188, 2228, 2252, 2364, 2388, 2436, 2556, 2580, 2668, 2692, 2764, 2788

Note: A bold number indicates the first allocated slot. Note further that the low-quality allocation from the interference-free case is shifted right, and all links, that cross the boundary at 2880, are removed. That is because all gathered low-quality allocations start with the same first slot (here: 52). However, regarding high-quality allocations, this slot is different.

Table A.3 Best allocation achieved by Simulated Annealing as presented in Section 6.5 (bandwidth: 72 MHz).

Situation	Allocation
before interference occurs	20, 57, 104, 120, 172, 193, 209, 272, 293, 660, 681, 697, 723, 744, 760, 781, 812, 833, 849, 870, 896, 933, 1940, 1961, 1977, 2003, 2024, 2040, 2061, 2092, 2113, 2129, 2150, 2176, 2192, 2213, 2564, 2580, 2601, 2617, 2643, 2664, 2680, 2701, 2732, 2753, 2769, 2790, 2816, 2832, 2853, 2869
after optimization	20, 57, 104, 120, 172, 193, 209, 272, 293, 375, 421, 451, 558, 582, 620, 1069, 1251, 1660, 1692, 1710, 1754, 1802, 1940, 1961, 1977, 2003, 2024, 2040, 2061, 2092, 2113, 2129, 2150, 2176, 2192, 2213, 2564, 2580, 2601, 2617, 2643, 2664, 2680, 2701, 2732, 2753, 2769, 2790, 2816, 2832, 2853, 2869

## SHIFT EXAMPLE

---

In the following example, we explain our data representation from Chapter 6 in detail by shifting the third link ( $k=3$ ) with an offset  $o = 5$  to the right. Our given allocation  $A$  hosts  $n = 3$  links and results after the shift operation in allocation  $A'$ :

$$A = \begin{pmatrix} 0 & 16 & 32 \end{pmatrix} \quad A' = \begin{pmatrix} 0 & 16 & \mathbf{37} \end{pmatrix}.$$

With this, we find the distances  $b_{i,j} = a_i - a_j$  between each link pair  $a_i, a_j$  for  $a_i \neq a_j \in A$  and  $i > j$ . Those distances can be written as the matrix  $B$  of size  $3 \times 3$ , with  $b_{i,j}$  its elements.

Considering  $B$ , the shift operation only affects the third row as we assumed this link to be shifted. So, we obtain  $B'$  as the distance matrix after shifting the third link by the offset with  $B$  the initial matrix of the distances:

$$B = \begin{pmatrix} \infty & 0 & 0 \\ 16 & \infty & 0 \\ 32 & 16 & \infty \end{pmatrix} \quad B' = \begin{pmatrix} \infty & 0 & 0 \\ 16 & \infty & 0 \\ \mathbf{37} & \mathbf{21} & \infty \end{pmatrix}.$$

The link distance utilities  $e_i$  can be calculated, e.g., for the first link as

$$e_1 = \sum_{j=2}^n u_B(b_{j,1}) = u_B(16) + u_B(32) = 10 + 10 = 20$$

resulting in

$$E = \begin{pmatrix} 20 & 20 & 20 \end{pmatrix} \quad E' = \begin{pmatrix} 20 & 20 & 20 \end{pmatrix}.$$

Here, the shift operation does not affect the utilities  $e_i$  of  $E$  since the initial values were already the maximum ones.

Having determined the distances between links and the resulting utilities, we calculate the IMPs applying (6.2), e.g.,

$$c_{2,1} = 2a_2 - a_1 = 2 \cdot 16 - 0 = 32.$$

The shift operation causes each element in the third column/row of  $C$  to be decremented/incremented by the offset and double the offset, respectively. So the initial  $C$  becomes  $C'$ :

$$C = \begin{pmatrix} \infty & -16 & -32 \\ 32 & \infty & 0 \\ 64 & 48 & \infty \end{pmatrix} \quad C' = \begin{pmatrix} \infty & -16 & \mathbf{-37} \\ 32 & \infty & \mathbf{-5} \\ \mathbf{74} & \mathbf{58} & \infty \end{pmatrix}.$$

Using  $A$  and  $C$ , we can calculate the distances between IMPs and links by applying (6.3), e.g.,

$$d_{2,1} = c_{2,1} \cdot H^T - A^T = 32 \cdot H^T - A^T = (32 \ 16 \ 0)^T.$$

Note that  $d_{i,j}$  is a vector as it describes the distance of the IMP of links  $a_i$  and  $a_j$  to each link  $a_k$  in the allocation.

To update matrix  $D$ , the elements need to be incremented by a specific offset as defined in (6.8). Remind that this is required because the elements of  $D$  are defined as vectors of size  $n$ . Each vector element of the third column/row in the matrix is decremented/incremented by the offset and the double offset, respectively. Note that there is an exception for the third vector element of these columns/rows that must be decremented/incremented by the double offset and offset, respectively. Furthermore, the third vector element of all remaining matrix elements must be decremented by the offset value. We write the specific offset coefficients to update matrix  $D$  in matrix  $S$ :

$$D = \begin{pmatrix} \left( \begin{array}{c} \infty \\ \infty \\ \infty \end{array} \right) & \left( \begin{array}{c} -16 \\ -32 \\ -48 \end{array} \right) & \left( \begin{array}{c} -32 \\ -48 \\ -64 \end{array} \right) \\ \left( \begin{array}{c} 32 \\ 16 \\ 0 \end{array} \right) & \left( \begin{array}{c} \infty \\ \infty \\ \infty \end{array} \right) & \left( \begin{array}{c} 0 \\ -16 \\ -32 \end{array} \right) \\ \left( \begin{array}{c} 64 \\ 48 \\ 32 \end{array} \right) & \left( \begin{array}{c} 48 \\ 32 \\ 16 \end{array} \right) & \left( \begin{array}{c} \infty \\ \infty \\ \infty \end{array} \right) \end{pmatrix} \quad S = \begin{pmatrix} \left( \begin{array}{c} \infty \\ \infty \\ \infty \end{array} \right) & \left( \begin{array}{c} 0 \\ 0 \\ -1 \end{array} \right) & \left( \begin{array}{c} -1 \\ -1 \\ -2 \end{array} \right) \\ \left( \begin{array}{c} 0 \\ 0 \\ -1 \end{array} \right) & \left( \begin{array}{c} \infty \\ \infty \\ \infty \end{array} \right) & \left( \begin{array}{c} -1 \\ -1 \\ -2 \end{array} \right) \\ \left( \begin{array}{c} 2 \\ 2 \\ 1 \end{array} \right) & \left( \begin{array}{c} 2 \\ 2 \\ 1 \end{array} \right) & \left( \begin{array}{c} \infty \\ \infty \\ \infty \end{array} \right) \end{pmatrix}.$$

By using the coefficients of  $S$ , we determine the new distances, e.g., of element  $d_{2,1}$  of matrix  $D$  as

$$d'_{2,1} = d_{2,1} + 0 \cdot s_{2,1} = (32 \ 16 \ 0)^T + 5(0 \ 0 \ -1)^T = (32 \ 16 \ -5)^T.$$

With the help of  $S$ , we evaluate all matrix elements of  $D$  resulting in  $D'$  holding the new distances:

$$D' = \begin{pmatrix} \left( \begin{array}{c} \infty \\ \infty \\ \infty \end{array} \right) & \left( \begin{array}{c} -16 \\ -32 \\ -53 \end{array} \right) & \left( \begin{array}{c} -37 \\ -53 \\ -74 \end{array} \right) \\ \left( \begin{array}{c} 32 \\ 16 \\ -5 \end{array} \right) & \left( \begin{array}{c} \infty \\ \infty \\ \infty \end{array} \right) & \left( \begin{array}{c} -5 \\ -21 \\ -42 \end{array} \right) \\ \left( \begin{array}{c} 74 \\ 58 \\ 37 \end{array} \right) & \left( \begin{array}{c} 58 \\ 42 \\ 21 \end{array} \right) & \left( \begin{array}{c} \infty \\ \infty \\ \infty \end{array} \right) \end{pmatrix}.$$

We find the individual utility between one IMP and a link, e.g., for element  $d_{2,1}$  of matrix  $D$  before the shift operation is performed as

$$\sum_n u_D(d_{2,1}) = u_D(32) + u_D(16) + u_D(0) = 3 + 3 - 4 = 2.$$

After the shift operation, we find the individual utility for element  $d'_{2,1}$  of matrix  $D'$  as

$$\sum_n u_D(d'_{2,1}) = u_D(32) + u_D(16) + u_D(-5) = 3 + 3 + 3 = 9.$$



With this, the overall utility of, e.g., the first link results in

$$f'_1 = \sum_{j=2}^n \sum_n (u_D(d'_{j,1}) + u_D(d'_{1,j})) = 9 + 9 + 9 + 9 = 36.$$

To this end, the shift influences the utility in a positive way, and the new allocation achieves the maximum utility, i.e., IM-freeness:

$$F = \begin{pmatrix} 29 & 22 & 29 \end{pmatrix} \quad F' = \begin{pmatrix} \mathbf{36} & \mathbf{36} & \mathbf{36} \end{pmatrix}.$$

During the selection of a link to shift, we observe that all utility values of  $E$  achieve the maximum value. This observation indicates that in the current allocation there is no adjacent-channel interference present. Thus, in this case the utility values of  $E$  do not indicate a candidate link to shift.

Regarding the utility values of  $F$ , we find that these values are not at their maximum and it follows that there is IM adjacent-channel interference present. To select a candidate, we could use the one that achieves the lowest utility which is in this case link  $a_2$  at slot 16. However, as we observe from the outcome of this example, the lowest utility does not indicate a suitable shift candidate in any case. As demonstrated, in the best case the shift of the third link with an offset of 5 to the right only requires a single shift operation to obtain an IM-free allocation.

To cope with this wrong candidate indication, the neighbor function of the presented SA scheme picks all links with the  $m$ -th lowest utility as possible candidates. For example, with  $m = 2$  all links, that obtain the second worst utility value or less, are selected as possible candidates to shift. In the presented shift example, the second worst utility value in  $F$  is 29 which results in a candidate set containing all links. The parameter  $m$  offers the scheme a large degree of freedom during operation to improve the given allocation and minimize IM adjacent-channel interference.



## BIBLIOGRAPHY

---

- [1] Boost C++ Libraries, 2014. URL <http://www.boost.org>.
- [2] Karen I. Aardal, Stan P.M. Van Hoesel, Arie M.C.A. Koster, Carlo Mannino, and Antonio Sassano. Models and Solution Techniques for Frequency Assignment Problems. *Ann. of Operations Research*, 153:79–129, 2007.
- [3] Ian F. Akyildiz, Won-Yeol Lee, Mehmet C. Vuran, and Shantidev Mohanty. NeXt generation/dynamic spectrum access/cognitive radio wireless networks: A survey. *Computer Networks*, 50(13):2127–2159, 2006.
- [4] Inder J. Bahl. *Fundamentals of RF and Microwave Transistor Amplifiers*. Wiley, 2009.
- [5] Lars Berlemann and Stefan Mangold. *Cognitive Radio and Dynamic Spectrum Access*. Wiley, 2009.
- [6] Uwe Beutnagel-Buchner, Norbert Hilbich, and Andreas Wilzeck. C-PMSE - Improved Spectrum Utilization and Coexistence by Cognitive PMSE Systems: A Strategic Application-oriented Research & Development Project in Germany. In *Int'l ICST Conf. CrownCom*, June 2011.
- [7] Ezio Biglieri, Andrea J. Goldsmith, Larry J. Greenstein, Narayan Mandayam, and Vincent H. Poor. *Principles of Cognitive Radio*. Cambridge University Press, 2012.
- [8] Christian Blum and Andrea Roli. Metaheuristics in combinatorial optimization: Overview and conceptual comparison. *ACM Comput. Surv.*, 35(3):268–308, September 2003.
- [9] Johannes Brendel, Steffen Riess, Andreas Stoeckle, Rafael Rummel, and Georg Fischer. A Spectrum Sensing Network for Cognitive PMSE Systems. *Frequenz*, 66(9-10):269–277, September 2012.
- [10] Johannes Brendel, Steffen Riess, Robert Weigel, and Georg Fischer. A Cognitive System for Future-Proof Wireless Microphones: Concept, Implementation and Results. In *Int'l Conf. on Telecommun. in Modern Satellite, Cable and Broadcast. Services*, October 2013.
- [11] Johannes Brendel, Axel Schmidt, and Georg Fischer. A Link Quality Indicator for Analog FM Transmission Systems. In *7th Int'l Conf. on Signal Process. and Commun. Syst.*, December 2013.

- [12] Frank Buschmann, Regine Meunier, Hans Rohnert, Peter Sommerlad, and Michael Stal. *Pattern-Oriented Software Architecture, Volume 1: A System of Patterns*. Wiley, 1996.
- [13] Martin Cave, Chris Doyle, and William Webb. *Essentials of Modern Spectrum Management*. Cambridge University Press, 2007.
- [14] Cisco. Cisco Visual Networking Index: Global Mobile Data Traffic Forecast Update, 2012–2017. *Cisco White Paper*, February 2013.
- [15] Clay Mathematics Institute. P vs. NP Problem, 2014. URL <http://www.claymath.org/millennium-problems/p-vs-np-problem>.
- [16] Paolo Colantonio, Franco Giannini, and Ernesto Limiti. *High Efficiency RF and Microwave Solid State Power Amplifiers*. Microwave and Optical Engineering. Wiley, 2009.
- [17] Stephen A. Cook. The Complexity of Theorem-Proving Procedures. In *Proc. of the third annu. ACM Symp. on Theory of Computing*. ACM, 1971.
- [18] James W. Cooley and John W. Tukey. An Algorithm for the Machine Calculation of Complex Fourier Series. *Math. Comp.*, 19(90):297–301, 1965.
- [19] Aleksandar Damnjanovic, Juan Montojo, Yongbin Wei, Tingfang Ji, Tao Luo, Madhavan Vajapeyam, Yoo Taesang, Song Osok, and Durga Malladi. A Survey on 3GPP Heterogeneous Networks. *IEEE Trans. Wireless Commun.*, 18(3):10–21, June 2011.
- [20] Sven Dortmund and Ilona Rolfes. Stochastic Frequency List Generation for Inter-Intermodulation Free Allocation of Professional Wireless Microphone Systems. In *German Microwave Conf.*, March 2009.
- [21] Linda E. Doyle. *Essentials of Cognitive Radio*. Cambridge University Press, 2009.
- [22] ECC. ECC Report 185 (complementary to ECC Report 159): Further Definition of Technical and Operational Requirements for the Operation of White Space Devices in the Band 470–790 MHz. *CEPT*, January 2013.
- [23] R. Edwards, J. Durkin, and Derek H. Green. Selection of intermodulation-free frequencies for multiple-channel mobile radio systems. *Proc. of the Institution of Electrical Engineers*, 1969.
- [24] Andreas Eisenblätter and Arie M.C.A. Koster. FAP web - A website about Frequency Assignment Problems, 2000-2007. URL <http://fap.zib.de>.

- [25] Erhan Erkut. The discrete p-dispersion problem. *European Journal of Operational Research*, 46(1):48–60, 1990.
- [26] EN 300 422-1 V1.3.2: *Wireless microphones in the 25 MHz to 3 GHz frequency range; Part 1: Technical characteristics and methods of measurement*. ETSI, March 2008.
- [27] TR 102 799 V1.1.1: *Operation methods and principles for spectrum access systems for PMSE technologies and the guarantee of a high sound production quality on selected frequencies utilising cognitive interference mitigation techniques*. ETSI, June 2010.
- [28] FCC. *Second Rep. and Order and Memorandum Opinion and Order, ET Docket No. 08-260*. FCC, November 2008.
- [29] FCC. *Second Memorandum Opinion and Order, ET Docket No. 10-174*. FCC, September 2010.
- [30] FCC. *Third Memorandum Opinion and Order, ET Docket No. 12-36*. FCC, April 2012.
- [31] Jean Baptiste Joseph Fourier. *Théorie analytique de la chaleur*. 1822.
- [32] Ghurumuruhan Ganesan and Ye Li. Cooperative Spectrum Sensing in Cognitive Radio Networks. In *1st IEEE Int'l Symp. on New Frontiers in Dynamic Spectrum Access Networks*, November 2005.
- [33] Michael R. Garey and David S. Johnson. *Computers and Intractability: A Guide to the Theory of NP-Completeness*. W. H. Freeman, 1979.
- [34] Fred Glover. Future Paths for Integer Programming and Links to Artificial Intelligence. *Computers & Operations Research*, 13(5): 533–549, 1986.
- [35] James S. Graham, Roberto Montemanni, Jim N. J. Moon, and Derek H. Smith. Frequency assignment, multiple interference and binary constraints. *Wireless Networks*, 14(4):449–464, 2008.
- [36] Daniel Gruner. *HF-Leistungsverstärker in modernen Silizium- und Verbindungshalbleiter-Technologien*. PhD thesis, TU Berlin, 2012.
- [37] William K. Hale. Frequency Assignment: Theory and Applications. *Proc. IEEE*, 68(12):1497–1514, 1980.
- [38] Garrett Hardin. The Tragedy of the Commons. *Science*, 162 (3859):1243–1248, 1968.
- [39] Kate Harrison, Shridhar Mubaraq Mishra, and Anant Sahai. How Much White-Space Capacity Is There? In *IEEE Symp. on New Frontiers in Dynamic Spectrum*, April 2010.

- [40] Ralph V. L. Hartley. Transmission of Information. *Bell System Technical J.*, 7(3):535–563, 1928.
- [41] Simon Haykin. Cognitive Radio: Brain-Empowered Wireless Communications. *IEEE J. Sel. Areas Commun.*, 23(2):201–220, 2005.
- [42] John H. Holland. *Adaptation in Natural and Artificial Systems: An Introductory Analysis with Applications to Biology, Control, and Artificial Intelligence*. Univ. of Michigan Press, 1975.
- [43] Oliver Holland, Pascal Cordier, Markus Mück, Laurent Mazet, Clemens Klöck, and Tobias Renk. Spectrum Power Measurements in 2G and 3G Cellular Phone Bands during the 2006 Football World Cup in Germany. In *Proc. IEEE DySPAN*, April 2007.
- [44] Stephen Hurley and Derek H. Smith. Fixed Spectrum Frequency Assignment Using Natural Algorithms. In *1st Int'l Conf. on Genetic Algorithms in Eng. Syst.: Innovations and Applicat.*, 1995.
- [45] Stephen Hurley, S. U. Thiel, and Derek. H. Smith. A Comparison of Local Search Algorithms for Radio Link Frequency Assignment Problems. In *Proc. of the 1996 ACM Symp. on Appl. Computing*, pages 251–257. ACM, 1996.
- [46] Stephen Hurley, Derek H. Smith, and S. U. Thiel. FASoft: A system for discrete channel frequency assignment. *Radio Science*, 1997.
- [47] Maria Stella Iacobucci. *Reconfigurable Radio Systems: Network Architectures and Standards*. Wiley, 2013.
- [48] IEEE. *Cognitive Wireless RAN Medium Access Control (MAC) and Physical Layer (PHY) Specifications: Policies and Procedures for Operation in the TV Bands (IEEE Std. 802.22-2011)*. Institute of Electrical and Electronics Engineers, Inc., July 2011.
- [49] IEEE. *Wireless LAN Medium Access Control (MAC) and Physical Layer (PHY) Specifications Amendment 5: Television White Spaces (TVWS) Operation (ANSI/IEEE Std. 802.11af-2013)*. Institute of Electrical and Electronics Engineers, Inc., December 2013.
- [50] IEEE. *IEEE Standard for Local and Metropolitan Area Networks: Overview and Architecture (IEEE Std. 802-2014)*. Institute of Electrical and Electronics Engineers, Inc., June 2014.
- [51] IEEE. *Low-Rate Wireless Personal Area Networks (LR-WPANs) - Amendment 6: TV White Space Between 54 MHz and 862 MHz Physical Layer (IEEE Std. 802.15.4m-2014)*. Institute of Electrical and Electronics Engineers, Inc., April 2014.

- [52] Md Habibul Islam, Choo Leng Koh, Ser Wah Oh, Xianming Qing, Yoke Yong Lai, Cavin Wang, Ying-Chang Liang, Bee Eng Toh, Francois Chin, Geok Leng Tan, and William Toh. Spectrum Survey in Singapore: Occupancy Measurements and Analyses. In *Proc. Int'l ICST Conf. CrownCom*, May 2008.
- [53] Anand Iyer, Krishna Chintalapudi, Vishnu Navda, Ramachandran Ramjee, Venkata N. Padmanabhan, and Chandra R. Murthy. SpecNet: Spectrum Sensing Sans Frontières. In *Proc. USENIX conf. Networked Syst. Design and Implementation*, March 2011.
- [54] Richard M. Karp. Reducibility Among Combinatorial Problems. In *Complexity of Computer Computations*. Plenum Press, 1972.
- [55] Scott Kirkpatrick, C. Daniel Gelatt, Jr., and Mario P. Vecchi. Optimization by Simulated Annealing. *Science*, 1983.
- [56] Christoph König and M. D. Perez-Guirao. A Cognitive Engine Architecture for Professional Wireless Microphone Systems. In *Int'l Conf. on Computing, Networking and Commun., CNC Workshop*. IEEE, 2015.
- [57] Christoph König, Michael Bredel, and M. D. Perez Guirao. Spectrum-Aware Frequency Planning for Professional Wireless Microphone Systems. In *IEEE Int'l Multi-Disciplinary Conf. on Cognitive Methods in Situation Awareness and Decision Support*, February 2013.
- [58] Christoph König, M. D. Perez Guirao, and Ralf Lübben. Distributed Indoor Spectrum Occupancy Measurements in the UHF TV Band. In *IEEE Int'l Conf. on Commun.*, June 2014.
- [59] Christoph König, Tobias Linde, and M. D. Perez-Guirao. Dynamic Frequency Allocation for Professional Wireless Microphone Systems. In *IEEE Consumer Commun. and Networking Conf. (MC)*. IEEE, 2015.
- [60] Arie M. C. A. Koster. *Frequency Assignment - Models and Algorithms*. PhD thesis, Maastricht University, 1999.
- [61] Herbert L. Krauss, Charles W. Bostian, and Frederick H. Raab. *Solid State Radio Engineering*. Wiley, 1980.
- [62] William Krenik and Anuj Batra. Cognitive Radio Techniques for Wide Area Networks. In *Proc. 42nd Design Automation Conf.* IEEE, 2005.
- [63] Bin Le, Thomas W. Rondeau, and Charles W. Bostian. Cognitive Radio Realities. *Wireless Commun. and Mobile Computing*, 7(9): 1037–1048, 2007.

- [64] Miguel López-Benítez and Fernando Casadevall. Methodological Aspects of Spectrum Occupancy Evaluation in the Context of Cognitive Radio. *European Trans. on Telecommun.*, 21(8):680–693, May 2010.
- [65] Miguel López-Benítez, Anna Umbert, and Fernando Casadevall. Evaluation of Spectrum Occupancy in Spain for Cognitive Radio Applications. In *Proc. IEEE VTC*, April 2009.
- [66] M. N. Lustgarten. A Method for Computing Intermodulation-Free Frequency Lists. In *IEEE Electromagnetic Compatibility Symp. Rec.*, July 1968.
- [67] Mark A. McHenry, Peter A. Tenhula, Dan McCloskey, Dennis A. Roberson, and Cynthia S. Hood. Chicago Spectrum Occupancy Measurements & Analysis and a Long-term Studies Proposal. In *ACM Int'l Workshop on Technology and Policy for Accessing Spectrum*, August 2006.
- [68] Shridhar Mubaraq Mishra, Anant Sahai, and Robert W. Brodersen. Cooperative Sensing among Cognitive Radios. In *IEEE Int'l Conf. on Commun.*, June 2006.
- [69] Joseph Mitola, III. and Gerald Q. Maguire, Jr. Cognitive Radio: Making Software Radios More Personal. *IEEE Personal Commun. Mag.*, 6, August 1999.
- [70] Roberto Montemanni, Jim N. J. Moon, and Derek H. Smith. An Improved Tabu Search algorithm for the Fixed-Spectrum Frequency-Assignment Problem. *IEEE Trans. Veh. Technol.*, 52(4):891–901, July 2003.
- [71] Robert A. Murphey, Panos M. Pardalos, and Mauricio G. C. Resende. Frequency Assignment Problems. In *Handbook of Combinatorial Optimization*. Springer, 1999.
- [72] Norddeutscher Rundfunk. Broadcast Stations Germany, 2013. URL <http://www.ueberallfernsehen.de/dvbt175.html>.
- [73] NVIDIA Cooperation. Compute Unified Device Architecture (CUDA), 2014. URL <http://www.nvidia.com/cuda/>.
- [74] Openstreetmap.org. Map of the area Messe Berlin, 2013. URL <http://osm.org/go/0MZuRdLe>.
- [75] Alexandros Palaios, Janne Riihijärvi, Oliver Holland, Andreas Achtzehn, and Petri Mähönen. Measurements of Spectrum Use in London: Exploratory Data Analysis and Study of Temporal, Spatial and Frequency-Domain Dynamics. In *Proc. IEEE DySPAN*, October 2012.



- [76] Vilfredo Pareto. *Cours d'economie politique*. Librairie Droz, 1896.
- [77] John Parr and Dick Blandford. *Introduction to Digital Signal Processing*. Pearson Education, 2012.
- [78] Luis Fernando Pedraza, Felipe Forero, and Ingrid Paez. Metropolitan Spectrum Survey in Bogota Colombia. In *Proc. Int'l Conf. AINA*, May 2013.
- [79] Edward Peh and Ying-Chang Liang. Optimization for Cooperative Sensing in Cognitive Radio Networks. In *Proc. IEEE Wireless Commun. and Networking Conf.*, March 2007.
- [80] Maria Dolores Perez Guirao, Wolfgang Bilz, Edgar Reihl, Radu Circa, Axel Schmidt, and Georg Fischer. Cognitive Systems for the Professional Audio Industry: a Step Forward. In *Proc. of 6th Karlsruhe Workshop on Software Radio*, March 2010.
- [81] Project Office C-PMSE. Website of the C-PMSE project, 2014. URL <http://cpmse.research-project.de>.
- [82] Sekharipuram S. Ravi, Daniel J. Rosenkrantz, and Giri K. Tayi. Facility dispersion problems: Heuristics and special cases. In Frank Dehne, Jörg-Rüdiger Sack, and Nicola Santoro, editors, *Algorithms and Data Structures*, volume 519 of *Lecture Notes in Computer Science*, pages 355–366. Springer, 1991.
- [83] Sekharipuram S. Ravi, Daniel J. Rosenkrantz, and Giri K. Tayi. Heuristic and Special Case Algorithms for Dispersion Problems. *Operations Research*, 42(2):299–310, 1994.
- [84] Christian J. Rieser, Thomas W. Rondeau, Charles W. Bostian, Walling R. Cyre, and Timothy M. Gallagher. Cognitive Radio Engine based on Genetic Algorithms in a Network, October 2007. US Patent 7,289,972.
- [85] Steffen Riess, Johannes Brendel, Andreas Stoeckle, Richard Rose, and Georg Fischer. Concept of an UHF Band Receiver for Spectrum Sensing Applications. In *Proc. Int'l Symp. Signals, Syst., and Electron.*, October 2012.
- [86] Thomas W. Rondeau. *Application of Artificial Intelligence to Wireless Communications*. PhD thesis, Virginia Polytechnic Institute and State University, 2007.
- [87] Frank H. Sanders. Broadband Spectrum Surveys in Denver, CO, San Diego, CA, and Los Angeles, CA: Methodology, Analysis, and Comparative Results. In *Proc. IEEE Int'l Symp. EMC*, August 1998.

- [88] Simon Schroeter, Lars Zimmermann, Oliver Schwender, Georg Fischer, and Alexander Koelpin. Demonstrator of a Scanning Receiver Subsystem for Cognitive Professional Wireless Microphone Systems. In *Proc. Tech. Symp. ITU Telecom World*, October 2011.
- [89] Claude Elwood Shannon. Communication in the Presence of Noise. *Proc. of the IRE*, 37(1):10–21, 1949.
- [90] Claude Elwood Shannon. The Mathematical Theory of Communication. *Univ. Illinois*, 1949.
- [91] Derek H. Smith, Stuart M. Allen, Stephen Hurley, and W. J. Watkins. Frequency Assignment: Methods and Algorithms. In *Symp. on Frequency Assignment, Sharing and Conservation in Syst. (Aerospace)*, 1998.
- [92] Derek H Smith, Stuart M Allen, and Steve Hurley. Characteristics of Good Meta-Heuristic Algorithms for the Frequency Assignment Problem. *Ann. of Operations Research*, 107(1-4):285–301, 2001.
- [93] Derek H. Smith, Richard K. Taplin, and Stephen Hurley. Frequency Assignment with Complex Co-Site Constraints. *IEEE Trans. Electromagn. Compat.*, 43:210–218, 2001.
- [94] Jack Smith. *Modern Communication Circuits*. McGraw-Hill, 1986.
- [95] Kenneth Sörensen and Fred W. Glover. Metaheuristics. In *Encyclopedia of Operations Research and Management Science*, pages 960–970. Springer, 2013.
- [96] Andreas Stoeckle, Johannes Brendel, Steffen Riess, Richard Rose, and Georg Fischer. A low cost ultra-wide-band inverted F-antenna for Cognitive PMSE Systems. In *Proc. IEEE ICWITS*, November 2012.
- [97] Chin-Sean Sum, Gabriel Porto Villardi, Mohammad Azizur Rahman, Tuncer Baykas, Ha Nguyen Tran, Zhou Lan, Chen Sun, Yohannes Alemseged, Junyi Wang, Chunyi Song, et al. Cognitive Communication in TV White Spaces: An Overview of Regulations, Standards, and Technology. *IEEE Commun. Mag.*, 51(7):138–145, 2013.
- [98] Andrew S. Tanenbaum. *Computer Networks*. Prentice Hall Professional Technical Reference, 4th edition, 2002.
- [99] The European Commission. *Commission Decision 2009/766/EC on the harmonisation of the 900 and 1800 MHz frequency bands*. The European Commission, 2009. URL <http://eur-lex.europa.eu/LexUriServ/LexUriServ.do?uri=OJ:L:2009:274:0032:0035:EN:PDF>.

- [100] The European Commission. *Commission Decision 2011/251/EC amending Decision 2009/766/EC on the harmonisation of the 900 MHz and 1800 MHz frequency bands*. The European Commission, 2011. URL <http://eur-lex.europa.eu/LexUriServ/LexUriServ.do?uri=OJ:L:2011:106:0009:0010:EN:PDF>.
- [101] Jaap van de Beek, Janne Riihijärvi, Andreas Achtzehn, and Petri Mähönen. TV White Space in Europe. *IEEE Trans. Mobile Comput.*, 11(2):178–188, 2012.
- [102] Pramod K. Varshney. Elements of Detection Theory. In *Distributed Detection and Data Fusion*, pages 6–35. Springer, 1997.
- [103] Matthias Wellens, Jin Wu, and Petri Mähönen. Evaluation of Spectrum Occupancy in Indoor and Outdoor Scenario in the Context of Cognitive Radio. In *Proc. Int'l ICST Conf. CrownCom*, October 2007.
- [104] Xuhang Ying, Jincheng Zhang, Lichao Yan, Guanglin Zhang, Minghua Chen, and Ranveer Chandra. Exploring Indoor White Spaces in Metropolises. In *Proc. ACM MobiCom*, September 2013.
- [105] Wei Zhang, Ranjan K. Mallik, and Khaled Ben Letaief. Cooperative Spectrum Sensing Optimization in Cognitive Radio Networks. In *Proc. IEEE Int'l Conf. on Commun.*, May 2008.
- [106] Qing Zhao and Brian M. Sadler. A Survey of Dynamic Spectrum Access. *IEEE Signal Process. Mag.*, 24(3):79–89, May 2007.
- [107] Youping Zhao, Bin Le, and Jeffrey H. Reed. Network Support: The Radio Environment Map. *Cognitive Radio Technology*, pages 325–366, 2006.



## OWN PUBLICATIONS

---

- Hanwen Cao, Christoph König, Andreas Wilzeck, and M. D. Perez Guirao. Cognitive Agile Networking Testbed. In *IEEE Radio and Wireless Symp. (RWS)*. IEEE, 2010.
- Gerrit Buhe, Qipeng Cai, Hanwen Cao, Christoph König, Maria Dolores Perez Guirao, Axel Schmidt, and Andreas Wilzeck. Wireless Audio Transmission System, Particularly a Wireless Microphone System, September 2012. URL [http://www.patentlens.net/patentlens/patent/US\\_2012\\_0224713\\_A1/](http://www.patentlens.net/patentlens/patent/US_2012_0224713_A1/).
- Christoph König, Michael Bredel, and M. D. Perez Guirao. Spectrum-Aware Frequency Planning for Professional Wireless Microphone Systems. In *IEEE Int'l Multi-Disciplinary Conf. on Cognitive Methods in Situation Awareness and Decision Support (CogSIMA)*. IEEE, 2013.
- Christoph König, M. D. Perez Guirao, and Ralf Lübben. Distributed Indoor Spectrum Occupancy Measurements in the UHF TV Band. In *IEEE Int'l Conf. on Commun. (ICC)*. IEEE, 2014.
- Christoph König, Tobias Linde, and M. D. Perez Guirao. Dynamic Frequency Allocation for Professional Wireless Microphone Systems. In *IEEE Consumer Commun. and Networking Conf. (CCNC), Mini-Conference*. IEEE, 2015.
- Christoph König and M. D. Perez Guirao. A Cognitive Engine Architecture for Professional Wireless Microphone Systems. In *Int'l Conf. on Computing, Networking and Commun. (ICNC), CNC Workshop*. IEEE, 2015.



## CURRICULUM VITAE

---

Name	Christoph Jürgen König
Day of birth	May 28, 1979 in Bremen
<b>Education</b>	
since 07/2008	Research Assistant and Ph.D. student, Institute of Communications Technology, Leibniz Universität Hannover.  Research in the field of Cognitive Radio and Networks.
10/2003 – 06/2008	Studies: Industrial Engineering, Leibniz Universität Hannover.  Diplom thesis at the Institute of Communications Technology, Leibniz Universität Hannover, titled " <i>Simulation von Handover-Prozessen in IEEE 802.11 Infrastrukturnetzen</i> "

Student project at the Institute of Information Systems Research, Leibniz Universität Hannover, titled "*Training eines künstlichen neuronalen Netzes für die Detektion von Verkehrsschildern*"

06/1998

High school: Fachgymnasium Wirtschaft, Berufsbildende Schulen Zeven

### Work Experience

07/2002 – 09/2003

Systems Engineer for Application Development, EDS Deutschland GmbH, Bremen

08/1999 – 06/2002

Vocational education as an IT Specialist for Application Development, EDS Deutschland GmbH, Bremen

### Teaching Experience

since 10/2010

Exercises on "*Cognitive Networks*"

since 03/2009

Lab exercises on "*Introduction to Discrete Event Simulation*" and "*Flow Control Algorithms*"

since 07/2008

Supervising several B.Sc. and M.Sc. theses



#### COLOPHON

This document was typeset using the typographical look-and-feel classicthesis developed by André Miede. The style was inspired by Robert Bringhurst's seminal book on typography "*The Elements of Typographic Style*".

*Final Version* as of July 22, 2015